FTUV-09-0723, IFIC-09-34, SISSA-43/2009/EP

FCNC and CP Violation Observables in a $SU(3)$–flavoured MSSM

L. Calibbi,[1] J. Jones Pérez,[2] A. Masiero,[3,4] Jae-hyeon Park,[3] W. Porod,[5] and O. Vives[2]

[1] *SISSA/ISAS and INFN, I-34013, Trieste, Italy.*

[2] *Departament de Física Teòrica and IFIC, Universitat de València-CSIC, E-46100, Burjassot, Spain.*

[3] *INFN, Sezione di Padova, via F Marzolo 8, I–35131, Padova, Italy*

[4] *Univ. of Padova, Physics Dept. "G. Galieli", Padova, Italy*

[5] *Institut für Theoretische Physik und Astrophysik, Universität Würzburg, D-97074 Würzburg, Germany.*

A non-Abelian flavour symmetry in a minimal supersymmetric standard model can explain the flavour structures in the Yukawa couplings and simultaneously solve the SUSY flavour problem. Similarly the SUSY CP problem can be solved if CP is spontaneously broken in the flavour sector. In this work, we present an explicit example of these statements with a $SU(3)$ flavour symmetry and spontaneous CP violation. In addition, we show that it is still possible to find some significant deviation from the SM expectations as far as FCNC and CP violation are concerned. We find that large contributions can be expected in lepton flavour violating decays, as $\mu \to e\gamma$ and $\tau \to \mu\gamma$, electric dipole moments, d_e and d_n and kaon CP violating processes as ϵ_K. We also show that without further modifications, it is unlikely for these models to solve the Φ_{B_s} anomaly at low-moderate $\tan\beta$. Thus, these flavoured MSSM realizations are phenomenologically sensitive to the experimental searches in the realm of flavor and CP violation physics.

I. INTRODUCTION

In the next few years, after a long impasse in the phenomenological searches for new physics in the energy frontier, all the high-energy particle physics community will be focused on the results from the LHC experiments. Its first goal will be the study of the physics of electroweak symmetry breaking, but besides this, we also expect some kind of new physics around the electroweak scale. Supersymmetry (SUSY) is perhaps the new physics option that is best motivated. The LHC should find some SUSY particles if SUSY is indeed the solution to the hierarchy problem and provides a candidate for the dark matter observed in the universe.

Supersymmetry has been extensively studied in the last decades, but most of these studies have been done in the framework of the so-called Constrained Minimal Supersymmetric Standard Model (CMSSM). The CMSSM is one of the simplest supersymmetric extensions of the Standard Model

as it assumes universality of the supersymmetric soft breaking terms and is completely determined by four parameters $(M_{1/2}, m_0, A_0, \tan\beta)$ plus a sign $(\mathrm{sg}(\mu))$. This simplified model is very useful to explore the main features of the SUSY spectrum in collider experiments, however, nobody really believes that the realization nature has chosen of supersymmetry is exactly the CMSSM, specially concerning flavour. In analogy to the known flavour structures in the Yukawa couplings, we naturally expect non-trivial flavour structures in the supersymmetry soft-breaking terms.

Therefore, we should consider other more general flavoured MSSM models as the SUSY models we can find when we analyze the experimental results from LHC experiments. Nevertheless, it is well-known that the presence of generic flavour structures in the SUSY soft-breaking terms causes the so-called "supersymmetric flavour problem". Flavour changing neutral currents (FCNC) and flavour-dependent CP violation observables receive too large contributions from loops involving SUSY particles and can not satisfy the stringent phenomenological bounds on these processes [1, 2]. Although this statement is still true, it is important to emphasize that the basis of this problem lies clearly on our total ignorance about the origin of the observed flavour and CP-violation in our theory, and this includes also the SM Yukawa couplings. The **real flavour problem** is simply our inability to understand the complicated structures in the quark and lepton Yukawa couplings, and likewise for the soft-breaking flavour structures in the MSSM. It has been recently shown in the literature [3, 4] that an MSSM model with a non-Abelian flavour symmetry allows a simultaneous understanding of the flavour structures in the Yukawa couplings and the SUSY soft-breaking terms, adequately suppressing FCNC and CP violating phenomena and solving the SUSY flavour problem.

In this work, we intend to exhibit a concrete example of such strategy considering an MSSM (with the limited number of new parameters present in the CMSSM) and showing that the presence of a non-Abelian family (horizontal) symmetry can simultaneously account for the solution of both flavor problems, namely that it is possible to successfully reproduce the correct fermion spectrum while adequately suppressing FCNC and CP violating phenomena. Regarding the phenomenology of these flavoured MSSM models, we do not expect large differences from the expectations in the CMSSM from the point of view of collider studies, as we know that the departures from flavour universality are strongly constrained by the present FCNC and CP violation experiments. Much probably the resolution of the new supersymmetric flavour structures will have to rely on FCNC and CP violation experiments. In the following we will analyze the FCNC and CP violation phenomenology of our flavoured MSSM example. We will show that it is still possible to find some significant deviation from the the SM expectations as far as the FCNC and CP violations are concerned, making these realizations phenomenologically sensitive to the experimental searches in

the realm of flavor physics.

In the next section, we introduce the flavour symmetries in SUSY and study its effects in the SUSY soft-breaking terms. Then, we illustrate these effects with an explicit model with a $SU(3)$ flavour symmetry. In section III, we analyze the different FCNC and CP violation observables in this model including lepton flavour violation, kaon physics, B physics and electric dipole moments. Section IV is devoted to a combined analysis of all the FCNC and CP violation observables and we show the correlations between the most interesting observables in this model. Finally, in section V we present our conclusions.

II. FLAVOUR SYMMETRIES IN SUSY

Flavour symmetries have been used with success in the past to try to extract some meaning from the complicated structures of fermion masses and mixings in the Standard Model (SM). Using the Froggat-Nielsen mechanism [5], flavour symmetries explain the structure of the SM Yukawa couplings as the result of a spontaneously broken symmetry associated with flavour. In different extensions of the SM, these flavour symmetries will also constrain the new couplings and masses. For instance, in the context of a supersymmetric theory, a flavour symmetry would apply equally to the fermion and scalar sectors. Therefore, this implies that in the limit of exact symmetry the soft-breaking scalar masses and the trilinear couplings must be invariant under the flavour symmetry and the structures in the soft-breaking terms will be generated after the spontaneous breaking of the flavour symmetry. Both the flavour structures in the Yukawa couplings and in the soft-breaking terms are generated by the same mechanism and thus we can expect a close relation between them[1].

The flavour-diagonal scalar masses, i.e. couplings $\phi^\dagger\phi$, are clearly invariant under any symmetry and are always allowed by the flavour symmetry. However, in general, this does not guarantee that they are family universal. In the case of an Abelian [5, 6, 7, 8, 9, 10, 11, 12] family symmetry, the symmetry does not relate different generations, and, generically, different fields will have different diagonal soft masses. On the other hand, a non-Abelian family symmetry groups two or three generations in a single multiplet with a common mass in the symmetric limit, thus helping to solve, in principle, the FCNC problem. This was one of the main motivations for the construction of the

[1] The relation between the soft-breaking terms and the Yukawa matrices is present in gravity mediation mechanisms, but it would not be present if the mediation mechanism is flavour blind, as in the case of gauge mediation or anomaly mediation

first $SU(2)$ flavour models [13, 14], where the first two generation sfermions, facing the strongest constraints, share a common mass. In the case of an $SU(3)$ flavour symmetry [3, 15, 16, 17], all three generations have the same mass in the unbroken family symmetry limit. On the contrary, trilinear couplings are completely equivalent to the Yukawa couplings from the point of view of the symmetry because they involve exactly the same fields (scalar or fermionic components). Thus, they are generated after symmetry-breaking as a function of small vevs. Therefore, to solve the "SUSY flavour problem", we will consider in this work non-Abelian family symmetries, and more exactly $SU(3)$ theories or discrete versions of this symmetry.

Apart from these renormalizable mass operators in the Lagrangian, we can construct non-renormalizable operators neutral under the flavour symmetry inserting an appropriate number of flavon fields. The flavon fields, charged under the symmetry, are responsible for the spontaneous symmetry breaking once they acquire a vev. Then, higher dimensional operators involving two SM fermions and a Higgs field, with several flavon vevs suppressed by a large mediator mass, generate the observed Yukawa couplings. In the same way, these flavon fields will couple to the scalar fields in all possible ways allowed by the symmetry and, after spontaneous symmetry breaking, they will generate a non-trivial flavour structure in the soft-breaking parameters. Therefore, by being generated by insertions of the same flavon vevs, we can expect the structures in the soft-breaking matrices and the Yukawa couplings to be related.

The structure in the Yukawa couplings is not completely determined by the observed values of fermionic masses and mixing angles. To solve this problem and fix the Yukawa couplings, we accept that the smallness of CKM mixing angles is due to the smallness of the off-diagonal elements in the Yukawa matrices with respect to the corresponding diagonal elements, and we make the additional simplifying assumption of choosing the matrices to be symmetric. With these two theoretical assumptions, and using the ratio of masses at the GUT scale to define the expansion parameters in the up and down sector as $\bar{\varepsilon} = \sqrt{m_s/m_b}$ and $\varepsilon = \sqrt{m_c/m_t}$, we can fix the Yukawa textures in the quark sector to be:

$$Y_d \propto \begin{pmatrix} 0 & x^d_{12}\,\bar{\varepsilon}^3 & x^d_{13}\,\bar{\varepsilon}^3 \\ x^d_{12}\,\bar{\varepsilon}^3 & \bar{\varepsilon}^2 & x^d_{23}\,\bar{\varepsilon}^2 \\ x^d_{13}\,\bar{\varepsilon}^3 & x^d_{23}\,\bar{\varepsilon}^2 & 1 \end{pmatrix}, \qquad Y_u \propto \begin{pmatrix} 0 & x^u_{12}\,\varepsilon^3 & x^u_{13}\,\varepsilon^3 \\ x^u_{12}\,\varepsilon^3 & \varepsilon^2 & x^u_{23}\,\varepsilon^2 \\ x^u_{13}\,\varepsilon^3 & x^u_{23}\,\varepsilon^2 & 1 \end{pmatrix}, \tag{1}$$

where $\bar{\varepsilon} \simeq 0.15$, $\varepsilon \simeq 0.05$ and the x^a_{ij} are $O(1)$ coefficients fixed by the observed values of fermion masses and mixings. In the Appendix we show the full structure of the Yukawas, and find the best fit values $x^d_{12} \simeq 1.7$, $x^d_{13} \simeq 0.4$, $x^d_{23} \simeq 1.8$, $x^u_{12} \simeq 1.4$, $x^u_{13} \simeq 2$, $x^u_{23} \simeq 2$. In the leptonic sector we will follow the same strategy as in Ref. [4] and require unification of charged lepton and down-quark

flavour matrices, i.e. we embed our model in a grand unified framework, for instance $SO(10)$, and we try to explain simultaneously quark and lepton Yukawas. The detailed structure of the leptonic Yukawa matrix is also shown in the Appendix.

Taking this Yukawa structure as our starting point, we will generate the flavour structure of the soft-breaking terms in generic non-Abelian $SU(3)$ flavour symmetries or discrete versions, like $\Delta(27)$ or $\Delta(54)$ [18, 19, 20, 21, 22]. Under these symmetries, the three generations of SM fields, both $SU(2)_L$-doublets and singlets, are triplets **3** and the Higgs fields are singlets. Therefore Yukawa couplings and trilinear terms are not allowed by the symmetry. In these models, we add several flavon fields. For instance in [3] we have θ_3, θ_{23} (anti-triplets $\overline{\mathbf{3}}$), $\bar{\theta}_3$ and $\bar{\theta}_{23}$ (triplets **3**), while in [17] we have also θ_{123} and $\bar{\theta}_{123}$. The symmetry is broken in several steps, first $SU(3)$ is broken into $SU(2)$ by the vev of θ_3 and $\bar{\theta}_3$, with $\langle\theta_3\rangle = (0,0,a)$ and a being of the same order as the mediator mass M_f, i.e. $a/M_f \simeq O(1)$. Subsequently θ_{23} and $\bar{\theta}_{23}$ get a smaller vev $\propto (0,b,b)$, with $b/M_d \simeq \bar{\varepsilon}$ and $b/M_u \simeq \varepsilon$. Notice that in principle, we have three different mediator masses, $M_f = M_L, M_u, M_d$, because the flavour symmetry must commute with the SM symmetry and therefore the vector-like mediator fields must have the SM quantum numbers of the usual particles[2]. In some models we also have θ_{123} and $\bar{\theta}_{123}$ getting a lower vev $\propto (c,c,c)$ with $c/M_d \simeq \bar{\varepsilon}^2$.

Notice that the mentioned vevs require a vacuum alignment mechanism. In this work we do not specify a particular mechanism, but we refer the interested reader to the examples in [3, 18, 23, 24, 25].

The basic structure of the Yukawa superpotential (for quarks and leptons) is then given by

$$W_{\rm Y} \;=\; H\psi_i\psi_j^c\left[\theta_3^i\theta_3^j + \theta_{23}^i\theta_{23}^j\left(\theta_3\overline{\theta}_3\right) + \epsilon^{ikl}\overline{\theta}_{23,k}\overline{\theta}_{3,l}\theta_{23}^j\left(\theta_{23}\overline{\theta}_3\right) + \dots\right], \tag{2}$$

in the absence of θ_{123} fields, or,

$$W_{\rm Y} \;=\; H\psi_i\psi_j^c\left[\theta_3^i\theta_3^j + \theta_{23}^i\theta_{23}^j + \theta_{23}^i\theta_{123}^j + \theta_{123}^i\theta_{23}^j\dots\right], \tag{3}$$

in the models with θ_{123}. All flavon fields in these equations should be understood as θ_i/M_f. Note, however, that the $SU(3)$ symmetry is not enough by itself to determine the required structure in the superpotential. Generically, we have to introduce additional global symmetries to forbid unwanted terms, like a mixed term $\theta_3\theta_{23}$, that would spoil the Yukawa structure. Nevertheless, the structure in Eqs. (2) and (3) is quite general for the different $SU(3)$ models we can build, and for additional details we refer to [3, 15, 16].

[2] For simplicity, we take M_d and $M_u = M_L$ in all our numerical calculations.

In the same way, the scalar soft masses deviate from exact universality after $SU(3)$ breaking. As explained above, $\phi_i^\dagger \phi_i$ is completely neutral under gauge and global symmetries and gives rise to a common contribution for the family triplet. However, after $SU(3)$ breaking, terms with additional flavon fields give rise to important corrections [3, 26, 27, 28]. Any invariant combination of flavon fields can also contribute to the sfermion masses (at least with Planck scale suppression). In this case, it is easy to see that the following terms will always contribute to the sfermion mass matrices (the presence of the θ_{123} field will depend on the model):

$$(M^2_{\tilde{f}})^j_i = m_0^2\Bigg(\delta^j_i + \frac{1}{M_f^2}\left[\theta^\dagger_{3i}\theta^j_3 + \overline{\theta}_{3,i}\overline{\theta}^{\dagger\,j}_3 + \theta^\dagger_{23i}\theta^j_{23} + \overline{\theta}_{23,i}\overline{\theta}^{\dagger\ \ j}_{23} + \theta^\dagger_{123i}\theta^j_{123} + \overline{\theta}_{123,i}\overline{\theta}^{\dagger\ \ j}_{123}\right] + \frac{1}{M_f^4}(\epsilon_{ikl}\overline{\theta}^{\dagger k}_3\overline{\theta}^{\dagger\ \ l}_{23})(\epsilon^{jmn}\overline{\theta}_{3,m}\overline{\theta}_{23,n}) + \quad \ldots \quad \Bigg), \tag{4}$$

where f represents the $SU(2)$ quark and lepton doublets or the up (neutrino) and down (charged-lepton) singlets, so that $M_f = M_L, M_u, M_d$. From here we see that taking $\langle\theta_{123}\rangle/M_d = \langle\bar{\theta}_{123}\rangle/M_d = \bar{\varepsilon}^2$, both models with and without θ_{123} have the same structure up to corrections $O(\varepsilon^4)$ that will be always subdominant in the relevant soft mass matrices in the basis of diagonal Yukawa matrices.

Notice that in Eq. (4) only the fields that enter the superpotential have their vevs and associated mediators masses fixed by the ε or $\bar{\varepsilon}$ parameters. For instance in the discrete model of Ref.[19], $\bar{\theta}_{123}$ (the **3**-field that in this reference is written as θ_{123}) does not enter the superpotential. Therefore, its contributions to the soft masses can be suppressed even having a large vev if the associated mediator mass is high enough[3]. However, in the continuous version of this model [17], the vevs of $\bar{\theta}_{123}/M_f$ and $\bar{\theta}_{123}/M_f$ are constrained to be both $O(\varepsilon^2)$ by D-flatness and thus they are not dangerous in the soft-mass matrices. Moreover, we have to remember that these deviations from universality in the soft-mass matrices proportional to flavour symmetry breaking come always through corrections in the Kähler potential and these effects will be important only in gravity-mediation SUSY models.

In the case of the trilinear couplings we have to emphasize that from the point of view of the flavour symmetry these couplings are completely equivalent to the corresponding Yukawa coupling. This means that they necessarily involve the same combination of flavon vevs, although order one coefficients are generically different because they require at least an additional coupling to a field mediating SUSY breaking (in general coupled in different ways in the various contributions). Therefore, from our point of view, we expect that the trilinear couplings have the same structure as the Yukawa matrices in the flavour basis. However in general they are **not** proportional to the Yukawas, because of different $O(1)$ coefficients in the different elements. Thus, we can expect that

[3] We thank G. G. Ross and I. de Medeiros Varzielas for clarifying this point.

going to the SCKM basis does not diagonalize the trilinear matrices. In fact, the trilinear matrices maintain the same structure as in the flavour basis and only the $O(1)$ coefficients are modified.

Therefore, we can see that in these $SU(3)$-like models with the three generations unified in a single field, we have basically the same "leading order" structures in the soft mass matrices and the trilinear couplings directly related to the structures in the Yukawa couplings. In the following we concentrate in the $SU(3)$ model of [3] because it has a complete phase structure in the flavon vevs consistent with the CKM phase. Remember however, that the main features of the soft terms are similar in other models and in principle the phase structure could be also adapted in these models.

A. SU(3) Flavour Model

Let us now specify more explicitely the $SU(3)$ flavour model that we use as our main example. The full superpotential is determined by $SU(3)$ and several global symmetries are used to forbid unwanted terms that would spoil the observed structure of the Yukawa couplings. Using the charges presented in Table II, the leading terms in the superpotential are,

$$\begin{aligned} W_{\rm Y} \;=\; & H\psi_i\psi_j^c\left[\theta_3^i\theta_3^j+\theta_{23}^i\theta_{23}^j\Sigma+\left(\epsilon^{ikl}\overline{\theta}_{23,k}\overline{\theta}_{3,l}\theta_{23}^j+\epsilon^{jkl}\overline{\theta}_{23,k}\overline{\theta}_{3,l}\theta_{23}^i\right)\left(\theta_{23}\overline{\theta}_3\right)+\right. \\ & \left.\epsilon^{ijl}\overline{\theta}_{23,l}\left(\theta_{23}\overline{\theta}_3\right)^2+\epsilon^{ijl}\overline{\theta}_{3,l}\left(\theta_{23}\overline{\theta}_3\right)\left(\theta_{23}\overline{\theta}_{23}\right)+\ldots\right], \end{aligned} \tag{5}$$

where to simplify the notation, the flavon fields have been normalized to the corresponding mediator mass, which means that all the flavon fields in this equation should be understood as θ_i/M_f. The field Σ is a Georgi-Jarlskog field that gets a vev in the $B-L$ direction, distinguishing leptons and quarks. Furthermore, as said above this model is embeded in a $SO(10)$ grand unified structure at high scales, which allow us to relate quark and lepton (including neutrino) Yukawa couplings. However, the $SU(2)_R$ subgroup of $SO(10)$ must be broken as we need different mediator masses for the up and down sector and, in fact θ_3 and $\overline{\theta}_3$ are $\mathbf{3}\oplus\mathbf{1}$ representations of $SU(2)_R$ which is broken by their vevs [3, 16, 29].

After spontaneous symmetry breaking the flavon fields get the following vevs:

$$\langle\theta_3\rangle=\begin{pmatrix}0\\0\\1\end{pmatrix}\otimes\begin{pmatrix}a_3^u & 0\\ 0 & a_3^d\,e^{i\chi}\end{pmatrix};\qquad \langle\bar{\theta}_3\rangle=\begin{pmatrix}0\\0\\1\end{pmatrix}\otimes\begin{pmatrix}a_3^u\,e^{i\alpha_u} & 0\\ 0 & a_3^d\,e^{i\alpha_d}\end{pmatrix};$$

$$\langle\theta_{23}\rangle=\begin{pmatrix}0\\ b_{23}\\ b_{23}\,e^{i\beta_3}\end{pmatrix};\qquad \langle\bar{\theta}_{23}\rangle=\begin{pmatrix}0\\ b_{23}\,e^{i\beta_2'}\\ b_{23}\,e^{i(\beta_2'-\beta_3)}\end{pmatrix}; \tag{6}$$

Flavon Phase	$\alpha_u - \alpha_d$	χ	β_3	β_2'
Allowed Values	$(-40 \pm 2)^\circ$	$(20 \pm 10)^\circ + 180^\circ n$	$-(20 \pm 10)^\circ + 180^\circ n$	Unconstrained

TABLE I: Flavon phases after imposing CKM constraints, with $n \in N$. Notice that the approximate errors we quote in χ and β_3 are highly correlated, as shown in the Appendix.

where we require the following relations:

$$\left(\frac{a_3^u}{M_u}\right)^2 = y_t, \qquad \left(\frac{a_3^d}{M_d}\right)^2 = y_b,$$
$$\frac{b_{23}}{M_u} = \varepsilon, \qquad \frac{b_{23}}{M_d} = \bar{\varepsilon}. \tag{7}$$

These relations are valid at the flavour breaking scale, that we take as the GUT scale in the numerical evaluation.

It is straight-forward to see that this superpotential reproduces correctly the required Yukawa structure in Eq. (1). For completeness, we also list in Table I the values that the flavon phases can take, given the constraints imposed by the CKM matrix. The analysis leading to such constraints is found in the Appendix.

We can now turn to the soft breaking terms. As mentioned in the previous section, a universal, flavour diagonal mass term will always be allowed. Moreover, in a SUSY theory, the same messenger fields as in the Yukawas will couple the flavons to the scalar fields in the soft terms. Thus, the ε and $\bar{\varepsilon}$ parameters still act as expansion parameters, and represent important corrections to the soft terms.

Clearly any coupling involving a flavon field and its hermitian conjugate (i.e. $\theta_3^{i\dagger}\theta_3^j$) is invariant under the flavour symmetry. From this we can deduce that the soft mass terms get a minimum structure determined uniquely by the flavon content of the model and on their vevs. This minimum structure is obtained from the following effective terms:

$$(M_{\tilde{f}}^2)_i^j = m_0^2\Bigg(\delta_i^j + \left[\theta_{3i}^\dagger\theta_3^j + \overline{\theta}_{3,i}\overline{\theta}_3^{\dagger\,j} + \theta_{23i}^\dagger\theta_{23}^j + \overline{\theta}_{23,i}\overline{\theta}_{23}^{\dagger\;\;j}\right]$$
$$+ (\epsilon_{ikl}\theta_3^k\theta_{23}^l)(\epsilon^{jmn}\theta_{3m}^\dagger\theta_{23n}^\dagger) + (\epsilon_{ikl}\overline{\theta}_3^{\dagger k}\overline{\theta}_{23}^{\dagger\;\;l})(\epsilon^{jmn}\overline{\theta}_{3,m}\overline{\theta}_{23,n}) + \quad \ldots \quad \Bigg). \tag{8}$$

In Table II we show a choice of global charges that reproduces the correct Yukawa structure and does not allow other terms at leading order in the Kähler potential (soft-masses).

In the squark sector, after rephasing the fields such that the CKM matrix elements V_{ud}, V_{us},

Field	ψ	ψ^c	H	Σ	θ_3	θ_{23}	$\bar{\theta}_3$	$\bar{\theta}_{23}$
SU(3)	3	3	1	1	$\bar{3}$	$\bar{3}$	3	3
U(1)	0	0	0	1	0	-1	1	0
U′(1)	-1	-1	0	2	1	0	-1	4
U″(1)	1	1	0	-3	-1	1	0	-4

TABLE II: Charges required to build the minimal RVV1 Model.

V_{cb} and V_{tb} are real, the soft masses in the SCKM basis are:

$$\left(M^2_{\tilde{u}^c_R}\right)^T = \begin{pmatrix} 1+\varepsilon^2\, y_t & -\varepsilon^3\, e^{i\omega'} & -\varepsilon^3\, e^{i(\omega'-2\chi)} \\ -\varepsilon^3\, e^{-i\omega'} & 1+\varepsilon^2 & \varepsilon^2\, e^{-2i\chi} \\ -\varepsilon^3\, e^{-i(\omega'-2\chi)} & \varepsilon^2\, e^{2i\chi} & 1+y_t \end{pmatrix} m_0^2 \tag{9a}$$

$$\left(M^2_{\tilde{d}^c_R}\right)^T = \begin{pmatrix} 1+\bar{\varepsilon}^2\, y_b & -\bar{\varepsilon}^3\, e^{i\omega_{us}} & -\bar{\varepsilon}^3\, e^{i\omega_{us}} \\ -\bar{\varepsilon}^3\, e^{-i\omega_{us}} & 1+\bar{\varepsilon}^2 & \bar{\varepsilon}^2 \\ -\bar{\varepsilon}^3\, e^{-i\omega_{us}} & \bar{\varepsilon}^2 & 1+y_b \end{pmatrix} m_0^2 \tag{9b}$$

$$M^2_{\tilde{Q}} = \begin{pmatrix} 1+\varepsilon^2\, y_t & -\varepsilon^2\bar{\varepsilon}\, e^{i\omega_{us}} & -\bar{\varepsilon}^3\, y_t e^{i\omega_{us}} \\ -\varepsilon^2\bar{\varepsilon}\, e^{-i\omega_{us}} & 1+\varepsilon^2 & \bar{\varepsilon}^2\, y_t \\ -\bar{\varepsilon}^3\, y_t e^{-i\omega_{us}} & \bar{\varepsilon}^2\, y_t & 1+y_t \end{pmatrix} m_0^2 \tag{9c}$$

$$\left(M^2_{\tilde{e}^c_R}\right)^T = \begin{pmatrix} 1+\bar{\varepsilon}^2\, y_b & -\bar{\varepsilon}^3 & -\bar{\varepsilon}^3\, e^{i(\chi-\beta_3)} \\ -\bar{\varepsilon}^3 & 1+\bar{\varepsilon}^2 & \bar{\varepsilon}^2\, e^{i(\chi-\beta_3)} \\ -\bar{\varepsilon}^3\, e^{-i(\chi-\beta_3)} & \bar{\varepsilon}^2\, e^{-i(\chi-\beta_3)} & 1+y_b \end{pmatrix} m_0^2 \tag{9d}$$

$$M^2_{\tilde{L}} = \begin{pmatrix} 1+\varepsilon^2\, y_t & -\varepsilon^2\bar{\varepsilon} & -\bar{\varepsilon}^3\, y_t\, e^{i(\chi-\beta_3)} \\ -\varepsilon^2\bar{\varepsilon} & 1+\varepsilon^2 & \bar{\varepsilon}^2\, y_t\, e^{i(\chi-\beta_3)} \\ -\bar{\varepsilon}^3\, y_t e^{-i(\chi-\beta_3)} & \bar{\varepsilon}^2\, y_t\, e^{-i(\chi-\beta_3)} & 1+y_t \end{pmatrix} m_0^2 \tag{9e}$$

where $M^2_{\tilde{Q}}$ ($M^2_{\tilde{L}}$) is in the basis where Y_d (Y_e) is diagonal, ω_{us} is related to the CKM phase, and $\omega' = \omega_{us} - (\delta_u - \delta_d)$. The ω_{us} and δ_i phases can be found in the Appendix. The structure of $M^2_{\tilde{Q}}$ in the basis where Y_u is diagonal is similar to $M^2_{\tilde{u}^c_R}$. Notice that, although the structure in terms of ε, $\bar{\varepsilon}$ in $M^2_{\tilde{e}^c_R}$ and $M^2_{\tilde{L}}$ is the same as that of $M^2_{\tilde{d}^c_R}$ and $M^2_{\tilde{Q}}$, respectively, the coefficients from the SCKM rotation and RGE evolution are different due to the Georgi-Jarlskog field Σ. This can be seen in the Appendix, and is summarized in Table V, in Section III A. The phase structure of the slepton matrices is different to the one of squarks, since the latter have been rephased in order for

Field	ψ	ψ^c	H	Σ	θ_3	θ_{23}	$\bar{\theta}_3$	$\bar{\theta}_{23}$
SU(3)	3	3	1	1	$\bar{3}$	$\bar{3}$	3	3
U(1)	-2	-2	0	-4	2	3	0	-2
U′(1)	0	0	0	1	0	-1	1	0

TABLE III: Charges for RVV2 Model.

the CKM matrix to follow the standard phase convention.[4]

In Eq. (9), we have written only the leading contribution in ε and $\bar{\varepsilon}$ to each element with a leading phase, omitting effective complex $O(1)$ coefficients. This sets the size of the modulus of the mass-insertion. The $O(1)$ coefficients are the remaining part of the full element, after factorizing the terms explicitly written in Eq. (9). There are many contributions to these coefficients: first, we have the real $O(1)$ constants in front of each term in the Kähler potential, at M_{GUT}. We also have contributions from the real $O(1)$ constants in the Yukawa matrices, coming from the rotation into the SCKM basis. A third contribution comes from the RGE evolution to the EW scale. And finally, it is possible to have further contributions from subleading terms in the Kähler potential, still at M_{GUT}.

All of these contributions can involve the flavon phases, so the effective $O(1)$ can be complex. As we are factorizing the leading phases, the phase in each coefficient shall only appear in subleading terms. If the leading phases cancel for a particular observable, these subleading phases shall be important. Such a cancellation can happen in EDMs. For example, in mass-insertion notation [30, 31], the corresponding effective $O(1)$ coefficients of $(\delta^d_{13})_{RR}$ and $(\delta^d_{13})_{LL}$ have the following structure:

$$D^{RR}_{13} \sim 1 - y_b\, e^{-2i(\chi-\beta_3)} \tag{10a}$$

$$Q^{LL}_{13} \sim 1 - (\varepsilon^2/\bar{\varepsilon}^2)\, e^{-2i(\chi-\beta_3)}. \tag{10b}$$

Although Eq. (8) is the minimal structure present for all possible models, it is possible, for particular choices of the global symmetries and charges, to build other symmetry-dependent soft-mass structures. In fact, the observed structure in the Yukawa couplings does not fix completely the introduced global charges and it is possible to add new invariant combinations of flavon fields to the Kähler potential without modifying the Yukawas.

The first example of these new combinations of flavon fields in the Kähler is achieved by allowing

[4] As physical observables are independent of phase conventions, we could also rephase the slepton superfields and use the same phase structure as squarks.

a $\theta_3^i \bar{\theta}_{23}^j$ term (RVV2). The required charges are shown in Table III. It is easy to check that, with these charges, the structure of the Yukawa couplings in the superpotential remains unchanged. This is due to the fact that the superpotential is a holomorphic function of the fields while the Kähler is only a real function. When rotated to the SCKM basis, the soft-mass matrices become:

$$\left(M^2_{\tilde{u}^c_R}\right)^T = \begin{pmatrix} 1+\varepsilon^2\, y_t & -\varepsilon^3\, e^{i\omega'} & -\varepsilon^2\, y_t^{0.5} e^{i(\omega'-2\chi+\beta_3-\beta_2')} \\ -\varepsilon^3\, e^{-i\omega'} & 1+\varepsilon^2 & \varepsilon\, y_t^{0.5} e^{-i(2\chi-\beta_3+\beta_2')} \\ -\varepsilon^2\, y_t^{0.5} e^{-i(\omega'-2\chi+\beta_3-\beta_2')} & \varepsilon\, y_t^{0.5} e^{i(2\chi-\beta_3+\beta_2')} & 1+y_t \end{pmatrix} m_0^2 \quad (11a)$$

$$\left(M^2_{\tilde{d}^c_R}\right)^T = \begin{pmatrix} 1+\bar{\varepsilon}^2\, y_b & -\bar{\varepsilon}^3\, e^{i\omega_{us}} & -\bar{\varepsilon}^2\, y_b^{0.5} e^{i(\omega_{us}-\chi+\beta_3-\beta_2')} \\ -\bar{\varepsilon}^3\, e^{-i\omega_{us}} & 1+\bar{\varepsilon}^2 & \bar{\varepsilon}\, y_b^{0.5} e^{-i(\chi-\beta_3+\beta_2')} \\ -\bar{\varepsilon}^2\, y_b^{0.5} e^{-i(\omega_{us}-\chi+\beta_3-\beta_2')} & \bar{\varepsilon}\, y_b^{0.5} e^{i(\chi-\beta_3+\beta_2')} & 1+y_b \end{pmatrix} m_0^2 \quad (11b)$$

$$M^2_{\tilde{Q}} = \begin{pmatrix} 1+\varepsilon^2\, y_t & -\varepsilon^2\bar{\varepsilon}\, e^{i\omega_{us}} & \varepsilon\bar{\varepsilon}\, y_t^{0.5} e^{i(\omega_{us}-2\chi+\beta_3+\beta_2')} \\ -\varepsilon^2\bar{\varepsilon}\, e^{-i\omega_{us}} & 1+\varepsilon^2 & \varepsilon\, y_t^{0.5} e^{-i(2\chi-\beta_3-\beta_2')} \\ \varepsilon\bar{\varepsilon}\, y_t^{0.5} e^{-i(\omega_{us}-2\chi+\beta_3+\beta_2')} & \varepsilon\, y_t^{0.5} e^{i(2\chi-\beta_3-\beta_2')} & 1+y_t \end{pmatrix} m_0^2 \quad (11c)$$

$$\left(M^2_{\tilde{e}^c_R}\right)^T = \begin{pmatrix} 1+\bar{\varepsilon}^2\, y_b & -\bar{\varepsilon}^3 & -\bar{\varepsilon}^2\, y_b^{0.5} e^{-i\beta_2'} \\ -\bar{\varepsilon}^3 & 1+\bar{\varepsilon}^2 & \bar{\varepsilon}\, y_b^{0.5} e^{-i\beta_2'} \\ -\bar{\varepsilon}^2\, y_b^{0.5} e^{i\beta_2'} & \bar{\varepsilon}\, y_b^{0.5} e^{i\beta_2'} & 1+y_b \end{pmatrix} m_0^2 \quad (11d)$$

$$M^2_{\tilde{L}} = \begin{pmatrix} 1+\varepsilon^2\, y_t & -\varepsilon^2\bar{\varepsilon} & \varepsilon\bar{\varepsilon}\, y_t^{0.5}\, e^{-i(\chi-\beta_2')} \\ -\varepsilon^2\bar{\varepsilon} & 1+\varepsilon^2 & \varepsilon\, y_t^{0.5}\, e^{-i(\chi-\beta_2')} \\ \varepsilon\bar{\varepsilon}\, y_t^{0.5}\, e^{i(\chi-\beta_2')} & \varepsilon\, y_t^{0.5}\, e^{i(\chi-\beta_2')} & 1+y_t \end{pmatrix} m_0^2 \quad (11e)$$

One can see that the effect of this term in $m^2_{\tilde{d}^c_R}$ is to exchange one power of $\bar{\varepsilon}$ by a $y_b^{0.5}$ suppression in $(\delta^d_{13})_{RR}$ and $(\delta^d_{23})_{RR}$. In $m^2_{\tilde{Q}}$, the same terms change an $\bar{\varepsilon}^2$ by an $\varepsilon\, y_t^{0.5}$. However, for $\tan\beta = 10$, and considering that $\varepsilon \approx \bar{\varepsilon}^2$, such replacements leave the structure of the mass matrices very similar numerically to the original one (notice that y_t and y_b are taken at M_{GUT}). Nonetheless, it must be remarked that the phase structure of the whole mass matrix is modified.

As in RVV1, it is crucial to take into account that relative phases exist within the effective $O(1)$ coefficients. For instance, although the global phase of $(\delta^d_{12})_{AA}$ is still ω_{us}, the $O(1)$ structure of $(\delta^d_{12})_{LL}$ in RVV2 is now:

$$(Q^{LL}_{12})^{RVV2} \sim 1 - \left(\bar{\varepsilon}^2/\varepsilon\right)\left(1 + e^{i(2\chi-\beta_3-\beta_2')}\right). \quad (12)$$

Notice that the factor $(\bar{\varepsilon}^2/\varepsilon) = 0.45$ does not really provide any suppression at all. This means that the imaginary part of $(\delta^d_{12})_{LL}$ is larger than just $\varepsilon^2\bar{\varepsilon}\sin\omega_{us}$. We label this new, larger, effective phase as ω'_{us}.

Field	ψ	ψ^c	H	Σ	θ_3	θ_{23}	$\bar{\theta}_3$	$\bar{\theta}_{23}$
SU(3)	3	3	1	1	$\bar{3}$	$\bar{3}$	3	3
U(1)	-1	-1	0	5	1	-2	0	6
U′(1)	0	0	0	-1	0	0	1	-2

TABLE IV: Charges for RVV3 Model.

A second possibility is to allow a $\left(\epsilon^{ikl}\theta_3^k\theta_{23}^l\right)\theta_3^j$ term (RVV3) in the Kähler, with the charges being shown in Table IV. The soft matrices, when rotated into the SCKM basis, have the following structure:

$$\left(M^2_{\tilde{u}^c_R}\right)^T = \begin{pmatrix} 1+\varepsilon^2\, y_t & -\varepsilon^3\, e^{i\omega'} & \varepsilon\, y_t e^{i(\omega'-2\chi+\beta_3-\delta_u)} \\ -\varepsilon^3\, e^{-i\omega'} & 1+\varepsilon^2 & \varepsilon^2\, e^{-2i\chi} \\ \varepsilon\, y_t e^{-i(\omega'-2\chi+\beta_3-\delta_u)} & \varepsilon^2\, e^{2i\chi} & 1+y_t \end{pmatrix} m_0^2 \tag{13a}$$

$$\left(M^2_{\tilde{d}^c_R}\right)^T = \begin{pmatrix} 1+\bar{\varepsilon}^2\, y_b & -\bar{\varepsilon}^3\, e^{i\omega_{us}} & \bar{\varepsilon}\, y_b e^{i(\omega_{us}+\beta_3-\delta_d)} \\ -\bar{\varepsilon}^3\, e^{-i\omega_{us}} & 1+\bar{\varepsilon}^2 & \bar{\varepsilon}^2 \\ \bar{\varepsilon}\, y_b e^{-i(\omega_{us}+\beta_3-\delta_d)} & \bar{\varepsilon}^2 & 1+y_b \end{pmatrix} m_0^2 \tag{13b}$$

$$M^2_{\tilde{Q}} = \begin{pmatrix} 1+\varepsilon^2\, y_t & -\varepsilon\bar{\varepsilon}^2\, y_t e^{i(\omega_{us}-2\chi+\beta_3+\delta_d)} & \varepsilon\, y_t e^{i(\omega_{us}-2\chi+\beta_3+\delta_d)} \\ -\varepsilon\bar{\varepsilon}^2\, y_t e^{-i(\omega_{us}-2\chi+\beta_3+\delta_d)} & 1+\varepsilon^2 & \bar{\varepsilon}^2\, y_t \\ \varepsilon\, y_t e^{-i(\omega_{us}-2\chi+\beta_3+\delta_d)} & \bar{\varepsilon}^2\, y_t & 1+y_t \end{pmatrix} m_0^2 \tag{13c}$$

$$\left(M^2_{\tilde{e}^c_R}\right)^T = \begin{pmatrix} 1+\bar{\varepsilon}^2\, y_b & -\bar{\varepsilon}^3 & \bar{\varepsilon}\, y_b e^{i(\chi-\delta_d)} \\ -\bar{\varepsilon}^3 & 1+\bar{\varepsilon}^2 & \bar{\varepsilon}^2\, e^{i(\chi-\beta_3)} \\ \bar{\varepsilon}\, y_b e^{-i(\chi-\delta_d)} & \bar{\varepsilon}^2\, e^{-i(\chi-\beta_3)} & 1+y_b \end{pmatrix} m_0^2 \tag{13d}$$

$$M^2_{\tilde{L}} = \begin{pmatrix} 1+\varepsilon^2\, y_t & -\varepsilon\bar{\varepsilon}^2\, y_t\, e^{-i(2\chi-\beta_3-\delta_d)} & \varepsilon\, y_t\, e^{-i(\chi-\delta_d)} \\ -\varepsilon\bar{\varepsilon}^2\, y_t\, e^{i(2\chi-\beta_3-\delta_d)} & 1+\varepsilon^2 & \bar{\varepsilon}^2\, y_t\, e^{i(\chi-\beta_3)} \\ \varepsilon\, y_t\, e^{i(\chi-\delta_d)} & \bar{\varepsilon}^2\, y_t\, e^{-i(\chi-\beta_3)} & 1+y_t \end{pmatrix} m_0^2 \tag{13e}$$

with δ_i defined in the Appendix.

This model shows larger deviations from RVV1 in the LL sector. It is important to notice that $(\delta^d_{12})_{LL}$ is now of order $\varepsilon\bar{\varepsilon}^2$ instead of $\varepsilon^2\bar{\varepsilon}$, which will have considerable consequences in processes such as $\mu \to e\gamma$. Likewise, $(\delta^d_{13})_{LL}$ is of order $\varepsilon\, y_t$ instead of $\bar{\varepsilon}^3$, so an enhancement in $\tau \to e\gamma$ should be expected. Regarding the RR sector, for $\tan\beta = 10$, the y_b suppression at M_{GUT} has roughly the same size as an $\bar{\varepsilon}$ suppression, so once again the structure of $m^2_{\tilde{d}^c_R}$ is numerically similar to RVV1 for this value of $\tan\beta$.

The trilinear couplings, on the other hand, follow the same symmetries as the Yukawas. Thus, they have the same flavon structure in RVV1, RVV2 and RVV3. Nonetheless, although they have the same structure, they do not have the same $O(1)$ constants, which means that the rotation into the SCKM basis does not diagonalize them. In the SCKM basis, after rephasing the fields, the trilinears have the following structure:

$$A_u = \begin{pmatrix} 0 & \varepsilon^3\, e^{-i\omega'} & \varepsilon^3\, e^{i(2\chi-\omega')} \\ \varepsilon^3\, e^{i\omega'} & \varepsilon^2\, \Sigma_u & \varepsilon^2\, \Sigma_u\, e^{2i\chi} \\ \varepsilon^3\, e^{i(\omega'+2\beta_3-2\chi)} & \varepsilon^2\, \Sigma_u\, e^{2i(\beta_3-\chi)} & 1 \end{pmatrix} A_0\, y_t \tag{14a}$$

$$A_d = \begin{pmatrix} 0 & \bar{\varepsilon}^3\, e^{-i\omega_{us}} & \bar{\varepsilon}^3\, e^{-i\omega_{us}} \\ \bar{\varepsilon}^3\, e^{-i\omega_{us}} & \bar{\varepsilon}^2\, \Sigma_d & \bar{\varepsilon}^2\, \Sigma_d \\ \bar{\varepsilon}^3\, e^{i(\omega_{us}+2\beta_3-2\chi)} & \bar{\varepsilon}^2\, \Sigma_d\, e^{2i(\beta_3-\chi)} & 1 \end{pmatrix} A_0\, y_b \tag{14b}$$

where we have neglected the $O(1)$ coefficients. One can get A_e by taking A_d with $\langle \Sigma_e \rangle = 3\, \langle \Sigma_d \rangle$.

The soft mass matrices in Eqs. (9,11,13,14) are given at the large scale $\sim M_{GUT}$. Then, we have to include also effects coming from the running from M_{GUT} to M_W. Although these effects produce further non-universal contributions, they are usually smaller than the terms presented here. In the quark sector, the misalignment of the Y_u and Y_d matrices gives sizeable contributions to the LL and LR sectors, analogous to the MFV contributions of CMSSM models. In the lepton sector with RH neutrinos, the same happens due to the misalignment of Y_ν and Y_e [32, 33, 34]. Both of these contributions are unavoidable, albeit the Y_ν contribution is highly model dependent.

Moreover, in the present case there are new contributions to the running given by the intrinsic non-universality of the soft mass matrices. Although these effects contribute even in the RR sector, it turns out that the magnitude of the generated off-diagonal terms are, at most, of the same order as those at M_{GUT}. This means that the addition of running effects will only change the already unknown $O(1)$ constants, such that the low-energy phenomenology can still be understood by analyzing Eqs. (9), (11), (13) and (14).

Finally, we have to emphasize once more that all the soft matrices presented here have unknown $O(1)$ coefficients in all non-universal terms. The flavour symmetry allows us to fix the order in ε and $\bar{\varepsilon}$ of the different entries but the final values could easily vary up or down by factors of two and this has to be taken into account when analyzing our numerical results.

III. FCNC AND CP VIOLATION OBSERVABLES

In the following, we shall study flavour and CP violating observables, presenting analytical estimates in mass insertion approximation (MIA). Moreover, we will perform a full numerical analysis in the SUGRA parameter space through a scan in m_0 and $M_{1/2}$ for fixed values of $\tan\beta$ and $a_0 = A_0/m_0$. The numerical analysis is done defining the Yukawa, trilinear and soft mass matrices at $M_{flav} = 2 \times 10^{16}$ GeV, for the three different versions of the model, as explained in Section II A. Then the different flavour matrices are evolved to the electro-weak scale, solving 1-loop RGEs with SPheno [35]. $O(1)$ coefficients in the Yukawa matrices are determined by requiring a good fit on the fermion masses and quark mixings at M_Z [36]. The result of such fit is presented in the Appendix.

Regarding the unknown $O(1)$ constants in both the superpotential and Kähler potential, as we do not have a full high-scale model, we shall fix each $O(1)$s at a random value, between 0.5 and 2. Notice they can be of either sign. Thus, a model is characterized by both the choice of symmetries involved, and by the particular $O(1)$s we have in front of each effective term. In Section IV we shall take into account their variation.

After running the resulting matrices down to the M_Z scale, we diagonalize the Yukawas in order to obtain the left and right mixing matrices and rotate the soft matrices into the SCKM basis. At the M_Z scale, for each point of the SUSY parameter space, we compute the SUSY spectrum and check that the electroweak symmetry breaking does take place and no tachyonic particles arise. Moreover, to be conservative, we require that the Lightest Supersymmetric Particle (LSP) is the lightest neutralino.

In this work we do not include the non-holomorphic corrections to the Yukawa couplings, so our results are valid for low and moderate values of $\tan\beta$. In this regime, the effects of these non-holomorphic corrections are usually small. The only exception is found in the case for the neutron EDM, where new imaginary parts induced by these corrections can give sizeable contributions. We give details on how we introduce such corrections to this observable in Section III D.

Finally, we apply the following constraints:

- Bounds on the sparticle masses from direct searches at LEP and Tevatron [37].
- Lower bound on Higgs masses from LEP [38]. Although the SM bound on the Higgs mass is of 114 GeV, in SUSY the modification of the lightest Higgs coupling could reduce this constraint. In order to take this effect into account, for each point we calculate the Higgs

mixing angle α and use Eq. (17) of Ref. [39] to estimate the correct Higgs mass bound. We then use SPheno to calculate the two loop Higgs mass, and take into account a theoretical uncertainty of 3 GeV [40, 41].

- $b \to s\gamma$. The experimental world average from the CLEO [42], Belle [43] and BaBar [44] collaborations is given by [45]:

$$\mathrm{BR}(B \to X_s\gamma)_{E_\gamma > 1.6\mathrm{GeV}} = (3.52 \pm 0.23 \pm 0.9) \times 10^{-4} \; . \tag{15}$$

  We have to compare these values with the MSSM predictions. In our numerical calculation, we use the expression presented in Ref. [46] in which the branching ratio is explicitly given in terms of arbitrary complex Wilson coefficients C_7 and C_8. At present, the SM contribution to this decay is already available at NNLO while the SUSY contribution in a general MSSM is partially known at NLO. In this work, we include the NLO SM contribution with a modified low value of the scale for the charm mass to reproduce the NNLO SM contribution ($\mathrm{BR}(B \to X_s\gamma)^{SM} = 3.15 \times 10^{-4}$) [47, 48, 49]. We add the supersymmetric contributions at one loop, and require that the total result does not deviate from the experimental value of Eq. (15) in more than 2-sigma.

- Muon anomalos magnetic moment, $a_\mu = (g-2)_\mu/2$. At present, the experimental result for this observable is given by [50],

$$a_\mu^{\mathrm{exp}} = 11\,659\,2080\,(63) \times 10^{-11}, \tag{16}$$

  while, computing the hadronic contribution by means of the hadronic e^+e^- annihilation data, the SM theoretical expectation is [51, 52, 53],

$$a_\mu^{\mathrm{SM}} = 11\,659\,181\,(8) \times 10^{-10}. \tag{17}$$

  The resulting discrepancy is:

$$\Delta a_\mu = a_\mu^{\mathrm{exp}} - a_\mu^{\mathrm{SM}} = +302(88) \times 10^{-11}. \tag{18}$$

  It is well-known that in the MSSM a_μ receives contributions from $\tilde{\chi}^0$–$\tilde{\mu}$ and $\tilde{\chi}^\pm$–$\tilde{\nu}$ loops [54]. Such contributions are approximately given by the following expression:

$$\frac{a_\mu^{\mathrm{MSSM}}}{1 \times 10^{-9}} \approx 1.5 \left(\frac{\tan\beta}{10}\right) \left(\frac{300\ \mathrm{GeV}}{m_{\tilde{\nu}}}\right)^2 \left(\frac{\mu M_2}{m_{\tilde{\nu}}^2}\right) \; . \tag{19}$$

  A comparison with Eq. (18) implies that the present discrepancy strongly favours the $\mu > 0$ region of the SUSY parameter space. In the case of the theoretical prediction based on τ

	$\lvert(\delta^e_{LL})_{12}\rvert$	$\lvert(\delta^e_{LL})_{13}\rvert$	$\lvert(\delta^e_{LL})_{23}\rvert$	$\lvert(\delta^e_{RR})_{12}\rvert$	$\lvert(\delta^e_{RR})_{13}\rvert$	$\lvert(\delta^e_{RR})_{23}\rvert$
RVV1	$\frac{1}{3}\varepsilon^2\bar{\varepsilon}$	$y_t\bar{\varepsilon}^3$	$3y_t\bar{\varepsilon}^2$	$\frac{1}{3}\bar{\varepsilon}^3$	$\frac{1}{3}\bar{\varepsilon}^3$	$\bar{\varepsilon}^2$
RVV2	$\frac{1}{3}\varepsilon^2\bar{\varepsilon}$	$\frac{1}{3}\sqrt{y_t}\varepsilon\bar{\varepsilon}$	$\sqrt{y_t}\varepsilon$	$\frac{1}{3}\bar{\varepsilon}^3$	$\frac{1}{3}\sqrt{y_b}\bar{\varepsilon}^2$	$\sqrt{y_b}\bar{\varepsilon}$
RVV3	$3y_t\varepsilon\bar{\varepsilon}^2$	$y_t\varepsilon$	$3y_t\bar{\varepsilon}^2$	$\frac{1}{3}\bar{\varepsilon}^3$	$y_b\bar{\varepsilon}$	$\bar{\varepsilon}^2$

TABLE V: Order of magnitude of LFV mass-insertions, for the three models.

	Present Bound	Future Sensitivity
$BR(\mu \to e\gamma)$	1.2×10^{-11} [56]	$\mathcal{O}(10^{-13})$ [57]
$BR(\tau \to \mu\gamma)$	1.6×10^{-8} [58, 59]	$\mathcal{O}(10^{-9})$ [60]
$BR(\tau \to e\gamma)$	1.1×10^{-7} [61]	$\mathcal{O}(10^{-8})$ [62]

TABLE VI: Present bounds and future experimental sensitivities of lepton flavour violating processes.

decay [55], the difference of Eq. (18) is reduced to $\sim 1\sigma$ [52] but it still requires a positive correction and disfavours strongly a sizable negative contribution.

A. Lepton Flavour Violation

As pointed out in [4], flavour models based on SU(3) give rise to potentially large rates of LFV processes, such that positive signals of LFV can be found in the currently running or near-future experiments, at least for SUSY masses within the reach of the LHC. The arising of large mixing among flavours relies on the features of the SU(3) model discussed in the previous sections: the presence of nonuniversal scalar masses already at the scale where the SUSY breaking terms appear, and the fact that the trilinear A_f matrices are in general not aligned with the corresponding Yukawa matrices. Let's start considering the case $A_0 = 0$, where the latter effect is strongly reduced so that, in terms of mass insertions, BR($l_i \to l_j\gamma$) mainly depends on $|(\delta^e_{LL})_{ij}|^2$ and $|(\delta^e_{RR})_{ij}|^2$. Looking at the structure of the slepton soft mass matrices in the three versions of the model (Table V), we see that RVV1 and RVV2 are expected to give similar predictions for BR($\mu \to e\gamma$) and BR($\tau \to \mu\gamma$), with possibly sizeable contributions coming from both the LL and the RR sector. In the case of RVV3, the prediction for BR($\tau \to \mu\gamma$) will be also similar to the previous two cases, while we expect BR($\mu \to e\gamma$) to be strongly enhanced. In fact, for RVV3, the LL mass insertion is larger by a factor $9\, y_t\, \bar{\varepsilon}/\varepsilon = \mathcal{O}(10)$ with respect to RVV1 and RVV2, and the BR($\mu \to e\gamma$) is consequently increased by two orders of magnitude.

To summarize, let's compare the expections for the different LFV processes. In the case $A_0 = 0$,

considering for simplicity only the contribution from δ^e_{LL}, we have:

$$\frac{BR(\tau \to e\,\gamma)}{BR(\mu \to e\,\gamma)} \;\approx\; \left(\frac{m_\tau}{m_\mu}\right)^5 \frac{\Gamma_\mu}{\Gamma_\tau} \frac{(\delta^e_{\rm LL})^2_{13}}{(\delta^e_{\rm LL})^2_{12}} \approx\; \mathcal{O}(1) \text{ (RVV1, RVV2, RVV3)} \tag{20}$$

$$\frac{BR(\tau \to \mu\,\gamma)}{BR(\mu \to e\,\gamma)} \;\approx\; \left(\frac{m_\tau}{m_\mu}\right)^5 \frac{\Gamma_\mu}{\Gamma_\tau} \frac{(\delta^e_{\rm LL})^2_{23}}{(\delta^e_{\rm LL})^2_{12}} \approx\; \mathcal{O}(10^3) \text{ (RVV1, RVV2)},\ \mathcal{O}(10) \text{ (RVV3)} \tag{21}$$

where Γ_μ (Γ_τ) is the μ (τ) full width. Given the present limits and future sensitivities of LFV processes shown in Tab. VI, we see that BR($\tau \to e\gamma$) is not able to constrain the parameter space better than BR($\mu \to e\gamma$) in none of the three models. On the other hand, we expect from Eq. (21) that the present constraints given by $\mu \to e\gamma$ and $\tau \to \mu\gamma$, that differ by three orders of magnitude, are comparable for RVV1 and RVV2, while $\mu \to e\gamma$ should give the strongest constraint in the case of RVV3.

In the case $A_0 \neq 0$, generally large δ^e_{LR} insertions arise as a consequence of the misalignment between A_f and the corresponding Yukawa matrix Y_f. In this case, the neutralino contribution to BR($\mu \to e\gamma$) gets strongly enhanced [4] and the present (or future) bound requires heavier SUSY masses to be fulfilled, specially in the region where the gaugino mass is much larger than the common sfermion mass. Nevertheless, we expect this effect to be visible only in the case of RVV1 and RVV2, while for RVV3 the very large $(\delta^e_{LL})_{12}$ should still give the dominant contribution.

Let us now consider the results of the numerical analysis for the LFV decays. After fixing the unknown $O(1)$ parameters to random values, we present in Fig. 1 the current bounds provided by $\mu \to e\gamma$ and $\tau \to \mu\gamma$ in the (m_0, $M_{1/2}$) plane, and also the final reach of the MEG experiment. In the first row, the $A_0 = 0$ case is displayed (for $\tan\beta = 10$). We see that, as expected, RVV1 and RVV2 give similar results both for BR($\mu \to e\gamma$) and BR($\tau \to \mu\gamma$). The regions of the parameter space excluded by the present bounds BR($\mu \to e\gamma$) $\lesssim 1.2{\cdot}10^{-11}$, BR($\tau \to \mu\gamma$) $\lesssim 1.6{\cdot}10^{-8}$ are comparable, as obtained by the naive estimate in Eq. (21), although $\tau \to \mu\gamma$ turns out to be more constraining for $m_0 > M_{1/2}$. The presently allowed region is approximately $(m_0,\ M_{1/2}) \gtrsim (700,\ 300)$ GeV. In the case of RVV3, $\mu \to e\gamma$ already gives a strong constraint, $(m_0,\ M_{1/2}) \gtrsim (1400,\ 800)$ GeV, which is much more stringent than the one provided by $\tau \to \mu\gamma$. Although the precise values may vary with different $O(1)$ parameters, these plots give an idea of the reach of these LFV experiments. As a consequence, for SUSY masses lying within the LHC reach, RVV3 results already rather disfavoured, while RVV1 and RVV2 are not strongly constrained. Considering the sensitivity expected at the MEG experiment for BR($\mu \to e\gamma$), $\mathcal{O}(10^{-13})$, we see that also RVV1 and RVV2 will be tested in most of the parameter space accessible to the LHC, while RVV3 will be completely probed well beyond the LHC reach. Moreover, in case of larger values of $\tan\beta$ (e.g. $\tan\beta = 30$),

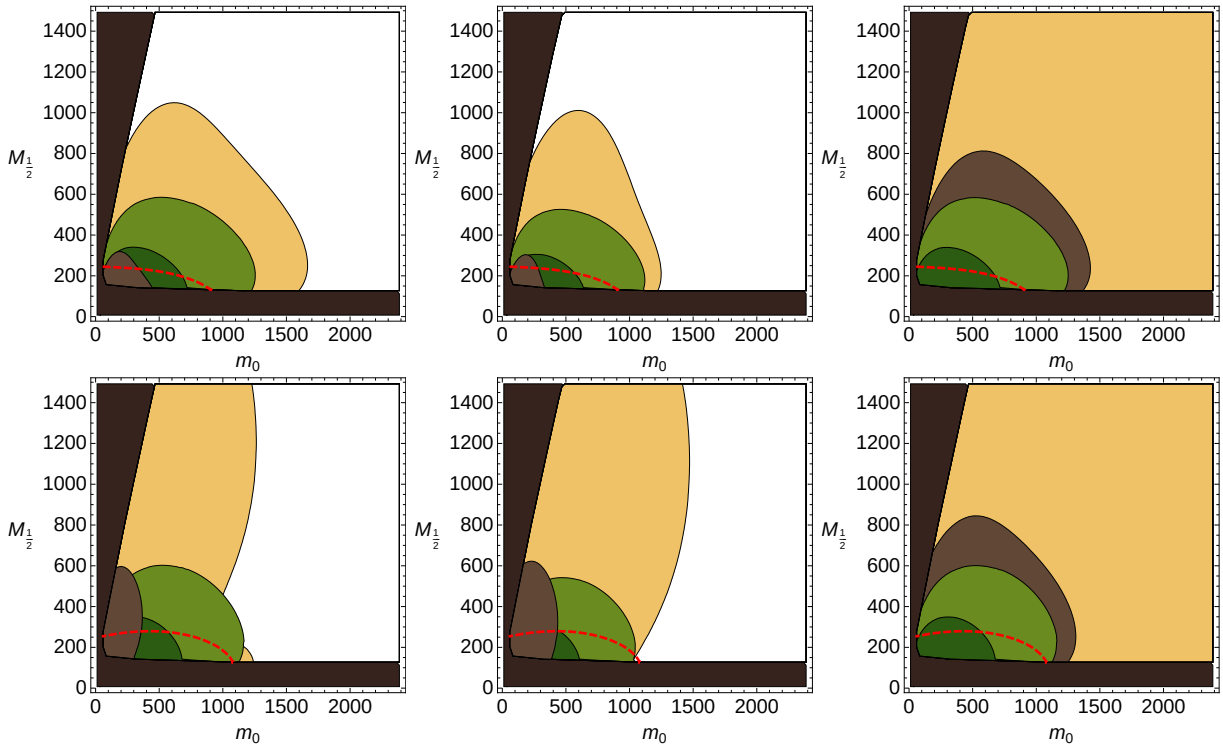

FIG. 1: Current LFV constraints in the m_0-$M_{1/2}$ plane, for RVV1 (left), RVV2 (center) and RVV3 (right) for $\tan\beta = 10$ and $A_0 = 0$ (first row), $A_0 = m_0$ (second row). The brown region corresponds to the present limit $\mathrm{BR}(\mu \to e\gamma) \lesssim 1.2 \cdot 10^{-11}$, the light brown region represents the sensitivity of the MEG experiment (10^{-13}). The present BaBar+Belle combined limit $\mathrm{BR}(\tau \to \mu\gamma) \lesssim 1.6 \cdot 10^{-8}$ is shown in dark green, and the light green region corresponds to the sensitivity of a Super Flavour Factory (10^{-9}). The dark brown region show areas excluded by having a charged LSP or by LEP, excepting the Higgs mass bound, which is shown in thick dashed red lines.

since $\mathrm{BR}(\mu \to e\gamma) \propto \tan^2\beta$, MEG will be able to test all the displayed parameter space also for RVV1 and RVV2 (cfr. [4], where a similar model has been studied).

In the second row of Fig. 1, the three versions of the model are displayed for the case $A_0 = m_0$, in order to show the potentially large flavour mixing induced by the A-terms. As expected, we see that, for RVV1 and RVV2, the $\mu \to e\gamma$ bound is increased with respect to the $A_0 = 0$ case, specially for $M_{1/2} \gtrsim m_0$, as a consequence of the large $(\delta^e_{LR})_{12}$ insertion contributing in diagrams with pure $\tilde{B}$ exchange. Also in this case, MEG has a very high capability of testing the parameter space. Indeed, for moderate slepton masses the neutralino contribution is so large that the models will be fully probed. Only in the case of rather heavy sleptons, the $\mathrm{BR}(\mu \to e\gamma)$ can be suppressed enough to escape the reach of MEG. In the case of RVV3, the contribution from LL insertion remains dominant and no substantial changes are observed with respect to the case of vanishing

trilinear terms.

As RVV3 is heavily constrained by LFV, in the following we shall exclude it from our analysis, and concentrate exclusively on RVV1 and RVV2.

B. Kaon physics

Supersymmetric contributions to K^0–$\overline{K}^0$ mixing are mainly determined by the mixing between the first two generations of down type squarks. In terms of mass insertions, a major hadronic constraint on $\Im m\{(\delta^d_{12})_{AB}\}$ comes from ϵ_K. The kaon mass difference, ΔM_K, does constrain $|(\delta^d_{12})_{AB}|$. However, this observable is less sensitive to small MIs since the long-distance effects are difficult to estimate.

On the experimental side, current data [37] shows that $|\epsilon_K^{\rm exp}| = (2.229 \pm 0.012) \times 10^{-3}$ and the phase of ϵ_K is $\phi_\epsilon = (43.51 \pm 0.05)^\circ$. On the theoretical side, many improvements are being made in the determination of input parameters needed to calculate the SM prediction of ϵ_K. We have good information on the CKM matrix elements thanks to the vast amount of data from B physics. Also available are new lattice estimates of the $\widehat{B}_K$ parameter which enters the $\Delta S = 2$ hadronic matrix element. However, these developments have lead to a puzzle in understanding the data. The authors of Refs. [63, 64] realized that within the SM, the theoretical prediction of ϵ_K might not be enough to account for the measured value if one accepts the unitarity triangle (UT) fit using B physics observables. One can summarize their result in the numerical form [63, 64],

$$
\begin{aligned}
|\epsilon_K^{\rm SM}| = 1.78 \cdot 10^{-3} \times & \left(\frac{\kappa_\epsilon}{0.92}\right) \left(\frac{\widehat{B}_K}{0.72}\right) \left(\frac{|V_{cb}|}{0.0412}\right)^2 \left(\frac{R_t}{0.914}\right) \times \\
& \left\{ 0.74 \times \left(\frac{|V_{cb}|}{0.0412}\right)^2 \left(\frac{R_t}{0.914}\right) \left(\frac{\sin 2\beta}{0.675}\right) \left(\frac{\eta_{tt}}{0.5765}\right) \left(\frac{S_0(x_t)}{2.30}\right) + \right. \\
& \left. \left(\frac{\sin\beta}{0.362}\right) \left[0.40 \times \left(\frac{\eta_{ct}}{0.47}\right) \left(\frac{S_0(x_c, x_t)}{0.00221}\right) - 0.14 \times \left(\frac{\eta_{cc}}{1.43}\right) \left(\frac{x_c}{0.000250}\right) \right] \right\}.
\end{aligned}
\tag{22}
$$

The definition of each symbol and its value can be found in the above references. Notice that the $\sin\beta$, $\sin 2\beta$ appearing in this equation refer to the UT angle β, not to the ratio of the Higgs vevs in SUSY. The denominator of each fraction is the central value of the input parameter appearing in the numerator, quoted in Ref. [63]. Major uncertainties are those in $\widehat{B}_K$, $|V_{cb}|^4$, R_t^2, which are 5%, 11%, 7%, respectively. One important refinement made in this expression, which had been overlooked in most of the literature, is the factor κ_ϵ that parameterizes suppression of the result due to $\phi_\epsilon \neq \pi/4$ and the imaginary part of the 0-isospin amplitude of $K \to \pi\pi$. In addition, latest

lattice values of $\widehat{B}_K$ are lower than previous determinations. Here we take $\widehat{B}_K = 0.720(13)(37)$ [65, 66] (see also [67]). These two facts cooperate to make $|\epsilon_K^{\rm SM}|$ insufficient for the central values, obtaining $|\epsilon_K^{\rm SM}| = 1.78 \times 10^{-3}$, which is smaller than the observed $|\epsilon_K|$ by 18%. This deficit should be compensated by some new source; since our model has extra sources of CP violation, we are lead to invoke these new sources to resolve the puzzle.

Before we proceed further, a clarification is in order regarding the ϵ_K puzzle. It stems from the tension among different observables used to determine the UT on the $(\overline{\rho}, \overline{\eta})$ plane. The regions preferred by ϵ_K, $S_{\psi K}$, and $\Delta M_{B_s}/\Delta M_{B_d}$ do not precisely overlap with one another (see Ref. [68] for example). As we said, if one accepts the regions determined by $S_{\psi K}$ and $\Delta M_{B_s}/\Delta M_{B_d}$, then ϵ_K should be modified. Conversely, one may also conceive a scenario where the ϵ_K region is in fact correct whereas one or more of the B sector observables have been contaminated by new physics effects. This could be an equally legitimate solution in a general case. However, it is not viable within our framework. The reason is that supersymmetric contributions to the above three observables are (up to $O(1)$ uncertainties) correlated and that the ϵ_K region is modified much more than the other two. We shall add more quantitative comments on this in the next subsection.

In order to evaluate the supersymmetric effects on ϵ_K, we should calculate $M_{K12}^{\rm SUSY} = \langle K|H_{\rm eff}^{\rm SUSY}|\overline{K}\rangle$. For this, we follow Ref. [69] which presents the $\Delta S = 2$ Wilson coefficients from the gluino-squark box graphs (which are the largest SUSY contributions in the presence of sizeable squark mass insertions) and the expressions for evolving those Wilson coefficients from the sparticle mass scale down to the hadronic scale. After that, the SUSY contribution to ϵ_K is given by the formula,

$$\epsilon_K^{\rm SUSY} = e^{i\phi_\epsilon} \sin\phi_\epsilon \, \frac{{\rm Im}(M_{K12}^{\rm SUSY})}{\Delta M_K}. \tag{23}$$

And then we can express the supersymmetric contribution to ϵ_K in terms of mass insertions as,

$$\begin{aligned}\frac{\epsilon_K^{\rm SUSY}}{\epsilon_K^{\rm exp}} = \sqrt{2}\sin\phi_\epsilon \, {\rm Im}\Bigg\{ & \frac{(\delta^d_{12})^2_{LL} + (\delta^d_{12})^2_{RR}}{0.0062^2}\left(\frac{\widehat{B}_K}{0.72}\right)\left[2.2\left(\frac{\tilde{f}_6(x)}{(-1/30)}\right) - 1.2\left(\frac{x f_6(x)}{1/20}\right)\right] - \\ & \frac{(\delta^d_{12})_{LL}(\delta^d_{12})_{RR}}{0.00013^2}\left(\frac{B_4(\mu)}{0.70}\right)\left[0.05\left(\frac{\tilde{f}_6(x)}{(-1/30)}\right) + 0.95\left(\frac{x f_6(x)}{1/20}\right)\right]\Bigg\}\left(\frac{500\ {\rm GeV}}{m_{\tilde{q}}}\right)^2,\end{aligned} \tag{24}$$

where $x \equiv m_{\tilde{g}}^2/m_{\tilde{q}}^2$ and functions $f_6(x)$ and $\tilde{f}_6(x)$ can be found in Ref. [69]. We have omitted the term proportional to $B_5(\mu)$ which happens to contribute only $O(1\%)$.

In the numerical analysis, we set $\widehat{B}_K = 0.72$ [65, 66] and use the central values of $B_{2,\ldots,5}(\mu)$ from Ref. [70].

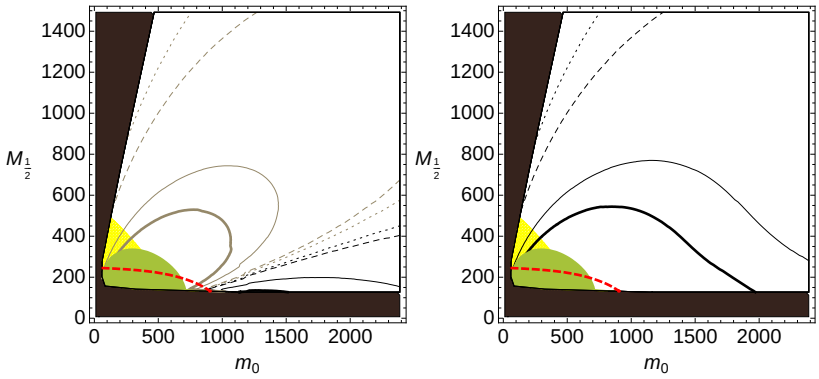

FIG. 2: Contours of $|\epsilon_K^{\rm SUSY}|$ for RVV1, in the m_0-$M_{1/2}$ plane for $\tan\beta = 10$ and $A_0 = 0$. The lines are (from thicker to dotted) $|\epsilon_K^{\rm SUSY}| = 10^{-3}, 5\times10^{-4}, 10^{-4}, 5\times10^{-5}$, respectively. We show predictions for positive (left) and negative (right) O(1)'s for $M^2_{\tilde{d}^c_R}$, giving in some cases ϵ_K^{SUSY} with the wrong phase, which are shown in grey. Current LFV bounds are also shown in green, and the $(g-2)_\mu$ favoured region is shown hatched in yellow. The dark brown region show areas excluded by having a charged LSP or by LEP, excepting the Higgs mass bound, which is shown in thick dashed red lines.

In our flavour models, RVV1 and RVV2, we have $|(\delta^d_{12})_{RR}| \sim \bar{\varepsilon}^3 \simeq 0.003$ and $|(\delta^d_{12})_{LL}| \sim \varepsilon^2\bar{\varepsilon} \simeq 0.0004$ with different phases in the two models, $\omega_{us} \sim O(\bar{\varepsilon})$ and $\omega'_{us} \sim O(1)$ respectively, as can be seen from Eq. (9) and the paragraph following Eq. (12). Therefore, we can expect that the supersymmetric contribution to ϵ_K can easily be comparable to $\epsilon_K^{\rm exp}$, in particular from the contribution in the second term in Eq. (24). The additional contribution might well be just what we need to fill the gap between $\epsilon_K^{\rm SM}$ and $\epsilon_K^{\rm exp}$, which could amount to 18% or more. In Figs. 2, we present contours of ϵ_K on the $(m_0, M_{1/2})$ plane for RVV1. The left and the right figures are for positive and negative O(1)'s for $M^2_{\tilde{d}^c_R}$, respectively.

The phase of $\epsilon_K^{\rm SUSY}$ can be either 43.51° or -136.49° which are respectively marked in black and gray in Figs. 2. Note that the phase of $\epsilon_K^{\rm SM}$ is 43.51° and that $\epsilon_K^{\rm SUSY}$ and $\epsilon_K^{\rm SM}$ should interfere constructively to fit the experimental value. Therefore, gray contours worsen compatibility between the theoretical and the experimental values of ϵ_K by increasing their discrepancy. The phase of $\epsilon_K^{\rm SUSY}$ is determined by the sign of Eq. (24). It is often dominated by the term proportional to $\mathrm{Im}[(\delta^d_{12})_{LL}(\delta^d_{12})_{RR}]$. In this case, the phase of $\epsilon_K^{\rm SUSY}$ can be shifted by π if one multiplies either $(\delta^d_{12})_{LL}$ or $(\delta^d_{12})_{RR}$ by -1 (of course, the modulus $|\epsilon_K^{\rm SUSY}|$ does not remain exactly the same due to the first term). For example, we can flip the sign of the RR insertion by changing the signs of the O(1) coefficients in $M^2_{\tilde{d}^c_R}$. This is the reason why the region with gray contours on the left plot turns to black on the right.

For RVV2, the phase in $(\delta^d_{12})_{LL}$ is much larger than that in RVV1, as we can see in Eq. (12). This

makes the SUSY $(\delta^d_{12})_{RR}(\delta^d_{12})_{LL}$ contribution to $\epsilon_K^{\rm SUSY}$ dominant in all of the evaluated parameter space, so only one of the two possible phases for $(\delta^d_{12})_{RR}$ solves the ϵ_K tension. Furthermore, each of the contours in Figure 2 would be scaled roughly by a factor $1/\bar{\varepsilon} \simeq 6$.

The requirement that the supersymmetric contribution solves the ϵ_K puzzle would define a strip in this plane which will be shown in all of the following plots, for both RVV1 and RVV2. One virtue of such a strip is that the parameter space therein will lead to a definite correlation between observables which are not apparently related to each other. We will elaborate on this in Sec. IV.

Another important quantity in kaonic CP violation is ϵ'/ϵ. It is specially sensitive to chirality-flipping mass insertions, $(\delta^d_{12})_{LR}$ and $(\delta^d_{12})_{RL}$ [30]. Using the formulae in Ref. [71], one can write the supersymmetric contribution to ϵ'/ϵ in the form,

$$\frac{(\epsilon')^{\rm SUSY}}{(\epsilon')^{\rm exp}} = {\rm Im}\left[\frac{(\delta^d_{12})_{LR} - (\delta^d_{12})_{RL}}{1.6\times 10^{-5}} \times B_G\right]\left(\frac{500\ {\rm GeV}}{m_{\tilde{q}}}\right), \tag{25}$$

which has been derived for $m^2_{\tilde{g}}/m^2_{\tilde{q}} = 1$. The $O(1)$ constant B_G parameterizes the uncertainty in the hadronic matrix element of the chromomagnetic operator. We have suppressed other factors that can change by $O(1)$ for $m^2_{\tilde{g}}/m^2_{\tilde{q}} \neq 1$, since the following argument depends only on the order of magnitude of ϵ'/ϵ.

In this model, there can be flavor-violating A-terms arising from mismatch of the $O(1)$ coefficients between the Yukawas and the A-terms. To estimate their possible effects, we define $A_0 \equiv a_0\ m_0$, with A_0 being the overall dimensionful coefficient of the A-terms. Using Eq. (14b) and (9b), one can get rough relationships among different 1–2 mass insertions,

$$(\delta^d_{12})_{LR} \sim (\delta^d_{12})_{RL} \sim a_0\ \frac{m_b}{m_0} \times (\delta^d_{12})_{RR} \sim a_0\ \frac{\bar{\varepsilon}^2}{\varepsilon^2}\frac{m_b}{m_0} \times (\delta^d_{12})_{LL}, \tag{26}$$

where m_b is the b-quark mass at the GUT scale. If we require that the size of the second term in Eq. (24) does not exceed unity, we find that the extra contribution to ϵ'/ϵ has an upper limit like

$$\left|\frac{(\epsilon')^{\rm SUSY}}{(\epsilon')^{\rm exp}}\right| \lesssim 8.1 \times \frac{\bar{\varepsilon}}{\varepsilon}\ a_0\ \frac{m_b}{m_0}, \tag{27}$$

for purely imaginary $(\delta^d_{12})_{LR}$ or $(\delta^d_{12})_{RL}$. In this case, the supersymmetric fraction within ϵ'/ϵ should be lower than 40% for a reasonably high $m_0 \gtrsim 100$ GeV. In fact, the phases of these flavor and chirality changing insertions are $\pm\omega_{us}$ which are smaller than maximal, as can be seen from Eq. (A5). Thus their effects on ϵ'/ϵ are smaller than the above estimate. We have numerically checked that the gluino-squark loop contribution to ϵ'/ϵ is less than 15% on the strip compatible with ϵ_K. Given the large theoretical uncertainty in ϵ'/ϵ, this amount of contamination by new physics should be hard to disentangle.

Another process that could, in principle, be interesting is the decay $K_L \to \pi^0 \nu\bar{\nu}$ [72, 73, 74]. The dominant contribution to this process requires the presence of CP violating phases, and therefore we could expect to have a contribution in our model. As, due to gauge invariance, this decay depends on $SU(2)_L$-breaking, it requires the presence of two Higgs vevs, either within δ_{LR} insertions in the squark sector, or within gaugino-higgsino mixing on the neutralino and chargino sectors. At moderate $\tan\beta$, this disfavours the gluino contribution, since δ^d_{LR} insertions are, at most, proportional to the bottom mass. Of much more interest is the chargino contribution, as the $(\delta^u_{33})_{LR}$ insertions are proportional to the top mass. Nonetheless, the required $(\delta^u_{23})_{LL}$ and $(\delta^u_{31})_{RR}$ insertions depend on powers of ε, instead of $\bar{\varepsilon}$, which constrains greatly any chargino contribution dependent on the $SU(3)$ structure. The chargino contribution will then be dominated by the flavour-changing of the CKM matrix, and thus cannot present any larger deviations than those predicted by MFV models.

C. B physics

Let us now discuss new physics effects on B_s mixing. For this, it is convenient to adopt the following parametrization [75]:

$$C_{B_s} e^{2i\phi_{B_s}} = \frac{M^{\rm SM}_{s12} + M^{\rm SUSY}_{s12}}{M^{\rm SM}_{s12}}. \tag{28}$$

The B_s–$\overline{B_s}$ transition amplitude is divided into two parts, one arising from the SM loops and the other from the gluino-squark which are the largest SUSY contributions in our model:

$$M^{\rm SM}_{s12} = \langle B_s | H^{\rm SM}_{\rm eff} | \overline{B_s} \rangle, \quad M^{\rm SUSY}_{s12} = \langle B_s | H^{\rm SUSY}_{\rm eff} | \overline{B_s} \rangle. \tag{29}$$

Here, we focus on the phase ϕ_{B_s} rather than on C_{B_s}, since the hadronic uncertainty in the latter is larger than the extra contributions that can be expected in this model.

The current data of B_s mixing phase is showing an interesting deviation from the SM prediction. A constrained fit, performed by HFAG, results in [76]:

$$\phi_{B_s} = -0.36^{+0.19}_{-0.17} \ \text{ or } \ -1.17^{+0.17}_{-0.19}. \tag{30}$$

Recall that non-vanishing ϕ_{B_s} is an indication of new physics. The above fit is away from the SM at the level of 2.4 σ, and the 90% CL range is:

$$\phi_{B_s} \in [-0.61, -0.045] \cup [-1.48, -0.92]. \tag{31}$$

It would be amusing to see whether or not our model could push this phase close to its best fit value.

In order to estimate maximal size of ϕ_{B_s} within this model, one should consider the ratio of $M_{s12}^{\rm SUSY}$ to $M_{s12}^{\rm SM}$ appearing in Eq. (28). We follow Ref. [77] to express the supersymmetric amplitude in terms of mass insertions. The SM amplitude is available in Ref. [78] for instance. For this, we use V_{ts} and V_{tb} from the full fit by the UTfit collaboration [79]. The result can be written in the form,

$$\frac{M_{s12}^{\rm SUSY}}{M_{s12}^{\rm SM}} = e^{2i\beta_s}\left[\frac{(\delta^d_{23})^2_{LL}+(\delta^d_{23})^2_{RR}}{0.71^2} - \frac{(\delta^d_{23})_{LL}(\delta^d_{23})_{RR}}{0.062^2}\right]\left(\frac{500\ {\rm GeV}}{m_{\tilde q}}\right)^2, \tag{32}$$

where we have taken the ratio $m^2_{\tilde g}/m^2_{\tilde q}=1$, since we need only the order of magnitude of the above ratio.

The first factor on the right hand side comes from the phase of $M_{s12}^{\rm SM}$ which is equal to $-2\beta_s = -0.04$. Now, from Eq. (28), it is clear that a change in the B_s phase, ${\rm Arg}\left[M_{s12}^{\rm SM}+M_{s12}^{\rm SUSY}\right]$, would require $|M_{s12}^{\rm SUSY}/M_{s12}^{\rm SM}| \simeq O(1)$ and a sizeable phase $\phi_{B_s}^{\rm SUSY} \equiv {\rm Arg}\left[M_{s12}^{\rm SUSY}/M_{s12}^{\rm SM}\right]$. This fact has strong implications on the size and phases of the mass insertions appearing above. These mass insertions differ in different variations of our model, for instance, that largest MIs can be expected in RVV2. In this model, the mass insertions are $(\delta^d_{23})_{LL} \sim \varepsilon \simeq 0.05$ and $(\delta^d_{23})_{RR} \sim \bar\varepsilon y_b^{0.5} \simeq 0.015\sqrt{\sec\beta}$, as one can find in Eqs. (11). The size of the RR insertion depends on $\tan\beta$ and taking $\tan\beta = 10$ for example, we have $(\delta^d_{23})_{RR} \sim 0.05$. These values appear to be large enough to make a significant change in the B_s phase from the second term of Eq. (32). Moreover, the product of these two insertions can have an $O(1)$ phase. Notice that this is possible only in RVV2 where the leading terms in these mass insertions have phases. In Fig. 3, we show the different contours of ϕ_{B_s}.

Indeed, in model RVV2 there is a region on the $(m_0, M_{1/2})$ plane where it is possible to shift ϕ_{B_s} into the interval in Eq. (31), at relatively high m_0 and low $M_{1/2}$ [80, 81]. However, these regions of large SUSY contributions to ϕ_{B_s} are excluded by LFV and tend to have a too large contribution to ϵ_K as well. If we confine ourselves on a strip allowed by ϵ_K, the maximal value of ϕ_{B_s} is around 10^{-4}. From the plots we can see that, in the case of RVV1, we are again in the same situation and for the strips allowed by ϵ_K we always have $\phi_{B_s} \lesssim 10^{-4}$. Although these values could in principle vary due to the unknown $O(1)$ coefficients in the soft terms, we can not expect variations in the order of magnitude. Thus, for low and moderate $\tan\beta$, our models are not able to provide a solution to the ϕ_{B_s} anomaly, and, in this situation, we would expect this anomaly to disappear with the inclusion of further data[5]. If this is the case, our predicted deviation should

[5] The authors of [83] claim to be able to satisfy the Φ_{B_s} anomaly and the ϵ_K tension in RVV2. We believe these

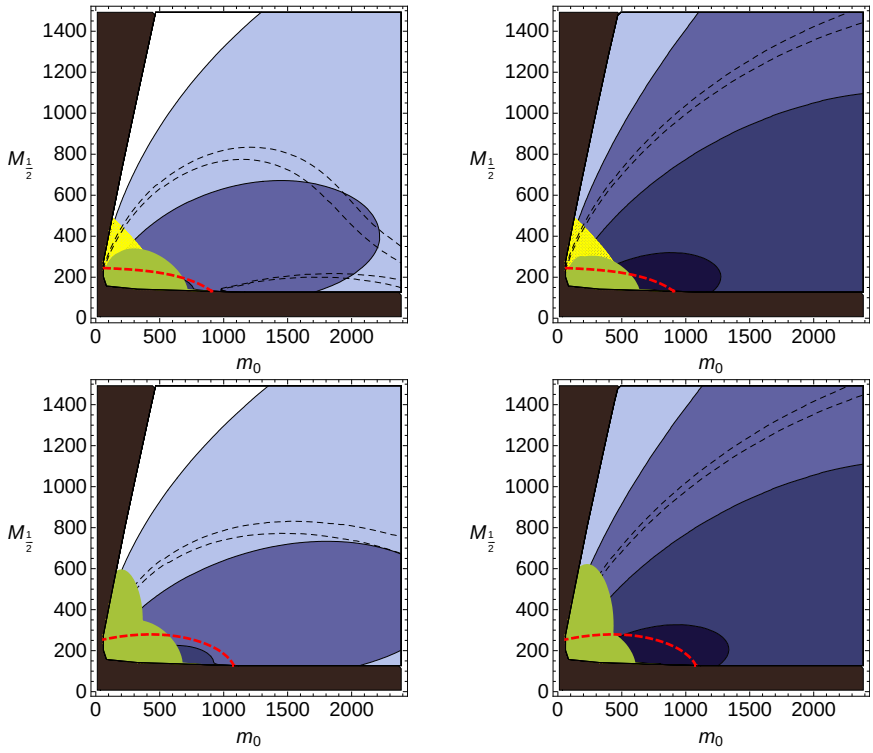

FIG. 3: Contours of ϕ_{B_s} for RVV1 (left) and RVV2 (right) in the m_0-$M_{1/2}$ plane for $\tan\beta = 10$ and $A_0 = 0$ (top) and $A_0 = m_0$ (bottom). The color of an area indicates the size of ϕ_{B_s}, which decreases as one moves in the order of dark to light blue. Each line between two adjacent areas is one of $\phi_{B_s} = 10^{-2}, 10^{-3}, 10^{-4}, 10^{-5}$ (the contour corresponding to $\phi_{B_s} = -0.045$, which would solve the discrepancy, is within the LFV excluded region in RVV2, and forbidden by direct bounds in RVV1). As in previous plots, green areas correspond to the currect LFV constraints and yellow area to the $(g-2)_\mu$ favoured region. The area between the dashed black lines solve the ϵ_K tension, and the dark brown region show areas excluded by having a charged LSP or by LEP, excepting the Higgs mass bound, which is shown in thick dashed red lines.

also be hard to observe at LHCb since it is much smaller than the precision of ϕ_{B_s} attainable after 5 years of run (10 fb^{-1}), which is estimated to be 5×10^{-3} [82].

Similarly, we can repeat a parallel discussion on B_d mixing with the following parameterization,

$$C_{B_d} e^{2i\Delta\beta} = \frac{M_{d12}^{\rm SM} + M_{d12}^{\rm SUSY}}{M_{d12}^{\rm SM}}, \tag{33}$$

where each M_{d12} is the same as that in Eqs. (29) with the replacement $s \to d$. The supersymmetric to SM contribution ratio is given by

$$\frac{M_{d12}^{\rm SUSY}}{M_{d12}^{\rm SM}} = e^{-2i\beta} \left[\frac{(\delta^d_{13})^2_{LL} + (\delta^d_{13})^2_{RR}}{0.15^2} - \frac{(\delta^d_{13})_{LL}(\delta^d_{13})_{RR}}{0.013^2} \right] \left(\frac{500 \text{ GeV}}{m_{\tilde{q}}} \right)^2 . \tag{34}$$

points correspond to a large value of $\tan\beta \gtrsim 50$. Moreover, we checked that the parameters can conspire to give Φ_{B_s} of $O(0.1)$, even for moderate values of $\tan\beta$.

One can get this result in the same way as for Eq. (32).

In this case, each denominator in the square brackets is smaller than the corresponding one in Eq. (32) by the factor $|V_{td}/V_{ts}|^2$. Again, we use the CKM matrix elements from the full fit by the UTfit collaboration [79]. In RVV2, we have $(\delta^d_{13})_{LL}(\delta^d_{13})_{RR} \sim \varepsilon\bar{\varepsilon}^3\, y_b^{0.5} \sim 1.7\times 10^{-5}\sqrt{\sec\beta}$, and thus we could expect a sizeable effect on $S_{\psi K}$ if it were not for ϵ_K. However, $\Delta S_{\psi K}$ is suppressed below 1×10^{-3} on an ϵ_K strip in the same way as ϕ_{B_s} is. This is below the sensitivity of a super B factory to $S_{\psi K}$ whose estimate is around 5×10^{-3} [60]. In RVV1, the new physics effect is even smaller, since the phases are suppressed. In the end, B_d–$\overline{B_d}$ mixing is not very much affected in both models. This fact, a posteriori, justifies the way we determine the $O(1)$ coefficients in Yukawas: we tune the coefficients so that they reproduce the CKM matrix elements which were obtained under the assumption of no new physics.

Let us come back to the alternative solutions of the ϵ_K puzzle that we mentioned in the previous subsection. If one is to blame the UT fit tension on $S_{\psi K}$, one would need a change due to new physics of the amount $\Delta S_{\psi K} \sim 0.07$ [68]. However, this is two orders of magnitude bigger than what can be maximally expected in our models when $\epsilon_K^{\rm SUSY}$ is at the level of 18%, as we have seen above. In an alternative solution, $\epsilon_K^{\rm SUSY}$ should be more suppressed, which in turn suppresses $\Delta S_{\psi K}$ as well, thereby making it far less sufficient. The other possibility of invoking modification of $\Delta M_{B_s}/\Delta M_{B_d}$ does not work for a similar reason. The authors of Ref. [83] need a new physics contribution to this ratio at the level of -22% in order to get an exact agreement. In our models however, the fractional change is about 0.5% at most, which is too small compared to what is needed.

Finally, we can look to the expected values in our model for the decays $b\to s\mu^+\mu^-$ and $b\to s\nu\bar{\nu}$ that are similar to $K_L\to\pi^0\nu\bar{\nu}$ in the B sector. We find that the values of the branching ratios for these processes, in both RVV1 and RVV2 models for $A_0=0$ and $A_0=m_0$, do not produce deviations from the SM values larger than the per cent level, in spite of the presence of sizeable flavour changing mass insertions. Therefore, these proceses are not interesting tests of new physics in our scenario. This is consistent with the work in [84], where it was found that the deviation from the SM prediction is small once the constraints from $b\to s\gamma$ and $B_s\to\mu^+\mu^-$ are taken into account.

D. Electric Dipole Moments

The EDMs of fermions, such as the electron and the neutron, provide very stringent constraints on CP-violation in new physics. In the SM, the electron EDM from the Kobayashi-Maskawa phase is predicted to be $\lesssim O(10^{-40})$ e cm^{-1} [85]. The SM expectation for the neutron EDM is of $O(10^{-31})$ e cm^{-1} [86], assuming a vanishing θ_{QCD}. We can see that EDMs are highly suppressed in the SM, and thus they are excellent observables where to look for new physics.

The electron EDM was studied in [4] within the context of RVV1. In these models CP is spontaneously broken in the flavour sector. Therefore, the phases in the μ parameter and diagonal A_f terms are very suppressed and can be neglected. In such a case, the imaginary parts required for EDMs only appear from flavour-changing mass insertions [89]. For the electron EDM, only neutralino-mediated diagrams contribute. The most important contribution to d_e, when $A_0 = 0$, comes from a bino-mediated diagram proportional to $\Im m\,[(\delta^e_{13})_{LL}(\delta^e_{33})_{LR}(\delta^e_{31})_{RR}]$, which is enhanced by $m_\tau \tan\beta$.

In this work, we have updated our analysis on the electron EDM, taking into account the constraints on the β_3 and χ phases imposed by the fit of CKM matrix and the $O(1)$ coefficients in Y_e (see the Appendix for details). The results are shown for the RVV1 and RVV2 models in Figure 4. An inspection of the slepton soft mass matrices indicates that, for RVV1, the leading phases in the product $(\delta^e_{13})_{LL}(\delta^e_{33})_{LR}(\delta^e_{31})_{RR}$ cancel and only subleading phases contribute, while RVV2 has non-vanishing leading phases. We then have the following predictions:

$$(d_e)_{\rm RVV1} \;\sim\; \bar{\varepsilon}^6\, y_b\, y_t \sin(2(\chi - \beta_3)) \tag{35}$$

$$(d_e)_{\rm RVV2} \;\sim\; \varepsilon\bar{\varepsilon}^3 \frac{(y_b\, y_t)}{9}^{0.5} \sin(\chi - 2\beta_2') \tag{36}$$

In Figure 4 we present the sensitivity of current [90] and future [91, 92] d_e experiments, for the two models. In this Figure, current constraints do not impose any restrictions on the parameter space of either RVV1 or RVV2. Nevertheless, electron EDM predictions are large enough to be probed at future EDM experiments. For relatively light SUSY masses we obtain $d_e \sim 10^{-29}$ e cm^{-1} and $d_e \sim 10^{-28}$ e cm^{-1}, for RVV1 and RVV2, respectively. The latter predicts a value of d_e about one order of magnitude larger than the former for any particular value of m_0 and $M_{1/2}$ due to the larger ε suppresion as seen in Eq. (35). This means that by reaching $d_e \sim 10^{-29}$ e cm^{-1} one could probe a much larger part of the evaluated parameter space, with $m_0 \lesssim 1500$ GeV, $M_{1/2} \lesssim 2000$ GeV. In particular, for RVV2, observation of SUSY at the LHC and solving the ϵ_K tension would force d_e to be larger than 10^{-29} e cm^{-1}. However, we have to take into account that these values

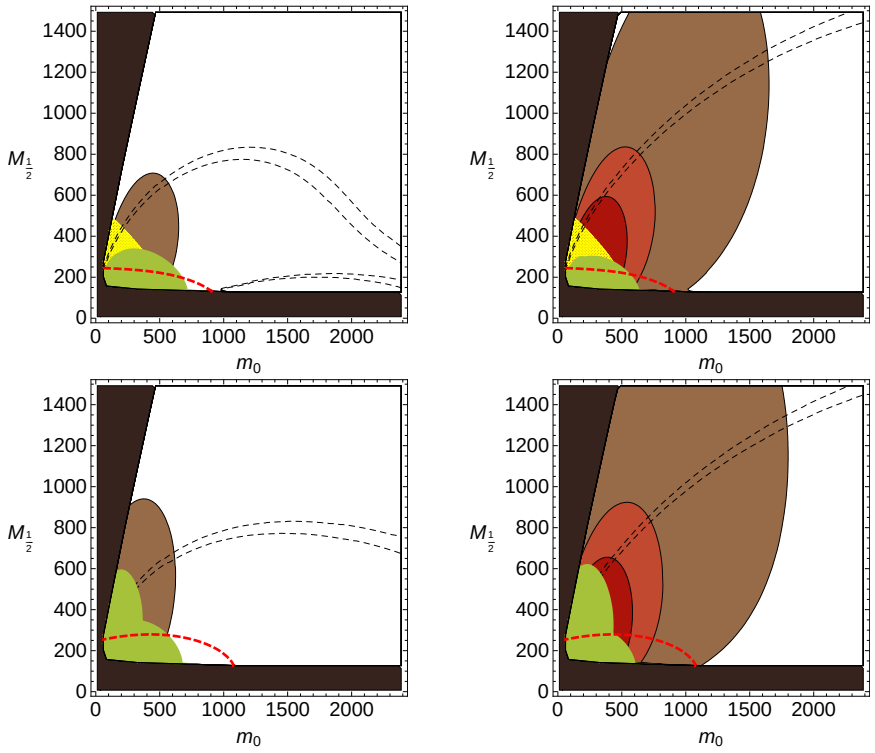

FIG. 4: Contours of $|d_e| = 1 \times 10^{-28}$ e cm (dark red), $|d_e| = 5 \times 10^{-29}$ e cm (light red) and $|d_e| = 1 \times 10^{-29}$ e cm (brown) in the m_0-$M_{1/2}$ plane for $\tan\beta = 10$ and $A_0 = 0$ (top), $A_0 = m_0$ (bottom). We show predictions for RVV1 (left) and RVV2 (right). Current LFV bounds are also shown in green, and the $(g-2)_\mu$ favoured region is shown hatched in yellow. The area between the dashed black lines solve the ϵ_K tension, and the dark brown region show areas excluded by having a charged LSP or by LEP, excepting the Higgs mass bound, which is shown in thick dashed red lines.

will vary by factors $O(1)$ because of the unknown $O(1)$ coefficients to the different MIs.

We now turn to the neutron EDM, d_n. In this observable we have an additional difficulty, since its calculation as a function of partonic EDMs is not straightforward. Here we use two different approaches to this problem, the quark-parton [93] and chiral quark [94] models for d_n.

In the quark-parton model [93], d_n is expressed in terms of the up, down and strange quark EDMs, weighed by the fractional contribution Δ_n^q of each quark to the spin of the neutron:

$$d_n^{QP} = \eta^E \left(\Delta_n^u d_u + \Delta_n^d d_d + \Delta_n^s d_s \right) \tag{37}$$

where $\eta^E = 0.61$ is a QCD correction factor [95] and typical values for Δ_n^q are $\Delta_n^u = -0.508$, $\Delta_n^d = 0.746$ and $\Delta_n^s = -0.226$.

The chiral quark model [94] uses naive dimensional analysis to establish:

$$d_n^{CQ} = \frac{4}{3}\tilde{d}_d - \frac{1}{3}\tilde{d}_u \tag{38}$$

where $\tilde{d}_q$ is the Wilson coefficient of the EDM operator at the hadronic scale. $\tilde{d}_q$ differs from d_q, which is calculated at the SUSY-breaking scale, since the former receives contributions from the quark chromo-electric dipole moment, d_q^c, and Weinberg's gluonic dimension-six operator, d_G [96, 97]:

$$\tilde{d}_q = \eta^E d_q + \eta^C \frac{e}{4\pi} d_q^c + \eta^G \frac{e\Lambda}{4\pi} d_G \tag{39}$$

These contributions arise from the operator mixing ocurring in the running from the electroweak scale to the hadronic scale. In our estimates, we take the QCD correction factor $\eta^C = 3.4$ [96], and ignore d_G, since it can be at most of the same order of d_q and d_q^c and we do not expect it to make big changes in our order of magnitude prediction.

The (C)EDM of each quark has contributions from diagrams with gluinos $d_q^{\tilde{g}}$, charginos $d_q^{\tilde{\chi}^\pm}$ and neutralinos $d_q^{\tilde{\chi}^0}$. For gluinos and neutralinos, we can use the same arguments as in [4] to establish that the main part of each contribution will come from $\Im m\left[(\delta^q_{i3})_{LL}(\delta^q_{33})_{LR}(\delta^q_{3i})_{RR}\right]$ insertions. Chargino contributions come from both pure higgsino and wino-higgsino diagrams. The mixed wino-higgsino diagrams require no LR flip on the squark line. Contrary to the case with leptons, it is possible to have only one δ_{LL} insertion, provided that the CKM matrix element V_{ij} is not flavour-diagonal. For instance, the largest contributions to the down quark (C)EDM are proportional to $\Im m\left[V_{qd}(\delta^u_{qq'})_{LL}V^*_{q'd}Y_d\right]$. Pure higgsino diagrams require a LR flip on the squark line. One would expect this contribution to be strongly suppressed, as there are two Yukawa couplings on the vertices. However, it is possible to exchange one of the small Yukawa couplings for a y_t or y_b coupling through a CKM off-diagonal term. As an example, the main contribution to the pure higgsino diagram for $d_d^{\tilde{\chi}^\pm}$ is proportional to $\Im m\left[V_{td}\, y_t (\delta^u_{33})_{RL}(\delta^u_{32})_{LL}V^*_{cd}\, y_d\right]$. Given the flavour structure of the $SU(3)$ models, we find that the pure higgsino part shall be larger than the mixed wino-higgsino part, and will dominate the chargino contribution to $d_q^{(c)}$.

It was noticed in [87] that, in addition to these contributions, it is important to consider beyond-leading-order (BLO) effects. These effects can be represented as new complex effective couplings [88], and although these are noticeable mainly for large values of $\tan\beta$, for EDMs they can also give significant contributions for moderate and small values of $\tan\beta$. In particular, diagrams with no imaginary part at LO can become complex from these effective vertices [89].

The most important BLO effect for the down quark EDM, for the values of $\tan\beta$ we are using, has been found to be the $H^\pm$ contribution [89]. Although the BLO corrections also affect the gluino, neutralino, chargino and neutral Higgs loops, these contributions represent only small corrections and do not play an important role. Therefore, the only BLO effects we shall include will come

from the $H^\pm$ diagrams.

The BLO effects can also enhance the coupling between the $H^\pm$ and fermions. At LO, the *flavour* suppression for an $H^\pm$-mediated dipole operator would be of order $\left[y_d V_{td}^* y_t^2 V_{td}\right] \sim \bar{\varepsilon}^{10}$. The BLO vertex allows us to change the $y_d V_{td}^*$ term for a $(\delta^d_{13})_{RR} y_b V_{tb}^*$ term, having then a total flavour suppression of order $\left[(\delta^d_{13})_{RR} y_b V_{tb}^* y_t^2 V_{td}\right] \sim \bar{\varepsilon}^6$. This is comparable to the gluino flavour suppression at LO.

Even though the flavour suppression of the BLO $H^\pm$ contribution is of an order of magnitude comparable to the LO gluino contribution, the question that needs to be answered is how much does the extra loop suppression affect the $H^\pm$ diagram. This calculation has been done in [87], for equal SUSY masses and moderate $\tan\beta$, giving:

$$\frac{d_d^{H^\pm}}{d_d^{\tilde{g}}} \sim \left[\frac{\alpha_2}{9\pi}\frac{m_t^2}{m_W^2}\right]\left[\frac{m_{\tilde{q}}^2}{m_{H^\pm}^2}\right]\left[\frac{\Im m\left[V_{td}^*(\delta^d_{31})_{RR}\right]}{\Im m\left[(\delta^d_{13})_{LL}(\delta^d_{31})_{RR}\right]}\right] f\left(\frac{m_t^2}{m_{H^\pm}^2}\right) \tag{40}$$

The first square bracket gives a factor of $O(0.1)$, which is compensated by the loop function $f(m_t^2/m_{H^\pm}^2)$, which is of $O(10)$. The third bracket is the flavour suppression ratio, which is of $O(1)$. Thus, in this approximation, the importance of the $H^\pm$ contribution with respect to the gluino contribution depends mainly on the ratio between the squark and charged Higgs masses squared. Higgs bosons decouple differently from squarks and gauginos, as gluino and squark masses increase faster than the $H^\pm$ mass for increasing m_0 and $M_{1/2}$, the BLO contributions shall be more important for large values of these parameters.

We shall include the $H^\pm$ contribution through the mass-insertion formulae of [89]. Such an approach contemplates three types of contributions. Two of them involve the CKM matrix, and are of the type $\Im m\left[V_{3i}^*(\delta^d_{3i})_{LL}\right]$ and $\Im m\left[V_{3i}^*(\delta^d_{3i})_{RR}\right]$. The third one is similar to that for the gluino loops: $\Im m\left[(\delta^d_{i3})_{LL}(\delta^d_{3i})_{RR}\right]$. The latter two shall be the ones that will allow us to avoid the y_d suppression. The second term shall be particularly important for RVV1, where the gluino contribution has a cancellation between $(\delta^d_{i3})_{LL}$ and $(\delta^d_{3i})_{RR}$.

The $SU(3)$ predictions for $\tan\beta = 10$ and $A_0 = 0$ are shown in Figure 5 for the quark-parton and chiral quark EDMs, respectively. The EDMs receive a significant contribution from the $H^\pm$ loop in d_d. Furthermore, d_n^{QP} is also dominated by gluino and $H^\pm$ contributions to d_s, while d_n^{CQ} is influenced by their contribution to d_d^c, for both RVV1 and RVV2. The other contributions are smaller by at least half an order of magnitude. We can see that current bounds are always weaker than the LEP and LFV constraints and do not appear in the Figure.

The observation of d_n in the near-future experiments is not always compatible with the solution of the ϵ_K tension. In RVV1, which is mostly dominated by the $H^\pm$ loops, a d_n of order 10^{-29}

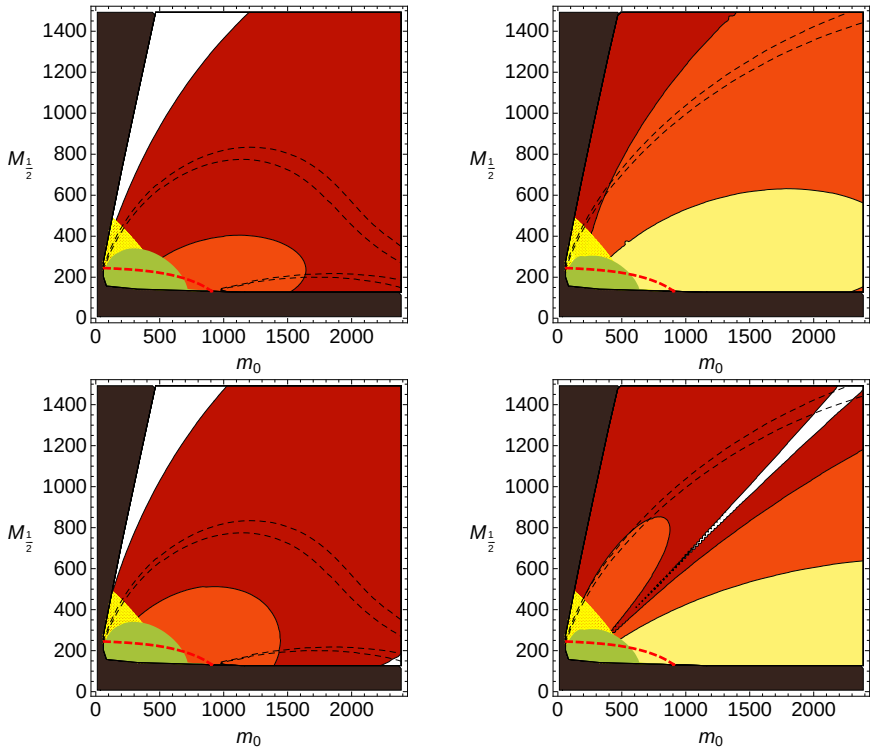

FIG. 5: Quark-parton (top) and chiral quark (bottom) contours of $|d_n| = 1 \times 10^{-27}$ e cm (yellow) $|d_n| = 1 \times 10^{-28}$ e cm (orange) and $|d_n| = 1 \times 10^{-29}$ e cm (red) in the m_0-$M_{1/2}$ plane for $\tan\beta = 10$ and $A_0 = 0$. We show predictions for RVV1 (left) and RVV2 (right). Current LFV bounds are also shown in green, and the $(g-2)_\mu$ favoured region is shown hatched in yellow.

e cm^{-1} is usually favoured, one order of magnitude under the reach of the next experiments [98]. In RVV2, both gluino and $H^\pm$ effects are comparable, the former dominating in the chiral-quark and the latter in the quark-parton models. In both situations it is possible to obtain an observable d_n which is compatible with the solution of the ϵ_K tension.

It is interesting to see that in some regions of the parameter space we have a cancellation. A careful analysis proves that close to these regions the phase of the $(\delta^d_{13})_{LL}$ term vanishes, and that can only be due to a cancellation between the initial term at M_{GUT} and the contributions from the running. This causes a change of sign in the gluino contribution, such that it can interfere destructively with the $H^\pm$ part. We can avoid the cancellations by changing the sign of the $O(1)$ terms at M_{GUT}, in which case the interference is constructive. This, of course, will turn the cancellation into a small enhancement, but in any case, d_n never exceeds its current bounds.

Finally, Figure 6 shows the same information for $A_0 = m_0$. In this situation, the inclusion of the off-diagonal $(\delta^d_{ij})_{LR}$ terms allow d_n contributions of the type $\Im m\left[(\delta^d_{ij})_{LL}(\delta^d_{ji})_{LR}\right]$ and $\Im m\left[(\delta^d_{ij})_{LR}(\delta^d_{ji})_{RR}\right]$. These are always proportional to m_b, although they do not receive a $\tan\beta$

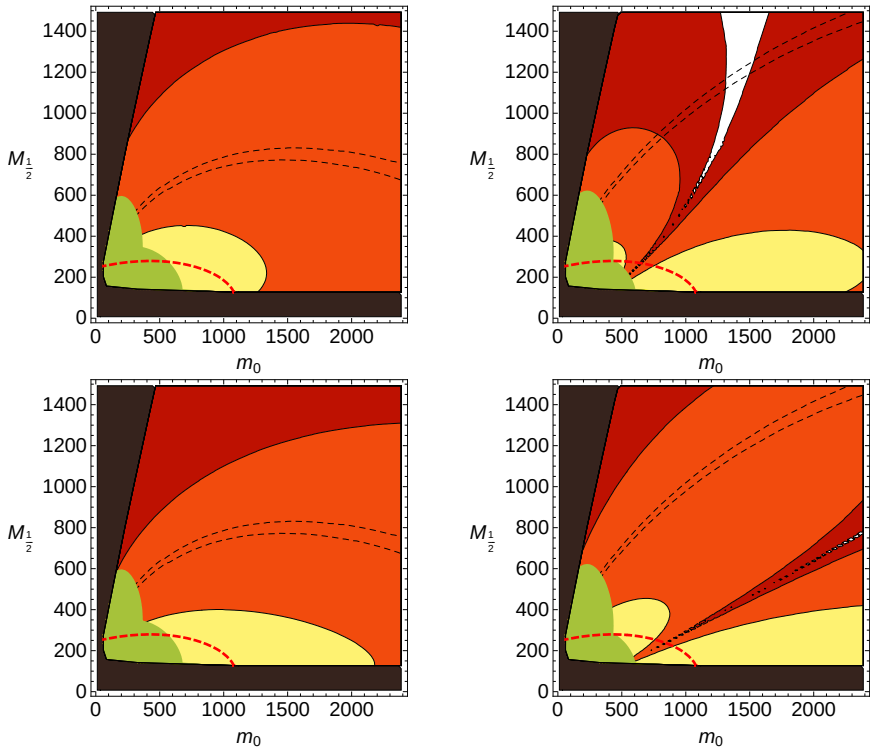

FIG. 6: Quark-parton (top) and chiral quark (bottom) contours of $|d_n| = 1 \times 10^{-27}$ e cm (yellow) $|d_n| = 1 \times 10^{-28}$ e cm (orange) and $|d_n| = 1 \times 10^{-29}$ e cm (red) in the m_0-$M_{1/2}$ plane for $\tan\beta = 10$ and $A_0 = m_0$. We show predictions for RVV1 (left), RVV2 (right). Current LFV bounds are also shown in green, and the $(g-2)_\mu$ favoured region is shown hatched in yellow.

enhancement. It was shown in [4] that these terms could be important, but they at most remained within the order of magnitude of the $\Im m\left[(\delta^d_{i3})_{LL}(\delta^d_{33})_{LR}(\delta^d_{3i})_{RR}\right]$ terms. Notice that for d_n the $(\delta^u_{ij})_{LR}$ insertions are of no interest: although RGE effects can make the off-diagonal terms as large as the $(\delta^d_{ij})_{LR}$ terms, they will usually enter the observables accompanied by a $(\delta^u_{ij})_{LL}$ or $(\delta^u_{ij})_{RR}$ insertion, which are proportional to powers of ε.

An important contribution that appears when $A_0 \neq 0$ comes from flavour-diagonal subleading phases in $(A_d)_{11}$. Although the rotation to the SCKM basis removes the leading phases in the flavour-diagonal elements of the trilinear couplings, the different $O(1)$ terms makes it impossible to remove the subleading phases in these terms. These phases are suppressed, but they still give important contributions, especially in RVV1, where the leading phases in the contributions from off-diagonal terms cancel. Such an effect is enhanced by the RGE evolution, and is particularly relevant for the squark sector.

In Figure 6 we can see that, barring the cancellations of the mass-insertion phases, both quark-parton and chiral quark EDMs are similar in magnitude. Although both RVV1 and RVV2 are still

not constrained by current bounds, the magnitude of the d_n within the ϵ_K strip is now larger by an order of magnitude, enough to be observed in the near future. The main reason for the similarity in the order of magnitude between models lies in an enhancement of the gluino contribution, due to the $(A_d)_{11}$ subleading phase mentioned in the previous paragraph. For RVV2, this contribution mostly presents a correction to the off-diagonal contributions, but for RVV1 it becomes the main source for d_n.

IV. COMBINED ANALYSIS IN THE SUSY PARAMETER SPACE

In this Section, we are going to present the results of a combined analysis of the observables studied in the previous sections. In particular, we will show the predictions of the model for LFV decays and EDMs in the regions of the parameter space where the SUSY contribution to ϵ_K can account for the possible tension between the measured value and the SM prediction, as discussed in [64]. Such a requirement, and always up to possible variations of $O(1)$ coefficients, is fulfilled in a restricted portion of the parameter space and allows, as we will see, to do quite definite predictions for the other flavour observables. If we require in addition that the $(g-2)_\mu$ discrepancy between SM and data is explained by SUSY, we are restricted in a region of rather light SUSY masses, where most of the observables are expected to be close to the present experimental bounds. Given both the presence of unknown $O(1)$ coefficients and the large theoretical uncertainties in the calculation which don't allow us to speak of a real failure of the SM, we cannot take what outlined above too seriously. Nevertheless, we think this can be a useful exercise in order to show how the interplay of various flavour observables can be used for testing this kind of flavour models.

In order to understand the impact of the $O(1)$ coefficients, in the following plots we shall set all of the $O(1)$s in the soft mass matrices equal to unity. The $O(1)$s of the trilinears shall be kept random, but fixed, since setting them to one aligns them with the Yukawas. At the end of this section we analyze the impact of varying the $O(1)$ coefficients, in order to understand how much they affect our correlations.

As explained in Section III B, the SUSY contribution to ϵ_K depends on the sign of the $O(1)$ coefficient of the entry $(\delta^d_{RR})_{12}$, since a negative sign can induce a partial cancellation between the contributions proportional to $(\delta^d_{RR})^2_{12}$ and $(\delta^d_{RR})_{12}(\delta^d_{LL})_{12}$. Therefore, we have to take into account both the possible signs for $(\delta^d_{RR})_{12}$. In Fig. 7, we show the leptonic observables as functions of the lightest slepton mass for the model RVV2 with $\tan\beta = 10$, $A_0 = 0$, $0 < m_0 < 2.5$ TeV, $0 < M_{1/2} < 1.5$ TeV. The green band corresponds to the points of the parameter space for which

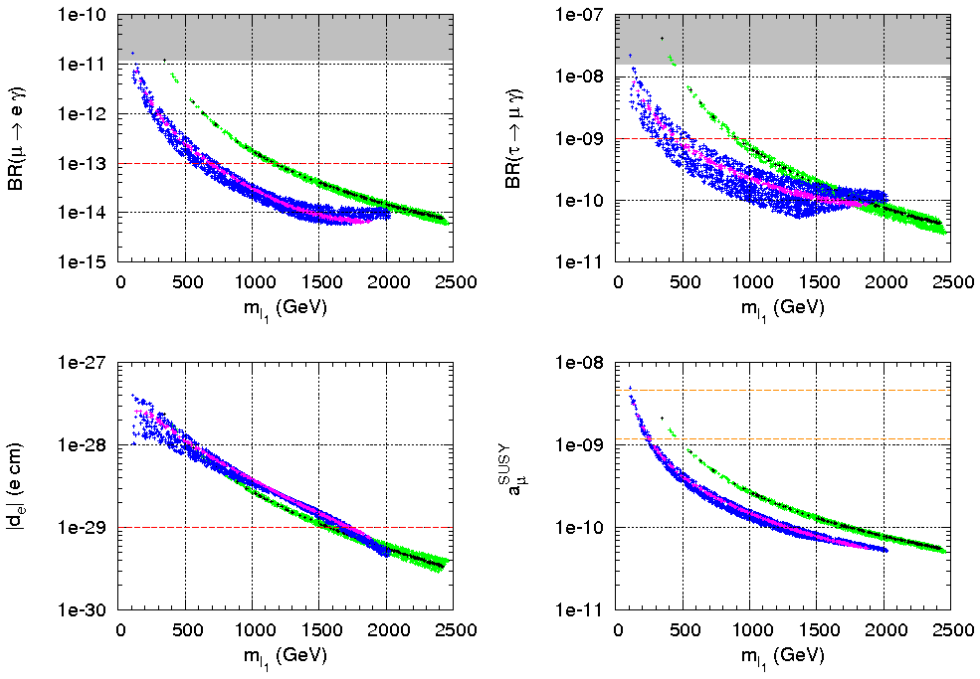

FIG. 7: Leptonic observables for model RVV2, $\tan\beta = 10$, $A_0 = 0$, as functions of the lightest slepton mass. See the text for details.

$(|\epsilon_K^{\rm SM} + \epsilon_K^{\rm susy}| - |\epsilon_K^{\rm exp}|) < \sigma^{\rm th}$, where we have checked that the correct sign has been obtained. For the SM contribution we took the central value computed in [63], $|\epsilon_K^{\rm SM}| = 1.78 \times 10^{-3}$, and $\sigma^{\rm th}$ is the corresponding theoretical error, $\sigma^{\rm th} = 0.25 \times 10^{-3}$. The blue band represents the same for the case of negative $(\delta^d_{RR})_{12}$. The black and purple strips correspond to the more strict requirement $(|\epsilon_K^{\rm SM} + \epsilon_K^{\rm susy}| - |\epsilon_K^{\rm exp}|) < 3\sigma^{\rm exp}$, with $\sigma^{\rm exp}$ being the experimental error, 0.012×10^{-3} (in other words for the strips we assume $|\epsilon_K^{\rm SM}|$ to take precisely to the central value in [63]). The shaded regions are ruled out by experiment, and the red lines indicate the future experimental sensitivity. For $(g-2)_\mu$, the area between the yellow lines solve the tension below 2σ.

The leptonic predictions in these "ϵ_K-favoured" regions are quite interesting. We see that BR($\mu \to e\gamma$) (top-left panel) gives at present practically no constraint, while the final MEG sensitivity ($\sim 10^{-13}$), will test the model up to slepton masses around 0.5-1.2 TeV. Very interestingly, the sensitivity of a Super Flavour Factory reaching BR($\tau \to \mu\gamma$) $\simeq 10^{-9}$ can be rather similar (top-right panel). The reason for this is that the "ϵ_K-favoured" region selects rather low values of $M_{1/2}$, where the future bounds of MEG and the Super Flavour Factory are comparable (see Fig. 1 in Section III A). Concerning eEDM (bottom-left panel), we see that reaching $d_e \sim 10^{-29}$ e cm^{-1} would test this case up to $m_{\tilde{l}_1} \simeq 1.5$ TeV, well beyond the reach of the LFV experiments. Finally,

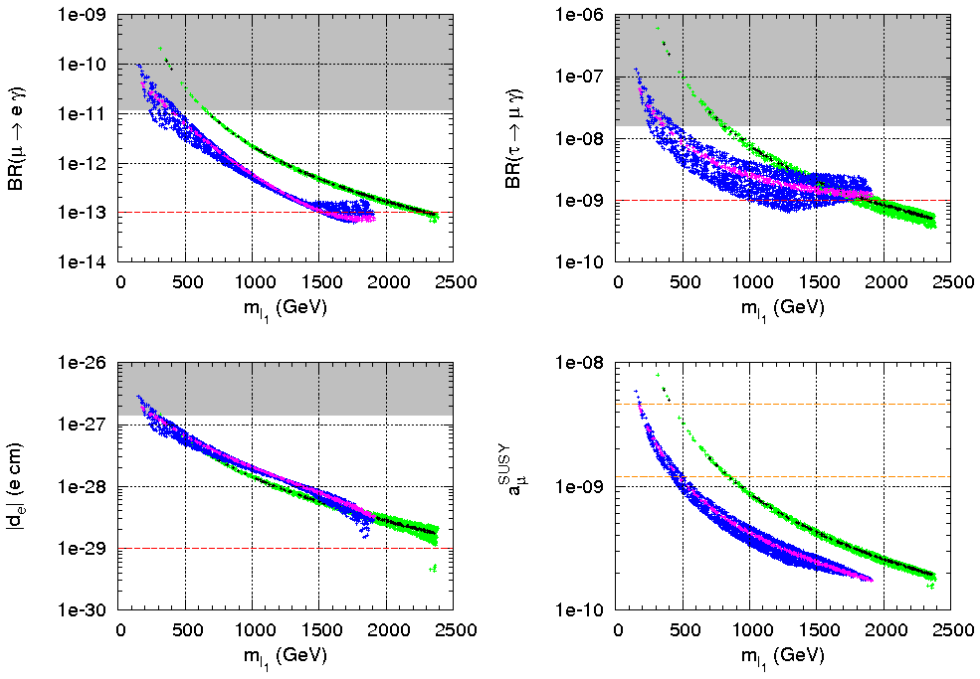

FIG. 8: Leptonic observables for model RVV2, $\tan\beta = 30$, $A_0 = 0$, as functions of the lightest slepton mass.

requiring that the SUSY contribution to $(g-2)_\mu$ (bottom-right panel) lowers the tension with the experiments below 2σ, a rather light spectrum is selected, $m_{\tilde{l}_1} \lesssim 250 - 500$ GeV, so that all the other observables should be in the reach of running/future experiments, with, in particular, branching ratios of LFV decays being just below the present experimental limits. We checked that model RVV1 gives results for LFV decays and $(g-2)_\mu$ which are similar to the ones of RVV2, while d_e is suppressed by approximately one order of magnitude: in this case, the future sensitivity on d_e will test the parameter space up to slepton masses around 500-750 GeV.

The predictions of Fig. 7 are rather stable also for $a_0 = 1$. In this case, both for RVV1 and RVV2, only BR($\mu \to e\gamma$) and d_e gets slightly increased. For larger values of $\tan\beta$ (~ 30) we expect, both for RVV1 and RVV2, the future sensitivities for LFV decays and d_e to completely test the parameter space in the range of parameters we considered, $0 < m_0 < 2.5$ TeV, $0 < M_{1/2} < 1.5$ TeV. This is shown in Fig. 8 for RVV2. Notice that, also in this case, it is possible to account for the $(g-2)_\mu$ and the ϵ_K discrepancies at the same time, even if the leptonic observables are in general predicted to be very close to the present experimental bounds.

In Fig. 9, we compare the discovery potential of the two most promising leptonic observables, $\mu \to e\gamma$ and the electron EDM. The correlation of BR($\mu \to e\gamma$) vs. $|d_e|$ is plotted for both RVV1 and RVV2, in the case $\tan\beta = 10$, $a_0 = 0$ (left), $\tan\beta = 10$, $a_0 = 1$ (center) and $\tan\beta = 30$, $a_0 = 0$

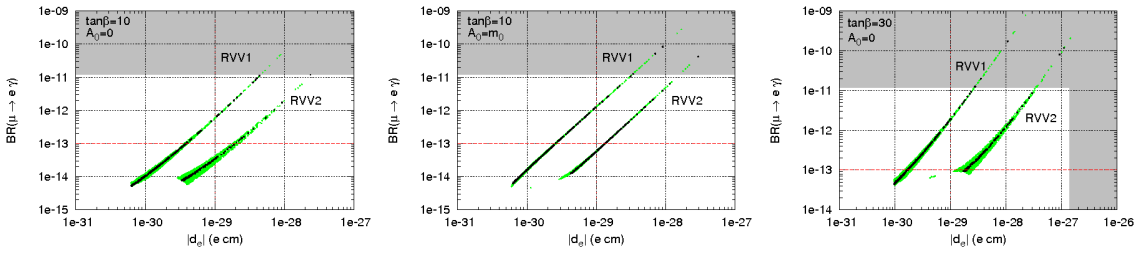

FIG. 9: BR($\mu \to e\gamma$) vs. $|d_e|$ for different scenarios. See the text for details.

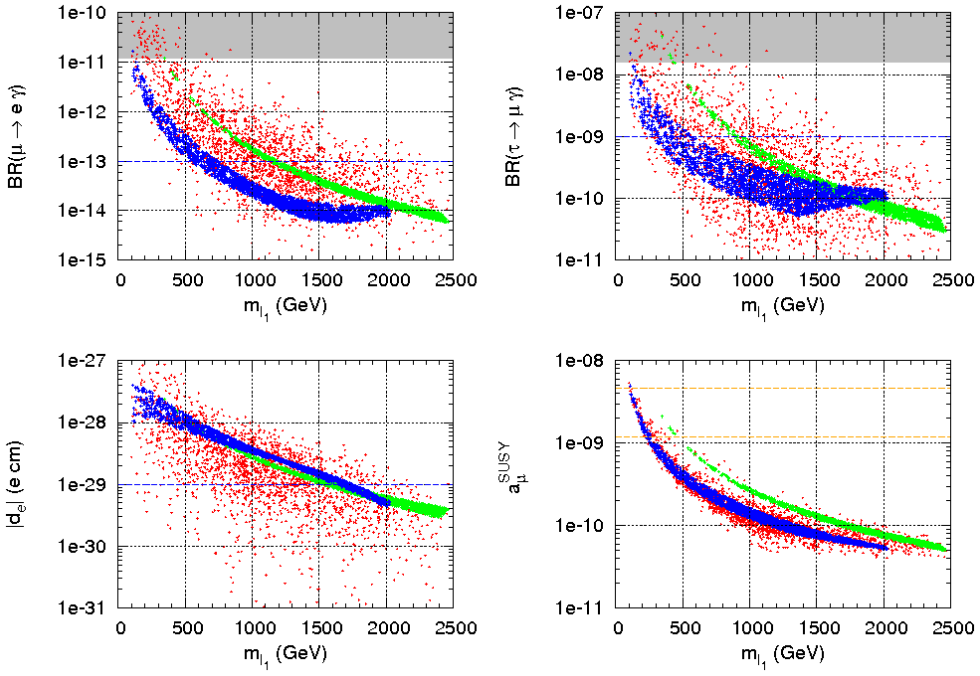

FIG. 10: Leptonic observables for model RVV2, $\tan\beta = 10$, $A_0 = 0$, as functions of the lightest slepton mass, for a random variation of the O(1) coefficients (red dots). See the text for details.

(right). As before we studied the mass range: $0 < m_0 < 2.5$ TeV, $0 < M_{1/2} < 1.5$ TeV. In the figures, only the "ϵ_K-favoured" region with positive $(\delta^d_{RR})_{12}$ has been plotted. The horizontal line corresponds to the final sensitivity of MEG, the vertical line to the sensitivity on $|d_e|$ of the running Yale-PdO experiment. We see that, for RVV1, $\mu \to e\gamma$ should be able to constrain the parameter space more strongly than eEDM, while for RVV2 it is $|d_e|$ the most sensitive observable (except for the large $\tan\beta$ case). These features could be useful in the future, in order to discriminate among different models and, more in general, shed light on the structure of mixings and phases in the slepton mass matrix.

Finally, let us briefly comment about the impact of the unknown $O(1)$ coefficients on the analysis

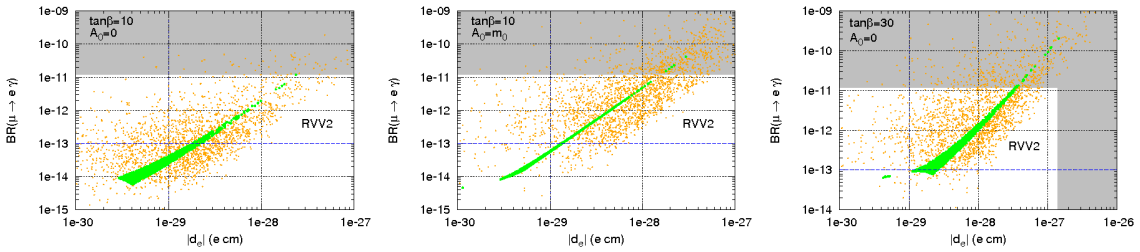

FIG. 11: Same as Fig. 9, but with a random variation of the O(1) coefficients (red dots). See the text for details.

outlined above. In Fig. 10, we plot the same observables of Fig. 7 (RVV2, $\tan\beta = 10$, $a_0 = 0$) in red, performing a random variation of all the O(1) coefficients between 0.5 and 2 (in absolute value). For comparison, we superimpose to the scatter plot the green and blue bands of Fig. 7. We do the same for Fig. 9 in Fig. 11, only for RVV2, in yellow, superimposing the green bands.

From these Figures we see that, although the lines are broadened by the variation of $O(1)$s, as expected, the correlations are roughly mantained. In some cases we can see variations of even several orders of magnitude for the predictions. This is due to two different sources. On one hand, for fixed values of m_0 and $M_{1/2}$ we can have a variation of a factor 4 or 1/4 in the product of two sleptonic $O(1)$ coefficients. On the other hand, if we allow the variation of $O(1)$ coefficients in ϵ_K, the lines in the (m_0, $M_{1/2}$) plane of Figure 2 become broad bands, increasing in turn the width of the bands of the sleptonic observables. Still, our predictions remain stable enough, especially for some observables such as BR($\mu \to e\gamma$), to conclude that the main qualitative features discussed above are not affected too much by the unknown O(1) coefficients.

V. CONCLUSIONS

In this work, we have studied the phenomenology of a MSSM with a $SU(3)$ flavour symmetry and spontaneous CP violation. We have shown that in this framework it is possible to fit the observed fermionic masses and mixings simultaneously solving the so-called SUSY flavour and CP problems. As a proof of existence, we have analyzed an explicit example based in the model of Ross, Velasco and Vives [3] that successfully overcomes the present FCNC and CP-violation constraints. At the same time, this model predicts a non-trivial flavour structure in the SUSY soft-breaking terms that will show up in near-future CP-violation, LFV and hadronic FCNC experiments. We have analyzed a model that includes the minimal set of contributions to the soft-breaking terms and we have presented two possible variations with additional contributions to soft-breaking terms.

In these models, we naturally expect to be able to observe the $\mu \to e\gamma$ decay at MEG for sfermion masses within LHC reach. Similarly, it is also possible to measure the $\tau \to \mu\gamma$ branching ratio at the future Super Flavour Factory. In the hadronic sector the main effect of the model is a sizeable contribution to ϵ_K that could explain the recently observed discrepancy between the SM and the measured value taking the latest lattice values for the B_K factor [63]. The electric dipole moment of the electron is also probably to be within reach of the present experiments while the neutron EDM will be just beyond the planned sensitivity of the experiments. It is unfortunate that, at low $\tan\beta$ and without any conspiration of $O(1)$ parameters, the evaluated versions of this model cannot provide the required contribution to ϕ_{B_s} in order to solve the discrepancy reported in [75]. This means that if the future data confirms the discrepancy, non-minimal versions of the model shall be required.

We have made a combined analysis of all the observables if we require that the ϵ_K discrepancy is solved by the SUSY contributions of the model. In this case we are able to relate the values of the different observables and again $\mu \to e\gamma$, $\tau \to \mu\gamma$ and d_e can be measured in the future experiments if SUSY is to be found at LHC.

Acknowledgments

We would like to thank G. G. Ross, I. de Medeiros Varzielas and M. Passera for useful discussions. L. C. wishes to thank the University of Valencia for the kind hospitality and partial support during various stages of this work. J. J. P. thanks the universities of Padova and Würzburg for hospitality during his visits to complete this work. A. M., J.-h. P. and O. V. would like to thank the Yukawa Institute, Kyoto and the research project YKIS for providing the opportunity to develop an important part of this work in a stimulating and active environment. We acknowledge support from the MEC-INFN agreements FPA2008-04065-E and INFN2008-016. The work of O. V. and J. J. P. was supported by the Spanish MICINN and FEDER (EC) Grant No. FPA2008-02878. O. V. was supported in part by European program MRTN-CT-2006-035482 "Flavianet" and the Generalitat Valenciana under the grant PROMETEO/2008/004. A. M. acknowledges partial support from the CARIPARO Project of Excellence (LHCosmology). W. P. is partially supported by the German Ministry of Education and Research (BMBF) under contract 05HT6WWA. J.-h. P. acknowledges Research Grants funded jointly by the Italian Ministero dell'Istruzione, dell'Università e della Ricerca (MIUR), by the University of Padova and by INFN within the *Astroparticle Physics Project*. A. M. and W. P. are partially supported by MRTN-CT-2006-035505 (Hep-Tools). A. M.

and J.-h. P. acknowledge partial support from the INFN FA51 Grant and from the RTN European Contracts MRTN-CT-2006-035863 (UniverseNet).

APPENDIX A: CKM FIT

The $SU(3)$ model generates the following leading structure for the Yukawa matrices, in terms of ε and $\bar{\varepsilon}$:

$$Y_d = \begin{pmatrix} 0 & x^d_{12}\,\bar{\varepsilon}^3\,e^{i\delta_d} & x^d_{13}\,\bar{\varepsilon}^3\,e^{i\delta_d+\beta_3} \\ x^d_{12}\,\bar{\varepsilon}^3\,e^{i\delta_d} & \Sigma_d\bar{\varepsilon}^2 & x^d_{23}\,\Sigma_d\,\bar{\varepsilon}^2\,e^{i\beta_3} \\ x^d_{13}\,\bar{\varepsilon}^3\,e^{i\delta_d+\beta_3} & x^d_{23}\,\Sigma_d\,\bar{\varepsilon}^2\,e^{i\beta_3} & e^{2i\chi} \end{pmatrix} y_b \tag{A1}$$

$$Y_u = \begin{pmatrix} 0 & x^u_{12}\,\varepsilon^3\,e^{i\delta_u} & x^u_{13}\,\varepsilon^3\,e^{i\delta_u+\beta_3} \\ x^u_{12}\,\varepsilon^3\,e^{i\delta_u} & \Sigma_u\varepsilon^2 & x^u_{23}\,\Sigma_u\,\varepsilon^2\,e^{i\beta_3} \\ x^u_{13}\,\varepsilon^3\,e^{i\delta_u+\beta_3} & x^u_{23}\,\Sigma_u\,\varepsilon^2\,e^{i\beta_3} & 1 \end{pmatrix} y_t \tag{A2}$$

where $\delta_f = 2\alpha_f + \beta_3 + \beta'_2$. It is necessary to fix the values for the x^α_{ij} parameters and the flavon phases. In the quark sector, this means that we need to reproduce the quark masses and CKM matrix and, in fact, we will see that the CKM matrix is the main source of constraints on x^u_{ij} and x^d_{ij}.

After diagonalizing the Yukawas, keeping terms up to order $\bar{\varepsilon}^3$, ε^2 and $\varepsilon\bar{\varepsilon}^2$, and rephasing fields such that V_{ud}, V_{us}, V_{cs}, V_{cb} and V_{tb} are real, we get the following CKM matrix:

$$V_{CKM} = \begin{pmatrix} \left|1 - \frac{1}{2}\left(\frac{x^d_{12}}{\Sigma_d}\right)^2 \Lambda_{ud}\,\bar{\varepsilon}^2\right| & \frac{x^d_{12}}{\Sigma_d}\,|\Lambda_{us}|\,\bar{\varepsilon} & x^d_{13}\,|\Lambda_{ub}|\,\bar{\varepsilon}^3\,e^{i(\omega_{ub}-\omega_{us}-\omega_{cb}-\omega_{ud})} \\ -\frac{x^d_{12}}{\Sigma_d}\,|\Lambda_{us}|\,\bar{\varepsilon} & \left|1 - \frac{1}{2}\left(\frac{x^d_{12}}{\Sigma_d}\right)^2 \Lambda_{ud}\,\bar{\varepsilon}^2\right| & x^d_{23}\Sigma_d\,|\Lambda_{cb}|\,\bar{\varepsilon}^2 \\ (x^d_{12}x^d_{23} - x^d_{13})\,\bar{\varepsilon}^3\,e^{i(\omega_{cb}+\omega_{us})} & -x^d_{23}\Sigma_d\,|\Lambda_{cb}|\,\bar{\varepsilon}^2\,e^{i\omega_{ud}} & 1 \end{pmatrix} \tag{A3}$$

where Λ_α are complex corrections due to subleading terms, with effective phase ω_α. These subleading terms play a very important role in the CKM phase δ_{CKM} which consists on a combination of subleading phases, the largest of these being ω_{ub}:

$$\begin{aligned} \omega_{ub} &= \arg(\Lambda_{ub}) \\ &= \arg\left(1 - x^d_{23}\left(\frac{x^u_{12}}{x^d_{13}}\right)\left(\frac{\Sigma_d}{\Sigma_u}\right)\frac{\varepsilon}{\bar{\varepsilon}}\,e^{-i(\delta_u-\delta_d)}\right), \end{aligned} \tag{A4}$$

followed by ω_{us}:

$$\omega_{us} = \arg\left(1 - \left(\frac{x^u_{12}}{x^d_{12}}\right)\left(\frac{\Sigma_d}{\Sigma_u}\right)\frac{\varepsilon}{\bar{\varepsilon}}\,e^{-i(\delta_u-\delta_d)} + (x^d_{12}x^d_{23} - x^d_{13})x^d_{23}\,\bar{\varepsilon}^2\,e^{2i(\beta_3-\chi)} + \ldots\right) \tag{A5}$$

Other Λ_α coefficients are $\Lambda_{ud}, \Lambda_{cb} \simeq 1+O(\bar{\varepsilon}^2)$ and do not play an important role in the fit. However, it is important to point out that the structure of these subleading terms is highly model dependent, and that the values we get for them shall be valid only in this model. Other $SU(3)$ models can have a completely different subleading structure.

The phenomenological fit of [36], based on structures similar to those in Eq. (A1), was used in previous works [3, 4] to fix the $O(1)$ parameters of the Yukawa matrices. In this work we make a new fit specifically for the $SU(3)$ model, taking into account also flavon phases. Although the variation of the latter make very small changes in the CKM elements, such variations could make these elements exceed the 3σ bounds in [37].

The values found in [37] for the CKM matrix are connected to a large number of flavour observables. The analysis assumes that the SM is the only source of flavour and CP violation. Nonetheless, the strong consistency in the SM between all flavour observables, in particular those participating in the construction of the unitarity triangle, suggests that new physics effects are small, and that the main source of the registered flavour and CP violation still lies in the CKM matrix. Thus, we shall adjust the $O(1)$ parameters in Y_u and Y_d such that the CKM matrix of [37] is reproduced, assuming that SUSY contributions do not affect the fit significantly.

To make a fit of the 11-dimensional parameter space of Eq. (A1), the Powell minimization method was used. The function to minimize was defined as a χ^2 on the quark masses and on the four CKM parameters in the Wolfenstein parametrization: λ, A, $\bar{\rho}$ and $\bar{\eta}$, as in [37]. We required the $O(1)$ parameters not to be larger than 2, and not smaller than 0.4. We found that the following values give a very good fit on the masses and mixings:

$$\begin{pmatrix} x^d_{12} \\ x^d_{13} \\ x^d_{23} \end{pmatrix} = \begin{pmatrix} 1.67 \\ 0.4 \\ 1.84 \end{pmatrix}; \qquad \begin{pmatrix} x^u_{12} \\ x^u_{13} \\ x^u_{23} \end{pmatrix} = \begin{pmatrix} 1.42 \\ 2.0 \\ 2.0 \end{pmatrix} \tag{A6a}$$

$$\alpha_u - \alpha_d = -0.69 \tag{A6b}$$

with β_2', β_3 and χ non-uniquely determined. The results for x^d_{ij} are similar to those in [36], with a larger discrepancy in x^d_{23}. The value of $(\alpha_u - \alpha_d)$ is mainly fixed by the CKM phase and $|V_{us}|$, as reported in [3]. To leading order, we can extract a 1σ uncertainty σ^d_{ij} on the x^d_{ij} constants from the errors on the CKM parameters [37]. We roughly expect $\sigma^d_{12} \approx 7 \times 10^{-3}$, $\sigma^d_{13} \approx 5 \times 10^{-2}$ and $\sigma^d_{23} \approx 4 \times 10^{-2}$. As the x^u_{ij} parameters participate only in subleading terms, such a rough estimation is not possible. However, by fixing these constants at the above values, we can estimate the uncertainty on $\alpha_u - \alpha_d$, being $\sigma_{(\alpha_u - \alpha_d)} \sim 0.04$.

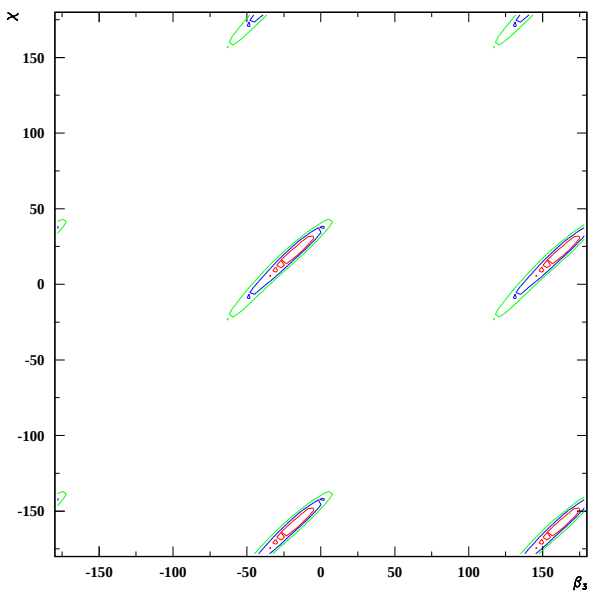

FIG. 12: Fit to Quark Masses and CKM matrix at one (red), two (blue) and three (green) sigma. There is a strong correlation between β_3 and χ, but β_2' does not affect CKM elements.

	m_u	m_c	m_t	m_d	m_s	m_b
$SU(3)$ (GeV)	2.9×10^{-3}	0.57	172.0	4.1×10^{-3}	71×10^{-3}	2.85
Reference (GeV)	$(1.4 \pm 0.5) \times 10^{-3}$	$0.63 \pm .08$	170.3 ± 2.4	$(3 \pm 1.2) \times 10^{-3}$	$(56 \pm 16) \times 10^{-3}$	2.89 ± 0.11

TABLE VII: $SU(3)$ predictions for quark masses at m_Z and corresponding values obtained by running to the same scale [99].

After fixing the determined $O(1)$s at these values, and taking $\alpha_d = 0$, we make a grid-based χ^2 analysis on the remaining three phases. We find out that the CKM matrix is completely independent of β_2', as expected from Eq. (A3). The result of the scan for β_3 and χ is shown in Figure 12. These two phases enter through subleading terms in the CKM matrix, and are severly constrained due to the precise determination of $|V_{us}|$, $|V_{cb}|$ and the diagonal elements. We are thus forced to place (β_3, χ) around $(-20°, 20°)$, or on any of four degenerate spots obtained by adding $180°$ to each. For definiteness, in the following we set $(\beta_3, \chi) = (-20°, 20°)$, and $\beta_2' = 0°$.

Using these values, we compare the results of the fit with the measured values for the CKM matrix and quark masses at m_Z [99]. The results are shown in Tables VII and VIII. We can see that the fit is very good and almost all of the SM parameters lie within their 1σ values.

Regarding the lepton sector, we shall unify the structure of quark and lepton flavoured matrices,

	λ	A	$\bar{\rho}$	$\bar{\eta}$
$SU(3)$	0.2250	0.805	0.156	0.327
Reference	$0.2257^{+0.0009}_{-0.0010}$	$0.814^{+0.021}_{-0.022}$	$0.135^{+0.031}_{-0.016}$	$0.349^{+0.015}_{-0.017}$

TABLE VIII: $SU(3)$ predictions for CKM elements and corresponding measured values, taken from [37].

	m_e	m_μ	m_τ
$SU(3)$ (GeV)	4.867808×10^{-4}	104.47907×10^{-3}	1.77634
Reference (GeV)	$4.866613(36) \times 10^{-4}$	$102.72899(44) \times 10^{-3}$	$1.74645^{+.00029}_{-.00026}$

TABLE IX: $SU(3)$ predictions for lepton masses at m_Z and corresponding values obtained by running to the same scale [99].

so the Yukawas can be written as:

$$Y_e = \begin{pmatrix} 0 & x^e_{12}\,\bar{\varepsilon}^3\,e^{i\delta_d} & x^e_{13}\,\bar{\varepsilon}^3\,e^{i\delta_d+\beta_3} \\ x^e_{12}\,\bar{\varepsilon}^3\,e^{i\delta_d} & \Sigma_e\bar{\varepsilon}^2 & x^e_{23}\,\Sigma_e\,\bar{\varepsilon}^2\,e^{i\beta_3} \\ x^e_{13}\,\bar{\varepsilon}^3\,e^{i\delta_d+\beta_3} & x^e_{23}\,\Sigma_e\,\bar{\varepsilon}^2\,e^{i\beta_3} & e^{2i\chi} \end{pmatrix} y_b, \tag{A7}$$

$$Y_\nu = \begin{pmatrix} 0 & x^u_{12}\,\varepsilon^3\,e^{i\delta_u} & x^u_{13}\,\varepsilon^3\,e^{i\delta_u+\beta_3} \\ x^u_{12}\,\varepsilon^3\,e^{i\delta_u} & 0 & 0 \\ x^u_{13}\,\varepsilon^3\,e^{i\delta_u+\beta_3} & 0 & 1 \end{pmatrix} y_t \tag{A8}$$

with and $\Sigma_e = 3\Sigma_d$ and $\Sigma_\nu = 0$. Notice that in Y_ν the zeroes are actually terms of order higher than ε^3. We use the same $O(1)$s in Y_u for Y_ν and we find that the $O(1)$s that fit best the charged lepton masses are:

$$\begin{pmatrix} x^e_{12} \\ x^e_{13} \\ x^e_{23} \end{pmatrix} = \begin{pmatrix} 1.31 \\ 2.0 \\ 2.0 \end{pmatrix} \tag{A9}$$

which give the values in Table IX. Note that lepton masses are known very precisely and thus subleading contributions will play an important role in the fit. For this reason, we did not try to fit exactly the reference values in Table IX.

For more details on how the $SU(3)$ model accomodates neutrino mixing, we refer the interested reader to [3].

APPENDIX B: $O(1)$ COEFFICIENTS IN THE SCKM BASIS AT THE GUT SCALE

In general, flavour symmetry models contain unknown $O(1)$ coefficients at the flavour scale. In CPV and FCNC studies we are interested in the leading real and imaginary contributions. However, we find that in some particular observables, leading phases might cancel. In such a situation it is important to know the structure of subleading complex terms in order to make verifiable predictions. For this purpose, we present here the structure of the $O(1)$ coefficients for the leading terms after the SCKM rotation.

In the following, we shall define $x^f_\delta = (x^f_{12}x^f_{23} - x^f_{13})$, with $f = u, d, e$.

1. RVV1

Our soft matrices in the flavour basis have the following structure at the GUT scale:

$$M^2_{\tilde{Q}} = \begin{pmatrix} 1 + Q_1\,\varepsilon^2\,y_t & 0 & 0 \\ 0 & 1 + Q_2\,\varepsilon^2 & Q_3\,\varepsilon^2\,e^{i\beta_3} \\ 0 & Q_3\,\varepsilon^2\,e^{-i\beta_3} & 1 + Q_4\,y_t \end{pmatrix} m_0^2,$$

with exactly the same structure, but different $O(1)$ constants U_i and L_i, for $M^2_{\tilde{u}^c_R}$ and $M^2_{\tilde{L}}$, respectively. For $M^2_{\tilde{d}^c_R}$ and $M^2_{\tilde{e}^c_R}$ we have an analogous structure, with ε replaced by $\bar{\varepsilon}$, y_t replaced by y_b, and different $O(1)$ constants D_i and E_i. This shall be true for all variations of the model, so in following subsections we shall only show $M^2_{\tilde{Q}}$ without repeating these specifications.

Rotation into the SCKM basis gives Eq (9), with the following $O(1)$ coefficients:

$$M^2_{\tilde{u}^c_R}(2,1) = (U_2 - U_1\,y_t)(x^u_{12}/\Sigma_u) \tag{B1a}$$

$$M^2_{\tilde{u}^c_R}(3,1) = U_3(x^u_{12}/\Sigma_u) - U_4\,x^u_\delta\,y_t\,e^{2i\beta_3} \tag{B1b}$$

$$M^2_{\tilde{u}^c_R}(3,2) = U_3 - U_4\,x^u_{23}\Sigma_u\,y_t\,e^{2i\beta_3} \tag{B1c}$$

$$M^2_{\tilde{d}^c_R}(2,1) = (D_2 - D_1\,y_b)(x^d_{12}/\Sigma_d) \tag{B2a}$$

$$M^2_{\tilde{d}^c_R}(3,1) = D_3(x^d_{12}/\Sigma_d) - D_4\,x^d_\delta\,y_b\,e^{-2i(\chi-\beta_3)} \tag{B2b}$$

$$M^2_{\tilde{d}^c_R}(3,2) = D_3 - D_4\,x^d_{23}\Sigma_d\,y_b\,e^{-2i(\chi-\beta_3)} \tag{B2c}$$

$$M^2_{\tilde{Q}}(2,1) \;=\; (Q_2 - Q_1\, y_t)(x^d_{12}/\Sigma_d) \tag{B3a}$$

$$M^2_{\tilde{Q}}(3,1) \;=\; -Q_4\, x^d_\delta + \frac{\varepsilon^2}{\bar{\varepsilon}^2}\frac{Q_3}{y_t}(x^d_{12}/\Sigma_d)\, e^{2i(\chi-\beta_3)} \tag{B3b}$$

$$M^2_{\tilde{Q}}(3,2) \;=\; Q_4\, x^d_{23}\, \Sigma_d - \frac{\varepsilon^2}{\bar{\varepsilon}^2}\,\frac{Q_3}{y_t}\, e^{2i(\chi-\beta_3)} \tag{B3c}$$

$$M^2_{\tilde{e}^c_R}(2,1) \;=\; (E_2 - E_1\, y_b)(x^e_{12}/\Sigma_e) \tag{B4a}$$

$$M^2_{\tilde{e}^c_R}(3,1) \;=\; E_3(x^e_{12}/\Sigma_e) - E_4\, x^e_\delta\, y_b\, e^{-2i(\chi-\beta_3)} \tag{B4b}$$

$$M^2_{\tilde{e}^c_R}(3,2) \;=\; E_3 - E_4\, x^e_{23}\Sigma_e\, y_b\, e^{-2i(\chi-\beta_3)} \tag{B4c}$$

$$M^2_{\tilde{L}}(2,1) \;=\; (L_2 - L_1\, y_t)(x^e_{12}/\Sigma_e) \tag{B5a}$$

$$M^2_{\tilde{L}}(3,1) \;=\; -L_4\, x^e_\delta + \frac{\varepsilon^2}{\bar{\varepsilon}^2}\frac{L_3}{y_t}(x^e_{12}/\Sigma_e)\, e^{2i(\chi-\beta_3)} \tag{B5b}$$

$$M^2_{\tilde{L}}(3,2) \;=\; L_4\, x^e_{23}\, \Sigma_e - \frac{\varepsilon^2}{\bar{\varepsilon}^2}\,\frac{L_3}{y_t}\, e^{2i(\chi-\beta_3)} \tag{B5c}$$

2. RVV2

The Kähler potential in RVV2 has got the minimal terms with the addition of the $\theta_3\bar{\theta}_{23}$ flavon vevs. This modifies the $(2,3)$ and $(3,2)$ elements of the soft mass matrices, giving them the following structure at the GUT scale:

$$M^2_{\tilde{Q}} = \begin{pmatrix} 1 + Q_1\,\varepsilon^2\, y_t & 0 & 0 \\ 0 & 1 + Q_2\,\varepsilon^2 & Q_5\,\varepsilon\, y_t^{0.5}\, e^{i\beta'_2} \\ 0 & Q_5\,\varepsilon\, y_t^{0.5}\, e^{-i\beta'_2} & 1 + Q_4\, y_t \end{pmatrix} m_0^2.$$

For simplicity, we have omitted the minimal X_3 ($X = U, D, Q, E, L$) $O(1)$s, replacing them by the corresponding X_5 that accompany the $\theta_3\bar{\theta}_{23}$ flavon vev. The $O(1)$ coefficients are:

$$M^2_{\tilde{u}^c_R}(2,1) \;=\; (U_2 - U_1\, y_t)(x^u_{12}/\Sigma_u) \tag{B6a}$$

$$M^2_{\tilde{u}^c_R}(3,1) \;=\; U_5(x^u_{12}/\Sigma_u) - \varepsilon\, U_4\, x^u_\delta\, y_t^{0.5}\, e^{i(\beta_3+\beta'_2)} \tag{B6b}$$

$$M^2_{\tilde{u}^c_R}(3,2) \;=\; U_5 - \varepsilon\, U_4\, x^u_{23}\, \Sigma_u\, y_t^{0.5}\, e^{i(\beta_3+\beta'_2)} \tag{B6c}$$

$$M^2_{\tilde{d}^c_R}(2,1) \;=\; (D_2 - D_1\, y_b)(x^d_{12}/\Sigma_d) \tag{B7a}$$

$$M^2_{\tilde{d}^c_R}(3,1) \;=\; D_5(x^d_{12}/\Sigma_d) - \bar{\varepsilon}\, D_4\, x^d_\delta\, y_b^{0.5}\, e^{-i(\chi-\beta_3-\beta'_2)} \tag{B7b}$$

$$M^2_{\tilde{d}^c_R}(3,2) \;=\; D_5 - \bar{\varepsilon}\, D_4\, x^d_{23}\, \Sigma_d\, y_b^{0.5}\, e^{-i(\chi-\beta_3-\beta'_2)} \tag{B7c}$$

$$\begin{aligned} M^2_{\tilde{Q}}(2,1) \;=\;& (Q_2 - Q_1\, y_t)(x^d_{12}/\Sigma_d) \\ & -\frac{\bar{\varepsilon}^2}{\varepsilon}\, Q_5\, y_t^{0.5} \left(x^d_\delta\, e^{i(-2\chi+\beta_3+\beta'_2)} + x^d_{12} x^d_{23}\, e^{-i(-2\chi+\beta_3+\beta'_2)} \right) \end{aligned} \tag{B8a}$$

$$M^2_{\tilde{Q}}(3,1) \;=\; Q_5(x^d_{12}/\Sigma_d) - \frac{\bar{\varepsilon}^2}{\varepsilon} Q_4\, x^d_\delta\, y_t^{0.5}\, e^{i(-2\chi+\beta_3+\beta'_2)} \tag{B8b}$$

$$M^2_{\tilde{Q}}(3,2) \;=\; Q_5 - \frac{\bar{\varepsilon}^2}{\varepsilon} Q_4\, x^d_{23}\, \Sigma_d\, y_t^{0.5}\, e^{i(-2\chi+\beta_3+\beta'_2)} \tag{B8c}$$

$$M^2_{\tilde{e}^c_R}(2,1) \;=\; (E_2 - E_1\, y_b)(x^e_{12}/\Sigma_e) \tag{B9a}$$

$$M^2_{\tilde{e}^c_R}(3,1) \;=\; E_5(x^e_{12}/\Sigma_e) - \bar{\varepsilon}\, E_4\, x^e_\delta\, y_b^{0.5}\, e^{-i(\chi-\beta_3-\beta'_2)} \tag{B9b}$$

$$M^2_{\tilde{e}^c_R}(3,2) \;=\; E_5 - \bar{\varepsilon}\, E_4\, x^e_{23}\, \Sigma_e\, y_b^{0.5}\, e^{-i(\chi-\beta_3-\beta'_2)} \tag{B9c}$$

$$\begin{aligned} M^2_{\tilde{L}}(2,1) \;=\;& (L_2 - L_1\, y_t)(x^e_{12}/\Sigma_e) \\ & -\frac{\bar{\varepsilon}^2}{\varepsilon}\, L_5\, y_t^{0.5} \left(x^e_\delta\, e^{i(-2\chi+\beta_3+\beta'_2)} + x^e_{12} x^e_{23}\, e^{-i(-2\chi+\beta_3+\beta'_2)} \right) \end{aligned} \tag{B10a}$$

$$M^2_{\tilde{L}}(3,1) \;=\; L_5(x^e_{12}/\Sigma_e) - \frac{\bar{\varepsilon}^2}{\varepsilon} L_4\, x^e_\delta\, y_t^{0.5}\, e^{i(-2\chi+\beta_3+\beta'_2)} \tag{B10b}$$

$$M^2_{\tilde{L}}(3,2) \;=\; L_5 - \frac{\bar{\varepsilon}^2}{\varepsilon} L_4\, x^e_{23}\, \Sigma_e\, y_t^{0.5}\, e^{i(-2\chi+\beta_3+\beta'_2)} \tag{B10c}$$

3. RVV Model 3

The addition of an effective term with the antisymmetric $(\theta_3\theta_{23})\theta_3$ flavon vevs gives the soft matrices the following structure, in the flavour basis, at the GUT scale:

$$M^2_{\tilde{Q}} = \begin{pmatrix} 1 + Q_1\, \varepsilon^2\, y_t & 0 & Q_6\, \varepsilon\, y_t \\ 0 & 1 + Q_2\, \varepsilon^2 & Q_3\, \varepsilon^2\, e^{i\beta_3} \\ Q_6\, \varepsilon\, y_t & Q_3\, \varepsilon^2\, e^{-i\beta_3} & 1 + Q_4\, y_t \end{pmatrix} m_0^2.$$

The additional term in the $(1,3)$ and $(3,1)$ sectors of the mass matrices induce large terms in the $(1,2)$ and $(2,1)$ sectors of the mass matrices, and have a moderate influence on the $(2,3)$ and $(3,2)$ sectors. The structure of the $O(1)$ coefficients follow:

$$M^2_{\tilde{u}^c_R}(2,1) \;=\; (U_2 - U_1\, y_t)(x^u_{12}/\Sigma_u) + U_6\, x^u_{23}\, \Sigma_u\, y_t\, e^{-i(\beta_3+\delta_u)} \tag{B11a}$$

$$M^2_{\tilde{u}^c_R}(3,1) \;=\; U_6 \tag{B11b}$$

$$M^2_{\tilde{u}^c_R}(3,2) \;=\; U_3 - U_4\, x^u_{23}\Sigma_u\, y_t\, e^{2i\beta_3} + U_6\, y_t\, (x^u_{12}/\Sigma_u)\, e^{i(\beta_3-\delta_u)} \tag{B11c}$$

$$M^2_{\tilde{d}^c_R}(2,1) \;=\; (D_2 - D_1\, y_b)(x^d_{12}/\Sigma_d) + D_6\, x^d_{23}\, \Sigma_d\, y_b\, e^{i(2\chi-\beta_3-\delta_d)} \tag{B12a}$$

$$M^2_{\tilde{d}^c_R}(3,1) \;=\; D_6 \tag{B12b}$$

$$M^2_{\tilde{d}^c_R}(3,2) \;=\; D_3 - D_4\, x^d_{23}\, \Sigma_d\, y_b\, e^{-2i(\chi-\beta_3)} + D_6\, y_b\, (x^d_{12}/\Sigma_d)\, e^{i(\beta_3-\delta_d)} \tag{B12c}$$

$$M^2_{\tilde{Q}}(2,1) \;=\; Q_6\, x^d_{23}\, \Sigma_d + \frac{\varepsilon}{\bar{\varepsilon}}\, \frac{(Q_2 - Q_1\, y_t)}{y_t} (x^d_{12}/\Sigma_d)\, e^{i(-2\chi+\beta_3+\delta_d)} \tag{B13a}$$

$$M^2_{\tilde{Q}}(3,1) \;=\; Q_6 \tag{B13b}$$

$$M^2_{\tilde{Q}}(3,2) \;=\; Q_4\, x^d_{23}\, \Sigma_d - \frac{\varepsilon}{\bar{\varepsilon}} \left[Q_6 (x^d_{12}/\Sigma_d) e^{-i\delta_d} + \frac{\varepsilon}{\bar{\varepsilon}} \frac{Q_3}{y_t} e^{-i\beta_3} \right] e^{i(2\chi-\beta_3)} \tag{B13c}$$

$$M^2_{\tilde{e}^c_R}(2,1) \;=\; (E_2 - E_1\, y_b)(x^e_{12}/\Sigma_e) + E_6\, x^e_{23}\, \Sigma_e\, y_b\, e^{i(2\chi-\beta_3-\delta_d)} \tag{B14a}$$

$$M^2_{\tilde{e}^c_R}(3,1) \;=\; E_6 \tag{B14b}$$

$$M^2_{\tilde{e}^c_R}(3,2) \;=\; E_3 - E_4\, x^e_{23}\, \Sigma_e\, y_b\, e^{-2i(\chi-\beta_3)} + E_6\, y_b\, (x^e_{12}/\Sigma_e)\, e^{i(\beta_3-\delta_d)} \tag{B14c}$$

$$M^2_{\tilde{L}}(2,1) \;=\; L_6\, x^e_{23}\, \Sigma_e + \frac{\varepsilon}{\bar{\varepsilon}}\, \frac{(L_2 - L_1\, y_t)}{y_t} (x^e_{12}/\Sigma_e)\, e^{i(-2\chi+\beta_3+\delta_d)} \tag{B15a}$$

$$M^2_{\tilde{L}}(3,1) \;=\; L_6 \tag{B15b}$$

$$M^2_{\tilde{L}}(3,2) \;=\; L_4\, x^e_{23}\, \Sigma_e - \frac{\varepsilon}{\bar{\varepsilon}} \left[L_6 (x^e_{12}/\Sigma_e) e^{-i\delta_d} + \frac{\varepsilon}{\bar{\varepsilon}} \frac{L_3}{y_t} e^{-i\beta_3} \right] e^{i(2\chi-\beta_3)} \tag{B15c}$$

4. A-Terms

For all of the evaluated models, the A-Terms will have the same structure the Yukawas have, but with different $O(1)$ constants. We parametrize them in the following way:

$$A_d = \begin{pmatrix} 0 & A_1^d\, x_{12}^d\, \bar{\varepsilon}^3\, e^{i\delta_d} & A_2^d\, x_{13}^d\, \bar{\varepsilon}^3\, e^{i(\beta_3+\delta_d)} \\ A_1^d\, x_{12}^d\, \bar{\varepsilon}^3\, e^{i\delta_d} & A_3^d\, \Sigma_d\, \bar{\varepsilon}^2 & A_4^d\, x_{23}^d\, \Sigma_d\, \bar{\varepsilon}^2\, e^{i\beta_3} \\ A_2^d\, x_{13}^d\, \bar{\varepsilon}^3\, e^{i(\beta_3+\delta_d)} & A_4^d\, x_{23}^d\, \Sigma_d\, \bar{\varepsilon}^2\, e^{i\beta_3} & A_5^d\, e^{2i\chi} \end{pmatrix} A_0\, y_b \tag{B16}$$

and similarly for A_u and A_e.

The A-Terms are rotated into the SCKM basis using the same unitary matrices that diagonalize the Yukawas. However, as the $O(1)$ constants in each entry are different from the ones in the Yukawas, the A-Terms are not diagonalized, and mantain the same structure. For squarks, the remaining off-diagonal terms are then affected by the rephasings, and we obtain:

$$A_u = \begin{pmatrix} 0 & A_2'^u\, x_{12}^u\, \varepsilon^3\, e^{-i\omega'} & A_2'^u\, x_{13}^u\, \varepsilon^3\, e^{i(2\chi-\omega')} \\ A_1'^u\, x_{12}^u\, \varepsilon^3\, e^{i\omega'} & A_3^u\, \Sigma_u\, \varepsilon^2 & A_4'^u\, x_{23}^u\, \Sigma_u\, \varepsilon^2\, e^{2i\chi} \\ A_2'^u\, x_{13}^u\, \varepsilon^3\, e^{i(\omega'+2\beta_3-2\chi)} & A_4'^u\, x_{23}^u\, \Sigma_u\, \varepsilon^2\, e^{2i(\beta_3-\chi)} & A_5^u \end{pmatrix} A_0\, y_t \tag{B17}$$

$$A_d = \begin{pmatrix} 0 & A_2'^d\, x_{12}^d\, \bar{\varepsilon}^3\, e^{-i\omega_{us}} & A_2'^d\, x_{13}^d\, \bar{\varepsilon}^3\, e^{-i\omega_{us}} \\ A_1'^d\, x_{12}^d\, \bar{\varepsilon}^3\, e^{-i\omega_{us}} & A_3^d\, \Sigma_d\, \bar{\varepsilon}^2 & A_4'^d\, x_{23}^d\, \Sigma_d\, \bar{\varepsilon}^2 \\ A_2'^d\, x_{13}^d\, \bar{\varepsilon}^3\, e^{i(\omega_{us}+2\beta_3-2\chi)} & A_4'^d\, x_{23}^d\, \Sigma_d\, \bar{\varepsilon}^2\, e^{2i(\beta_3-\chi)} & A_5^d \end{pmatrix} A_0\, y_b \tag{B18}$$

$$A_e = \begin{pmatrix} 0 & A_2'^e\, x_{12}^e\, \bar{\varepsilon}^3 & A_2'^e\, x_{13}^e\, \bar{\varepsilon}^3\, e^{i(\beta_3-\chi)} \\ A_1'^e\, x_{12}^e\, \bar{\varepsilon}^3 & A_3^e\, \Sigma_e\, \bar{\varepsilon}^2 & A_4'^e\, x_{23}^e\, \Sigma_e\, \bar{\varepsilon}^2\, e^{i(\beta_3-\chi)} \\ A_2'^e\, x_{13}^e\, \bar{\varepsilon}^3\, e^{i(\beta_3-\chi)} & A_4'^e\, x_{23}^e\, \Sigma_e\, \bar{\varepsilon}^2\, e^{i(\beta_3-\chi)} & A_5^e \end{pmatrix} A_0\, y_b \tag{B19}$$

with:

$$A_1'^f = (A_1^f - A_3^f) \tag{B20a}$$

$$A_2'^f = (A_2^f - A_5^f) - (A_4^f - A_5^f)(x_{12}^f x_{23}^f / x_{13}^f) \tag{B20b}$$

$$A_4'^f = (A_4^f - A_5^f) \tag{B20c}$$

with no subleading phases generated by the SCKM rotation. Notice that if the initial $A_i^f = 1$, the A-terms are aligned with the Yukawas. Thus, the new $A_i'^f$ go to zero, and the A-terms are diagonal at the SCKM basis.

APPENDIX C: O(1) CONSTANTS DUE TO RGES

Using the leading log approximation, we can estimate the effect of the running on the flavoured matrices. For this we define the negative parameter Δ, such that:

$$|\Delta| = \frac{1}{16\pi}\left|\log\frac{M_{SUSY}}{M_{GUT}}\right| \gtrsim \mathcal{O}(\bar{\varepsilon})$$

The rotation to the SCKM basis must be done at M_W. However, since the off-diagonal RGE contributions to the Yukawa matrices are negligible, we can perform the rotation at the GUT scale, and then apply the corrections from the running.

For $M_{\tilde{L}}$, one must take into account that only the $(3,3)$ term of Y_ν gives a significant contribution to the running. This parameter only participates until the heavy $(\nu_R^c)_3$ decouples, at the scale M_3. To take into account this effect, we introduce the parameter:

$$\Delta_\nu = \frac{1}{\Delta}\frac{1}{16\pi}\log\frac{M_3}{M_{GUT}}$$

With the exception of the A-Terms, the general result for all models is that the structure in terms of ε and $\bar{\varepsilon}$ remains unchanged. Even though the generated parameters are not necessarily of $O(1)$, the Δ parameter provides an additional suppression, which approximately keeps the matrix structure very similar to the one at the GUT scale.

These induced coefficients can have two parts: one independent of the flavour structure of the soft masses (the MFV contribution, generated by the misalignment of the Yukawa matrices), and one dependent on the flavour structure. In the following equations, those parts independent of the soft mass flavour structure can be distinguished because they do not vanish when the X_i terms $(X = U, D, Q, E, L)$ are set to zero and when the A_i terms are set to one (this also sets all primed variables to zero). They are only present in the $M^2_{\tilde{Q}}$, $M^2_{\tilde{L}}$ and A_i matrices.

In the following, we shall denote $M^2_{\tilde{X}}(i,j)$, at the scale μ, as X^μ_{ij}, with $X = U, D, Q, E, L$. For all soft mass terms, we shall factorize the $\bar{\varepsilon}$ and ε factors that appear in the mass matrices presented in Eq. (9), as well as the leading phase. Since we shall also factorize m_0^2, we define $a_0 = A_0/m_0$.

1. RVV Model 1

$$U_{21}^{EW} = U_{21}^{GUT} \tag{C1a}$$

$$U_{31}^{EW} = U_{31}^{GUT} + 2\left\{U_{31}^{GUT} - 2a_0^2\, A_2'^u\, A_5^u\, x_{13}^u\, e^{2i\beta_3}\right\} y_t^2\,\Delta \tag{C1b}$$

$$U_{32}^{EW} = U_{32}^{GUT} + 2\left\{U_{32}^{GUT} + 2a_0^2\, A_4'^u\, A_5^u\, x_{23}^u\, \Sigma_u\, e^{2i\beta_3}\right\} y_t^2\,\Delta \tag{C1c}$$

$$D_{21}^{EW} = D_{21}^{GUT} \tag{C2a}$$

$$D_{31}^{EW} = D_{31}^{GUT} + 2\left\{D_{31}^{GUT} - 2a_0^2\, A_2^{\prime d}\, A_5^d\, x_{13}^d\, e^{-2i(\chi-\beta_3)}\right\} y_b^2\, \Delta \tag{C2b}$$

$$D_{32}^{EW} = D_{32}^{GUT} + 2\left\{D_{32}^{GUT} + 2a_0^2\, A_4^{\prime d}\, A_5^d\, x_{23}^d\, \Sigma_d\, e^{-2i(\chi-\beta_3)}\right\} y_b^2\, \Delta \tag{C2c}$$

$$\begin{aligned} Q_{21}^{EW} &= Q_{21}^{GUT} - 2\frac{\bar{\varepsilon}^4}{\varepsilon^2}(3 + a_0^2 (A_5^u)^2) x_\delta^d\, x_{23}^d\, \Sigma_d\, y_t^2\, \Delta \\ &\quad + \frac{\bar{\varepsilon}^4}{\varepsilon^2}\left\{2(Q_4\, y_t + U_4\, y_t) x_\delta^d\, x_{23}^d\, y_t^2 + 2a_0^2 (A_2^{\prime d} A_4^{\prime d} x_{13}^d x_{23}^d + A_1^{\prime d} A_3^d x_{12}^d) y_b^2\right\} \Sigma_d\, \Delta \end{aligned} \tag{C3a}$$

$$\begin{aligned} Q_{31}^{EW} &= Q_{31}^{GUT} - 2(3 + a_0^2\, (A_5^u)^2) x_\delta^d\, y_t\, \Delta + 2\frac{\varepsilon^2}{\bar{\varepsilon}^2}(3 + a_0^2 A_4^u A_5^u)(x_{12}^d/\Sigma_d) x_{23}^u\, \Sigma_u\, y_t\, e^{2i\chi}\, \Delta \\ &\quad - \left\{Q_{31}^{GUT}\, (y_b^2 + y_t^2) + (Q_4 + 2U_4) x_\delta^d y_t^2 + 2a_0^2\, A_2^{\prime d}\, A_5^d\, x_{13}^d\, \frac{y_b^2}{y_t}\right\} \Delta \\ &\quad + \frac{\varepsilon^2}{\bar{\varepsilon}^2}(Q_4 + 2U_4)(x_{12}/\Sigma_d) x_{23}^u \Sigma_u\, y_t^2\, e^{2i\chi}\, \Delta \end{aligned} \tag{C3b}$$

$$\begin{aligned} Q_{32}^{EW} &= Q_{32}^{GUT} + 2(3 + a_0^2\, (A_5^u)^2) x_{23}^d\, \Sigma_d\; y_t\, \Delta - 2\frac{\varepsilon^2}{\bar{\varepsilon}^2}(3 + a_0^2 A_4^u A_5^u) x_{23}^u\, \Sigma_u\, y_t e^{2i\chi} \Delta \\ &+ \left\{\frac{Q_{32}^{GUT}}{x_{23}^d \Sigma_d}(y_b^2 + y_t^2) + (Q_4 + 2U_4)\left(1 - \frac{\varepsilon^2}{\bar{\varepsilon}^2}\frac{x_{23}^u \Sigma_u}{x_{23}^d \Sigma_d} e^{2i\chi}\right) y_t^2 - 2a_0^2 A_4^{\prime d} A_5^d \frac{y_b^2}{y_t}\right\} x_{23}^d \Sigma_d \Delta \end{aligned} \tag{C3c}$$

$$E_{21}^{EW} = E_{21}^{GUT} \tag{C4a}$$

$$E_{31}^{EW} = E_{31}^{GUT} + 2\left\{E_{31}^{GUT} - 2a_0^2\, A_2^{\prime e}\, A_5^e\, x_{13}^d\, e^{-2i(\chi-\beta_3)}\right\} y_b^2\, \Delta \tag{C4b}$$

$$E_{32}^{EW} = E_{32}^{GUT} + 2\left\{E_{32}^{GUT} + 2a_0^2\, A_4^{\prime e}\, A_5^e\, x_{23}^e\, \Sigma_e\, e^{-2i(\chi-\beta_3)}\right\} y_b^2\, \Delta \tag{C4c}$$

$$\begin{aligned} L_{21}^{EW} &= L_{21}^{GUT} - 4\frac{\bar{\varepsilon}^4}{\varepsilon^2} x_\delta^e\, x_{23}^e\, \Sigma_e\, y_t^2\, \Delta_\nu\, \Delta \\ &\quad + \frac{\bar{\varepsilon}^4}{\varepsilon^2}\left\{2(L_4\, y_t) x_\delta^e\, x_{23}^e\, y_t^2\, \Delta_\nu + 2a_0^2 (A_2^{\prime e} A_4^{\prime e} x_{13}^e x_{23}^e + A_1^{\prime e} A_3^e x_{12}^e) y_b^2\right\} \Sigma_e\, \Delta \end{aligned} \tag{C5a}$$

$$\begin{aligned} L_{31}^{EW} &= Q_{31}^{GUT} - 4x_\delta^e\, y_t\, \Delta_\nu\, \Delta \\ &\quad - \left\{Q_{31}^{GUT}\, (y_b^2 + y_t^2\, \Delta_\nu) + L_4 x_\delta^e y_t^2\, \Delta_\nu + 2a_0^2\, A_2^{\prime e}\, A_5^e\, x_{13}^e\, \frac{y_b^2}{y_t}\right\} \Delta \end{aligned} \tag{C5b}$$

$$\begin{aligned} L_{32}^{EW} &= Q_{32}^{GUT} + 4x_{23}^e\, \Sigma_e\; y_t\, \Delta_\nu\, \Delta \\ &+ \left\{\frac{Q_{32}^{GUT}}{x_{23}^e \Sigma_e}(y_b^2 + y_t^2\, \Delta_\nu) + L_4 y_t^2\, \Delta_\nu - 2a_0^2 A_4^{\prime e} A_5^e \frac{y_b^2}{y_t}\right\} x_{23}^e \Sigma_e \Delta \end{aligned} \tag{C5c}$$

2. RVV Model 2

$$U_{21}^{EW} = U_{21}^{GUT} \tag{C6a}$$

$$U_{31}^{EW} = U_{31}^{GUT} + 2\left\{U_{31}^{GUT} - 2a_0^2\,\frac{\varepsilon}{y_t^{0.5}} A_2'^u\, A_5^u\, x_{13}^u\, e^{i(\beta_3+\beta_2')}\right\} y_t^2\,\Delta \tag{C6b}$$

$$U_{32}^{EW} = U_{32}^{GUT} + 2\left\{U_{32}^{GUT} + 2a_0^2\,\frac{\varepsilon}{y_t^{0.5}} A_4'^u\, A_5^u\, x_{23}^u\, \Sigma_u\, e^{i(\beta_3+\beta_2')}\right\} y_t^2\,\Delta \tag{C6c}$$

$$D_{21}^{EW} = D_{21}^{GUT} \tag{C7a}$$

$$D_{31}^{EW} = D_{31}^{GUT} + \left\{2D_{31}^{GUT} - 2a_0^2\,\frac{\bar\varepsilon}{y_b^{0.5}}\, A_2'^d\, A_5^d\, x_{13}^d\, e^{-i(\chi-\beta_3-\beta_2')}\right\} y_b^2\Delta \tag{C7b}$$

$$D_{32}^{EW} = D_{32}^{GUT} + 2\left\{D_{32}^{GUT} + 2a_0^2\,\frac{\bar\varepsilon}{y_b^{0.5}}\, A_4'^d\, A_5^d\, x_{23}^d\, \Sigma_d\, e^{-i(\chi-\beta_3-\beta_2')}\right\} y_b^2\,\Delta \tag{C7c}$$

$$\begin{aligned} Q_{21}^{EW} &= Q_{21}^{GUT} + 2\frac{\bar\varepsilon^4}{\varepsilon^2}(3 + a_0^2(A_5^u)^2) x_\delta^d\, x_{23}^d\, \Sigma_d\, y_t^2\,\Delta \\ &\quad + \frac{\bar\varepsilon^4}{\varepsilon^2}\left\{2(Q_4\, y_t + U_4\, y_t) x_\delta^d\, x_{23}^d\, y_t^2 + 2a_0^2(A_2'^d A_4'^d x_{13}^d x_{23}^d + A_1'^d A_3^d x_{12}^d) y_b^2\right\}\Sigma_d\,\Delta \\ &\quad - \frac{\bar\varepsilon^2}{\varepsilon}\, Q_5\, y_t^{0.5}\left(x_\delta^d\, e^{i(-2\chi+\beta_3+\beta_2')} + x_{12}^d x_{23}^d\, e^{i(2\chi-\beta_3-\beta_2')}\right) y_t^2\Delta \end{aligned} \tag{C8a}$$

$$\begin{aligned} Q_{31}^{EW} &= Q_{31}^{GUT} + 2\frac{\bar\varepsilon^2}{\varepsilon}(3 + a_0^2(A_5^u)^2)\frac{x_\delta^d}{y_t^{0.5}} y_t^2 e^{i(-2\chi+\beta_3+\beta_2')}\Delta \\ &\quad - \left\{Q_{31}^{GUT}(y_t^2 + y_b^2) - \frac{\bar\varepsilon^2}{\varepsilon}\left((Q_4 + 2U_4) x_\delta^d y_t^{0.5} y_t^2 + 2a_0^2 A_2'^d A_5^d x_{13}^d \frac{y_b^2}{y_t^{0.5}}\right) e^{i(-2\chi+\beta_3+\beta_2')}\right\}\Delta \end{aligned} \tag{C8b}$$

$$\begin{aligned} Q_{32}^{EW} &= Q_{32}^{GUT} - 2\frac{\bar\varepsilon^2}{\varepsilon}(3 + a_0^2\,(A_5^u)^2)\frac{x_{23}^d\,\Sigma_d}{y_t^{0.5}}\, y_t^2\,\Delta \\ &\quad + \left\{Q_{32}^{GUT}(y_t^2 + y_b^2) - \frac{\bar\varepsilon^2}{\varepsilon}\left((Q_4 + 2U_4) y_t^{0.5} y_t^2 + 2a_0^2 A_4'^d A_5^d \frac{y_b^2}{y_t^{0.5}}\right) x_{23}^d \Sigma_d e^{i(-2\chi+\beta_3+\beta_2')}\right\}\Delta \end{aligned} \tag{C8c}$$

$$E_{21}^{EW} = E_{21}^{GUT} \tag{C9a}$$

$$E_{31}^{EW} = E_{31}^{GUT} + \left\{2E_{31}^{GUT} - 2a_0^2\,\frac{\bar\varepsilon}{y_b^{0.5}}\, A_2'^e\, A_5^e\, x_{13}^e\, e^{-i(\chi-\beta_3-\beta_2')}\right\} y_b^2\Delta \tag{C9b}$$

$$E_{32}^{EW} = E_{32}^{GUT} + 2\left\{E_{32}^{GUT} + 2a_0^2\,\frac{\bar\varepsilon}{y_b^{0.5}}\, A_4'^e\, A_5^e\, x_{23}^e\, \Sigma_e\, e^{-i(\chi-\beta_3-\beta_2')}\right\} y_b^2\,\Delta \tag{C9c}$$

$$
\begin{aligned}
L_{21}^{EW} &= L_{21}^{GUT} + 4\frac{\bar{\varepsilon}^4}{\varepsilon^2} x_\delta^e \, x_{23}^e \, \Sigma_e \, y_t^2 \, \Delta_\nu \, \Delta \\
&\quad + \frac{\bar{\varepsilon}^4}{\varepsilon^2} \left\{ 2(L_4 \, y_t) x_\delta^e \, x_{23}^e \, y_t^2 \, \Delta_\nu + 2a_0^2 (A_2'^e A_4'^e x_{13}^e x_{23}^e + A_1'^e A_3^e x_{12}^e) y_b^2 \right\} \Sigma_e \, \Delta \\
&\quad - \frac{\bar{\varepsilon}^2}{\varepsilon} \, L_5 \, y_t^{0.5} \left(x_\delta^e \, e^{i(-2\chi+\beta_3+\beta_2')} + x_{12}^e x_{23}^e \, e^{i(2\chi-\beta_3-\beta_2')} \right) y_t^2 \, \Delta_\nu \Delta
\end{aligned} \tag{C10a}
$$

$$
\begin{aligned}
L_{31}^{EW} &= L_{31}^{GUT} + 4\frac{\bar{\varepsilon}^2}{\varepsilon} \frac{x_\delta^d}{y_t^{0.5}} y_t^2 e^{i(-2\chi+\beta_3+\beta_2')} \, \Delta_\nu \, \Delta \\
&\quad - \left\{ L_{31}^{GUT} (y_t^2 \, \Delta_\nu + y_b^2) - \frac{\bar{\varepsilon}^2}{\varepsilon} \left(L_4 x_\delta^d y_t^{0.5} y_t^2 \, \Delta_\nu + 2a_0^2 A_2'^d A_5^d x_{13}^d \frac{y_b^2}{y_t^{0.5}} \right) e^{i(-2\chi+\beta_3+\beta_2')} \right\} \Delta
\end{aligned} \tag{C10b}
$$

$$
\begin{aligned}
L_{32}^{EW} &= L_{32}^{GUT} - 4\frac{\bar{\varepsilon}^2}{\varepsilon} \frac{x_{23}^e \, \Sigma_e}{y_t^{0.5}} \, y_t^2 \, \Delta_\nu \, \Delta \\
&\quad + \left\{ L_{32}^{GUT} (y_t^2 \, \Delta_\nu + y_b^2) - \frac{\bar{\varepsilon}^2}{\varepsilon} \left(L_4 y_t^{0.5} y_t^2 \, \Delta_\nu + 2a_0^2 A_4'^e A_5^e \frac{y_b^2}{y_t^{0.5}} \right) x_{23}^e \Sigma_e e^{i(-2\chi+\beta_3+\beta_2')} \right\} \Delta
\end{aligned} \tag{C10c}
$$

3. RVV Model 3

$$
U_{21}^{EW} = U_{21}^{GUT} \tag{C11a}
$$

$$
U_{31}^{EW} = U_{31}^{GUT} + 2U_{31}^{GUT} \, y_t^2 \Delta \tag{C11b}
$$

$$
U_{32}^{EW} = U_{32}^{GUT} + 2 \left\{ U_{32}^{GUT} + 2a_0^2 \, A_4'^u A_5^u \, \Sigma_u \, e^{2i\beta_3} \right\} y_t^2 \Delta \tag{C11c}
$$

$$
D_{21}^{EW} = D_{21}^{GUT} \tag{C12a}
$$

$$
D_{31}^{EW} = D_{31}^{GUT} + 2D_{31}^{GUT} \, y_b^2 \Delta \tag{C12b}
$$

$$
D_{32}^{EW} = D_{32}^{GUT} + 2 \left\{ D_{32}^{GUT} + 2a_0^2 \, A_4'^d A_5^d \, \Sigma_d \, e^{-2i(\chi-\beta_3)} \right\} y_b^2 \Delta \tag{C12c}
$$

$$
Q_{21}^{EW} = Q_{21}^{GUT} + \left(1 + \frac{\varepsilon^2}{\bar{\varepsilon}^2} \frac{x_{23}^u \Sigma_u}{x_{23}^d \Sigma_d} e^{-2i\chi} \right) (Q_6 \, x_{23}^d \Sigma_d) y_t^2 \Delta \tag{C13a}
$$

$$
Q_{31}^{EW} = Q_{31}^{GUT} + Q_6 (y_t^2 + y_b^2) \Delta \tag{C13b}
$$

$$
\begin{aligned}
Q_{32}^{EW} &= Q_{32}^{GUT} + 2(3 + a_0^2 \, (A_5^u)^2) x_{23}^d \Sigma_d \, y_t \, \Delta - 2\frac{\varepsilon^2}{\bar{\varepsilon}^2} (3 + a_0^2 A_4^u A_5^u) x_{23}^u \, \Sigma_u \, y_t e^{2i\chi} \Delta \\
&\quad + \left\{ \frac{Q_{32}^{GUT}}{x_{23}^d \Sigma_d} (y_b^2 + y_t^2) + (Q_4 + 2U_4) \left(1 - \frac{\varepsilon^2}{\bar{\varepsilon}^2} \frac{x_{23}^u \Sigma_u}{x_{23}^d \Sigma_d} e^{2i\chi} \right) y_t^2 - 2a_0^2 \, A_5^d \, A_4'^d \, \frac{y_b^2}{y_t} \right\} x_{23}^d \Sigma_d \, \Delta
\end{aligned} \tag{C13c}
$$

$$E_{21}^{EW} = E_{21}^{GUT} \tag{C14a}$$

$$E_{31}^{EW} = E_{31}^{GUT} + 2E_{31}^{GUT}\, y_b^2 \Delta \tag{C14b}$$

$$E_{32}^{EW} = E_{32}^{GUT} + 2\left\{ E_{32}^{GUT} + 2a_0^2\, A_4'^e\, A_5^e\, \Sigma_e\, e^{-2i(\chi-\beta_3)} \right\} y_b^2 \Delta \tag{C14c}$$

$$L_{21}^{EW} = L_{21}^{GUT} + (L_6\, x_{23}^e \Sigma_e) y_t^2\, \Delta_\nu\, \Delta \tag{C15a}$$

$$L_{31}^{EW} = L_{31}^{GUT} + L_6(y_t^2\, \Delta_\nu + y_b^2)\Delta \tag{C15b}$$

$$\begin{aligned} L_{32}^{EW} &= L_{32}^{GUT} + 4x_{23}^e \Sigma_e\, y_t\, \Delta_\nu\, \Delta \\ &+ \left\{ \frac{L_{32}^{GUT}}{x_{23}^e \Sigma_e} (y_b^2 + y_t^2\, \Delta_\nu) + L_4 y_t^2\, \Delta_\nu - 2a_0^2\, A_5^e\, A_4'^e\, \frac{y_b^2}{y_t} \right\} x_{23}^e \Sigma_e\, \Delta \end{aligned} \tag{C15c}$$

4. A-Terms

To write the RGE contribution for the A-Terms, we shall first denote:

$$\kappa_d^A = -\frac{7}{15} g_1^2 - 3g_2^2 - \frac{16}{3} g_3^2 + 3y_b^2 + y_\tau^2 \tag{C16a}$$

$$\kappa_d^Y = \frac{7}{15} g_1^2 M_1 + 3g_2^2 M_2 + \frac{16}{3} g_3^2 M_3 + (3y_b^2 A_5^d + y_\tau^2 A_5^e) A_0 \tag{C16b}$$

$$\kappa_u^A = -\frac{13}{15} g_1^2 - 3g_2^2 - \frac{16}{3} g_3^2 + 3y_t^2 + \sum_i y_{\nu,i}^2 \tag{C16c}$$

$$\kappa_u^Y = \frac{13}{15} g_1^2 M_1 + 3g_2^2 M_2 + \frac{16}{3} g_3^2 M_3 + 3y_t^2 A_5^u A_0 \tag{C16d}$$

$$\kappa_e^A = -\frac{9}{5} g_1^2 - 3g_2^2 + 3y_b^2 + y_\tau^2 \tag{C16e}$$

$$\kappa_e^Y = \frac{9}{5} g_1^2 M_1 + 3g_2^2 M_2 + (3y_b^2 A_5^d + y_\tau^2 A_5^e) A_0 \tag{C16f}$$

As the A-Terms are not hermitian matrices, the RGE evolution is different for each off-diagonal term. For each element, we shall factorize in Eq. (B17) the leading order of magnitude in terms of

ε or $\bar{\varepsilon}$, the phase, and the global term $A_0\, y_i$. Then, after the running, we get:

$$
\begin{aligned}
A_d(1,1) &= \mathcal{O}(\bar{\varepsilon}^4) && \text{(C17a)}\\
A_d(1,2) &= (1+\kappa_d^A\Delta)A_1'^d x_{12}^d && \text{(C17b)}\\
A_d(1,3) &= \left(1+(\kappa_d^A + A_{13}^{d,run})\Delta\right) A_2'^d x_{13}^d && \text{(C17c)}\\
A_d(2,1) &= A_d(1,2) && \text{(C17d)}\\
A_d(2,2) &= \left(1+\left(\kappa_d^A + 2\frac{\kappa_d^Y}{A_3^d A_0}\right)\Delta\right) A_3^d\,\Sigma_d && \text{(C17e)}\\
A_d(2,3) &= \left(1+(\kappa_d^A + A_{23}^{d,run})\Delta\right) A_4'^d\, x_{23}^d\,\Sigma_d && \text{(C17f)}\\
A_d(3,1) &= \left(1+(\kappa_d^A + 5y_b^2 + y_t^2)\Delta\right) A_2'^d\, x_{13}^d && \text{(C17g)}\\
A_d(3,2) &= \left(1+(\kappa_d^A + 5y_b^2 + y_t^2)\Delta\right) A_4'^d\, x_{23}^d\,\Sigma_d && \text{(C17h)}\\
A_d(3,3) &= \left(1+\left(9y_b^2 + \frac{(A_5^d+2A_5^u)}{A_5^d}y_t^2 + \kappa_d^A + 2\frac{\kappa_d^Y}{A_5^d A_0}\right)\Delta\right) A_5^d && \text{(C17i)}\\
& && \text{(C17j)}
\end{aligned}
$$

$$
\begin{aligned}
A_u(1,1) &= \mathcal{O}(\varepsilon^4) && \text{(C18a)}\\
A_u(1,2) &= (1+\kappa_u^A\Delta)A_1'^u x_{12}^u && \text{(C18b)}\\
A_u(1,3) &= \left(1+(\kappa_u^A + A_{13}^{u,run})\Delta\right) A_2'^u x_{13}^u && \text{(C18c)}\\
A_u(2,1) &= A_u(1,2) && \text{(C18d)}\\
A_u(2,2) &= \left(1+\left(\kappa_u^A + 2\frac{\kappa_u^Y}{A_3^u A_0}\right)\Delta\right) A_3^u\,\Sigma_u && \text{(C18e)}\\
A_u(2,3) &= \left(1+\left(\kappa_u^A + A_{23}^{u,run}\right)\Delta\right) A_4'^u x_{23}^u\,\Sigma_u && \text{(C18f)}\\
A_u(3,1) &= \left(1+(\kappa_u^A + 5y_t^2 + y_b^2)\Delta\right) A_2'^u\, x_{13}^u && \text{(C18g)}\\
A_u(3,2) &= \left(1+(\kappa_u^A + 5y_t^2 + y_b^2)\Delta\right) A_4'^u\, x_{23}^u\,\Sigma_u && \text{(C18h)}\\
A_u(3,3) &= \left(1+\left(9y_t^2 + \frac{(A_5^u+2A_5^d)}{A_5^u}y_b^2 + \kappa_u^A + 2\frac{\kappa_u^Y}{A_5^u A_0}\right)\Delta\right) A_5^u && \text{(C18i)}
\end{aligned}
$$

with:

$$
\begin{aligned}
A_{13}^{d,run} &= 4y_b^2 + \left(\frac{2A_5^u + A_5^d}{A_2'^d}\right)\frac{x_\delta^d}{x_{13}^d}y_t^2 - \frac{\varepsilon^2}{\bar{\varepsilon}^2}\left(\frac{2A_4^u + A_5^d}{A_2'^d}\right)\left(\frac{x_{12}^d x_{23}^u \Sigma_u}{x_{13}^d\Sigma_d}\right) y_t^2\, e^{2i\chi} && \text{(C19a)}\\
A_{23}^{d,run} &= 4y_b^2 - 3\frac{A_5^d}{A_4'^d}y_t^2 + \frac{\varepsilon^2}{\bar{\varepsilon}^2}\left(\frac{2A_4^u + A_5^d}{A_4'^d}\right)\left(\frac{x_{23}^u\Sigma_u}{x_{23}^d\Sigma_d}\right) y_t^2\, e^{2i\chi} && \text{(C19b)}\\
A_{13}^{u,run} &= 4y_t^2 + \frac{\bar{\varepsilon}^3}{\varepsilon^3}\left[\left(\frac{2A_2^d + A_5^u}{A_2'^u}\right)\frac{x_{13}^d}{x_{13}^u}\, e^{i(\omega'-\omega_{us})} - \frac{\varepsilon}{\bar{\varepsilon}}\left(\frac{2A_4^d + A_5^u}{A_2'^u}\right)\frac{x_{12}^u x_{23}^d \Sigma_d}{x_{13}^u\Sigma_u}\right] y_b^2\, e^{-2i\chi} && \text{(C19c)}\\
A_{23}^{u,run} &= 4y_t^2 - \left(\frac{2A_5^d + A_5^u}{A_4'^u}\right) y_b^2 + \frac{\bar{\varepsilon}^2}{\varepsilon^2}\left(\frac{2A_4^d + A_5^u}{A_4'^u}\right)\left(\frac{x_{23}^d\Sigma_d}{x_{23}^u\Sigma_u}\right) y_b^2\, e^{-2i\chi} && \text{(C19d)}\\
& && \text{(C19e)}
\end{aligned}
$$

We see that the running can generate subleading phases, which are contained within the $A_{ij}^{f,run}$ terms. In particular, it is noticeable that these phases do not vanish when aligning the A-Terms with the Yukawas (setting all $A_i'^f \to 0$), which means they belong to a MFV contribution.

It is also important to remark the fact that $A_{13}^{u,run}$ and $A_{23}^{u,run}$ contain terms of order $(\bar{\varepsilon}/\varepsilon)^3$ and $(\bar{\varepsilon}/\varepsilon)^2$, which are enhancement factors. Again, these are due to MFV contributions. Thus, the RGE evolution has the potential of changing the structure of A_u noticeably.

We do not list the A_e matrices, since their structure is identical to A_d, with the replacements $y_t^2 \to y_t^2\,\Delta_\nu$, $\kappa_d^\alpha \to \kappa_e^\alpha$, $x_i^d \to x_i^e$, $A_i^d \to A_i^e$ and $A_i^u \to 0$. One must also consider $\Sigma_e = 3\Sigma_d$ and $\Sigma_\nu = 0$.

---

[1] A. Masiero and O. Vives, Ann. Rev. Nucl. Part. Sci. **51** (2001) 161 [arXiv:hep-ph/0104027].

[2] A. Masiero, S. K. Vempati and O. Vives, arXiv:0711.2903 [hep-ph].

[3] G. G. Ross, L. Velasco-Sevilla and O. Vives, Nucl. Phys. B **692**, 50 (2004) [arXiv:hep-ph/0401064]

[4] L. Calibbi, J. Jones-Perez and O. Vives, Phys. Rev. D **78** (2008) 075007 [arXiv:0804.4620 [hep-ph]].

[5] C. D. Froggatt and H. B. Nielsen, Nucl. Phys. B **147** (1979) 277.

[6] M. Leurer, Y. Nir and N. Seiberg, Nucl. Phys. B **398** (1993) 319 [arXiv:hep-ph/9212278].

[7] A. Pomarol and D. Tommasini, Nucl. Phys. B **466**, 3 (1996) [arXiv:hep-ph/9507462].

[8] P. Binetruy, S. Lavignac and P. Ramond, Nucl. Phys. B **477** (1996) 353 [arXiv:hep-ph/9601243].

[9] E. Dudas, C. Grojean, S. Pokorski and C. A. Savoy, Nucl. Phys. B **481**, 85 (1996) [arXiv:hep-ph/9606383].

[10] H. K. Dreiner, H. Murayama and M. Thormeier, Nucl. Phys. B **729** (2005) 278 [arXiv:hep-ph/0312012].

[11] G. L. Kane, S. F. King, I. N. R. Peddie and L. Velasco-Sevilla, JHEP **0508** (2005) 083 [arXiv:hep-ph/0504038].

[12] P. H. Chankowski, K. Kowalska, S. Lavignac and S. Pokorski, Phys. Rev. D **71** (2005) 055004 [arXiv:hep-ph/0501071].

[13] R. Barbieri, G. R. Dvali and L. J. Hall, Phys. Lett. B **377**, 76 (1996) [arXiv:hep-ph/9512388].

[14] R. Barbieri, L. J. Hall, S. Raby and A. Romanino, Nucl. Phys. B **493**, 3 (1997) [arXiv:hep-ph/9610449].

[15] S. F. King and G. G. Ross, Phys. Lett. B **520**, 243 (2001) [arxiv:hep-ph/0108112]

[16] S. F. King and G. G. Ross, Phys. Lett. B **574**, 239 (2003) [arxiv:hep-ph/0307190]

[17] I. de Medeiros Varzielas and G. G. Ross, Nucl. Phys. B **733** (2006) 31 [arXiv:hep-ph/0507176].

[18] I. de Medeiros Varzielas, S. F. King and G. G. Ross, Phys. Lett. B **644** (2007) 153 [arXiv:hep-ph/0512313].

[19] I. de Medeiros Varzielas, S. F. King and G. G. Ross, Phys. Lett. B **648** (2007) 201 [arXiv:hep-ph/0607045].

[20] T. Kobayashi, H. P. Nilles, F. Ploger, S. Raby and M. Ratz, Nucl. Phys. B **768** (2007) 135 [arXiv:hep-ph/0611020].

[21] H. Ishimori, T. Kobayashi, H. Okada, Y. Shimizu and M. Tanimoto, JHEP **0904** (2009) 011 [arXiv:0811.4683 [hep-ph]].

[22] H. Ishimori, T. Kobayashi, H. Okada, Y. Shimizu and M. Tanimoto, arXiv:0907.2006 [hep-ph].

[23] G. Altarelli and F. Feruglio, Nucl. Phys. B **720** (2005) 64 [arXiv:hep-ph/0504165].

[24] T. Kobayashi, Y. Omura and K. Yoshioka, Phys. Rev. D **78** (2008) 115006 [arXiv:0809.3064 [hep-ph]].

[25] G. Seidl, arXiv:0811.3775 [hep-ph].

[26] G. G. Ross and O. Vives, Phys. Rev. D **67**, 095013 (2003) [arXiv:hep-ph/0211279]

[27] S. Antusch, S. F. King and M. Malinsky, arXiv:0708.1282 [hep-ph].

[28] K. A. Olive and L. Velasco-Sevilla, arXiv:0801.0428 [hep-ph].

[29] G. G. Ross and L. Velasco-Sevilla, Nucl. Phys. B **653** (2003) 3 [arXiv:hep-ph/0208218].

[30] F. Gabbiani, E. Gabrielli, A. Masiero and L. Silvestrini, Nucl. Phys. B **477** (1996) 321 [arXiv:hep-ph/9604387].

[31] J. S. Hagelin, S. Kelley and T. Tanaka, Nucl. Phys. B **415** (1994) 293.

[32] F. Borzumati and A. Masiero, Phys. Rev. Lett. **57** (1986) 961

[33] J. A. Casas and A. Ibarra, Nucl. Phys. B **618**, 171 (2001) [arXiv:hep-ph/0103065].

[34] A. Masiero, S. K. Vempati and O. Vives, Nucl. Phys. B **649**, 189 (2003) [arXiv:hep-ph/0209303].

[35] W. Porod, Comput. Phys. Commun. **153** (2003) 275 [arXiv:hep-ph/0301101].

[36] R. G. Roberts, A. Romanino, G. G. Ross and L. Velasco-Sevilla, Nucl. Phys. B **615** (2001) 358 [arXiv:hep-ph/0104088].

[37] C. Amsler *et al.* [Particle Data Group], Phys. Lett. B **667**, 1 (2008).

[38] R. Barate *et al.* [LEP Working Group for Higgs boson searches and ALEPH Collaboration and and], Phys. Lett. B **565** (2003) 61 [arXiv:hep-ex/0306033].

[39] A. Djouadi, M. Drees and J. L. Kneur, JHEP **0108** (2001) 055 [arXiv:hep-ph/0107316].

[40] B. C. Allanach, A. Djouadi, J. L. Kneur, W. Porod and P. Slavich, JHEP **0409**, 044 (2004) [arXiv:hep-ph/0406166].

[41] S. Heinemeyer, W. Hollik, H. Rzehak and G. Weiglein, Eur. Phys. J. C **39** (2005) 465 [arXiv:hep-ph/0411114].

[42] S. Chen *et al.* [CLEO Collaboration], Phys. Rev. Lett. **87** (2001) 251807 [arXiv:hep-ex/0108032].

[43] Belle Collaboration, talk by A. Limosani at Moriond EW (2008)

[44] B. Aubert *et al.* [BABAR Collaboration], Phys. Rev. D **72** (2005) 052004 [arXiv:hep-ex/0508004].

[45] Heavy Flavor Averaging Group web page: http://www.slac.stanford.edu/xorg/hfag/

[46] T. Hurth, E. Lunghi and W. Porod, Nucl. Phys. B **704** (2005) 56 [arXiv:hep-ph/0312260].

[47] G. Degrassi, P. Gambino and P. Slavich, Comput. Phys. Commun. **179** (2008) 759 [arXiv:0712.3265 [hep-ph]].

[48] T. Becher and M. Neubert, Phys. Rev. Lett. **98** (2007) 022003 [arXiv:hep-ph/0610067].

[49] E. Lunghi and J. Matias, JHEP **0704** (2007) 058 [arXiv:hep-ph/0612166].

[50] G. W. Bennett *et al.* [Muon G-2 Collaboration], Phys. Rev. D **73** (2006) 072003 [arXiv:hep-ex/0602035].

[51] J. P. Miller, E. de Rafael and B. L. Roberts, Rept. Prog. Phys. **70** (2007) 795 [arXiv:hep-ph/0703049].

[52] M. Passera, W. J. Marciano and A. Sirlin, Phys. Rev. D **78** (2008) 013009 [arXiv:0804.1142 [hep-ph]].

[53] F. Jegerlehner and A. Nyffeler, Phys. Rept. **477** (2009) 1 [arXiv:0902.3360 [hep-ph]].

[54] T. Moroi, Phys. Rev. D **53** (1996) 6565 [Erratum-ibid. D **56** (1997) 4424] [arXiv:hep-ph/9512396].

[55] M. Davier, S. Eidelman, A. Hocker and Z. Zhang, Eur. Phys. J. C **27** (2003) 497 [arXiv:hep-ph/0208177].

[56] M. Ahmed *et al.* [MEGA Collaboration], Phys. Rev. D **65** (2002) 112002 [arXiv:hep-ex/0111030].

[57] MEG Experiment: http://meg.psi.ch.

[58] S. Banerjee, Nucl. Phys. Proc. Suppl. **169** (2007) 199 [arxiv:hep-ex/0702017]

[59] A. Lusiani, [arXiv:0709.1599 [hep-ex]]

[60] M. Bona *et al.*, arXiv:0709.0451 [hep-ex].

[61] B. Aubert *et al.* [BABAR Collaboration], Phys. Rev. Lett. **96** (2006) 041801 [arXiv:hep-ex/0508012].

[62] A. G. Akeroyd *et al.* [SuperKEKB Physics Working Group], arXiv:hep-ex/0406071.

[63] A. J. Buras and D. Guadagnoli, arXiv:0901.2056 [hep-ph].

[64] A. J. Buras and D. Guadagnoli, Phys. Rev. D **78** (2008) 033005 [arXiv:0805.3887 [hep-ph]].

[65] D. J. Antonio *et al.* [RBC Collaboration and UKQCD Collaboration], Phys. Rev. Lett. **100** (2008) 032001 [arXiv:hep-ph/0702042].

[66] C. Allton *et al.* [RBC-UKQCD Collaboration], Phys. Rev. D **78** (2008) 114509 [arXiv:0804.0473 [hep-lat]].

[67] C. Aubin, J. Laiho and R. S. Van de Water, arXiv:0905.3947 [hep-lat].

[68] E. Lunghi and A. Soni, Phys. Lett. B **666** (2008) 162 [arXiv:0803.4340 [hep-ph]].

[69] M. Ciuchini *et al.*, JHEP **9810** (1998) 008 [arXiv:hep-ph/9808328].

[70] Y. Nakamura *et al.* [CP-PACS Collaboration], PoS **LAT2006** (2006) 089 [arXiv:hep-lat/0610075].

[71] A. J. Buras, G. Colangelo, G. Isidori, A. Romanino and L. Silvestrini, Nucl. Phys. B **566** (2000) 3 [arXiv:hep-ph/9908371].

[72] Y. Nir and M. P. Worah, Phys. Lett. B **423** (1998) 319 [arXiv:hep-ph/9711215].

[73] A. J. Buras, A. Romanino and L. Silvestrini, Nucl. Phys. B **520** (1998) 3 [arXiv:hep-ph/9712398].

[74] G. Colangelo and G. Isidori, JHEP **9809** (1998) 009 [arXiv:hep-ph/9808487].

[75] M. Bona *et al.* [UTfit Collaboration], arXiv:0803.0659 [hep-ph].

[76] E. Barberio *et al.* [Heavy Flavor Averaging Group], arXiv:0808.1297 [hep-ex].

[77] D. Becirevic *et al.*, Nucl. Phys. B **634** (2002) 105 [arXiv:hep-ph/0112303].

[78] G. Buchalla, A. J. Buras and M. E. Lautenbacher, Rev. Mod. Phys. **68** (1996) 1125 [arXiv:hep-ph/9512380].

[79] UTFit web page: http://www.utfit.org/

[80] B. Dutta and Y. Mimura, Phys. Rev. D **78** (2008) 071702 [arXiv:0805.2988 [hep-ph]].

[81] P. Ko, J. h. Park and M. Yamaguchi, JHEP **0811** (2008) 051 [arXiv:0809.2784 [hep-ph]].

[82] [LHCb Collaboration], Expression of interest for an LHCb upgrade, CERN/LHCC/2008-007.

[83] W. Altmannshofer, A. J. Buras, S. Gori, P. Paradisi and D. M. Straub, arXiv:0909.1333 [hep-ph].

[84] Y. Yamada, Phys. Rev. D **77**, 014025 (2008) [arXiv:0709.1022 [hep-ph]].

[85] M. E. Pospelov and I. B. Khriplovich, Sov. J. Nucl. Phys. **53** (1991) 638

[86] I. B. Khriplovich and A. R. Zhitnitsky, Phys. Lett. B **109** (1982) 490

[87] J. Hisano, M. Nagai and P. Paradisi, Phys. Lett. B **642** (2006) 510 [arXiv:hep-ph/0606322].

[88] A. J. Buras, P. H. Chankowski, J. Rosiek and L. Slawianowska, Nucl. Phys. B **659** (2003) 3 [arXiv:hep-ph/0210145].

[89] J. Hisano, M. Nagai and P. Paradisi, arXiv:0812.4283 [hep-ph].

[90] B. C. Regan and E. D. Commins and C. J. Schmidt and D. DeMille, Phys. Rev. Lett. **88** (2002) 071805

[91] S. K. Lamoreaux, [arXiv:nucl-ex/0109014]

[92] Cs and Rb eEDM Experiment: http://www.phys.psu.edu/research/amo/
HfF^+ eEDM Experiment: http://jilawww.colorado.edu/bec/index.html
PbO eEDM Experiment: http://www.yale.edu/demillegroup/
YbF eEDM Experiment: http://www3.imperial.ac.uk/ccm/research/edm

[93] J. R. Ellis and R. A. Flores, Phys. Lett. B **377** (1996) 83 [arXiv:hep-ph/9602211].

[94] A. Manohar and H. Georgi, Nucl. Phys. B **234** (1984) 189.

[95] G. Degrassi, E. Franco, S. Marchetti and L. Silvestrini, JHEP **0511** (2005) 044 [arXiv:hep-ph/0510137].

[96] R. L. Arnowitt, J. L. Lopez and D. V. Nanopoulos, Phys. Rev. D **42** (1990) 2423.

[97] S. Weinberg, Phys. Rev. Lett. **63** (1989) 2333.

[98] CryoEDM Experiment: http://hepwww.rl.ac.uk/EDM/index_files/CryoEDM.htm
PNPI nEDM Experiment: http://nrd.pnpi.spb.ru/LabSereb/neutronedm.htm
PSI nEDM Experiment: http://nedm.web.psi.ch/
SNS nEDM Experiment: http://p25ext.lanl.gov/edm/edm.html

[99] I. Dorsner, P. Fileviez Perez and G. Rodrigo, Phys. Rev. D **75** (2007) 125007 [arXiv:hep-ph/0607208].